

National & Kapodistrian University of Athens

Faculty of Geology and Geoenvironment

MSc. Program in Oceanography and Management of Marine
Environment

Title of Thesis

**THE CARBONATE FACTORY OVER THE LAST
20.000 YEARS IN THE NW SARONIKOS GULF**



Submitted by

Kristiana Karakigianou

A thesis in partial
fulfillment of the requirements for the degree of
Master of Science in Oceanography and Management of the Marine Environment

Master's Committee

Supervisor: Anastasakis G., Professor

Committee Member: Drinia C., Professor

Committee Member: Karageorgis A., Research Director in Hellenic Centre for Marine Research

Athens, December 2017

CONTENTS

ACKNOWLEDGMENTS	3
ΠΕΡΙΛΗΨΗ	4
ABSTRACT	5
CHAPTER 1. Introduction	6
CHAPTER 2. Geodynamic Setting	19
CHAPTER 3. Carbonate Chemistry	27
Control Factors	
3.1 Presence of Ions.....	28
3.2 Partial Pressure of Carbon dioxide.....	30
3.3 Mg: Ca ratio.....	33
3.4 Saturation State.....	36
3.5 Temperature.....	44
3.6 Salinity.....	46
3.7 O ₂	51
CHAPTER 4. Results	55
4.1 Magnetic Susceptibility.....	56
4.2 Description of Lithologic Units.....	60
4.3 XRD Analyses.....	82
4.4 AMS Chronology.....	99
4.5 SEM Photographs.....	101
CHAPTER 5. Conclusions	106
REFERENCES	107
ACRONYMS AND ABBREVIATIONS	125
LIST OF FIGURES	126
LIST OF TABLES	130

ACKNOWLEDGMENTS

I would first like to express my deep appreciation to my M.Sc. thesis advisor Professor George Anastasakis of the School of Science/ Faculty of Geology and Geoenvironment at National & Kapodistrian University of Athens. The door to Prof. Anastasakis office was always open, whenever I ran into a trouble spot or had a question about my research or writing. He consistently allowed this thesis to be my own work, but steered me in the right direction whenever he thought I needed it. Without his passionate participation and patience, this thesis could not have been successfully conducted. My sincere thanks are also due to the other two members of my thesis committee, Prof. Drinia and Dr. Karageorgis for making many constructive comments that greatly proved this thesis.

I would also like to express my deep gratitude to Koumoutsakou Olga for her valuable technical support on this project. Her willingness to give her time so generously has been very much appreciated. I am particularly grateful for the assistance given by my colleagues Foutrakis Panagiotis, Anastasakos Dionysis, Kontogonis George, Aggelos Bougiouris and Koutrouli Anna.

Special thanks go to my colleague Louvari Melina for sharing with me her notes regarding the contained microfauna of my samples.

I also wish to acknowledge the support of the Onassis Foundation, in the form of a Postgraduate Grant that enabled me to attend this Master Program and for which I am gratefully indebted to them.

Finally, I wish to thank my family and friends for their support and encouragement throughout my study.

Author

Kristiana Karakigianou

ΠΕΡΙΛΗΨΗ

Σύμφωνα με προηγούμενες μελέτες στην περιοχή του βορειοδυτικού Σαρωνικού, η λεκάνη των Μεγάρων επανειλημμένα αποκοπτόταν από την ανοιχτή θάλασσα στο παρελθόν, όταν η παγκόσμια θαλάσσια στάθμη έπεφτε. Η απομόνωση αυτή της λεκάνης είχε ως αποτέλεσμα την μετάβαση σε συνθήκες ανθρακικής ιζηματογένεσης και απόθεσης κυρίως αραγωνίτη.

Στόχος της διπλωματικής αυτής εργασίας είναι η διερεύνηση των συνθηκών που οδήγησαν στην δημιουργία ενός φυσικού ανθρακικού εργαστηρίου και στην εναπόθεση ανθρακικών ακολουθιών κατά το τέλος του Πλειστόκαινου.

Με βάση τα αποτελέσματα μας, προς το τέλος της τελευταίας Παγετώδους περιόδου, η λεκάνη των Μεγάρων ήταν πράγματι μία αποκομμένη αλμυρή λεκάνη, σχετικά ρηχή και υπερκορεσμένη σε ανθρακικό ασβέστιο, και πιο συγκεκριμένα σε αραγωνίτη, δίχως σημαντική τροφοδότηση από τις περιβάλλουσες λεκάνες απορροής, ωστόσο δεν κατάφερε ποτέ να φτιάξει γύψο.

Επιπρόσθετα, το ανθρακικό αυτό εργαστήριο, αν και δείχνει να επηρεάστηκε σε ένα μικρό βαθμό από το ψυχρό επεισόδιο HS1, πολύ γρήγορα όχι μόνο επανήλθε αλλά αύξησε την παραγωγή του σε αραγωνίτη, εξαιτίας της ανόδου της θερμοκρασίας κατά τη διάρκεια του Bølling-Allerød, με τα ποσοστά του ορυκτού να φτάνουν τα 80-90%.

Τέλος, η κατανομή των ανθρακικών ορυκτών κατά μήκος της λεκάνης μας οδηγεί στο συμπέρασμα ότι ο δυτικός Σαρωνικός καθυστέρησε αρκετά να επανενωθεί με την ανοιχτή θάλασσα και όχι πριν η θαλάσσια στάθμη φτάσει τα -82 μ.

ABSTRACT

Previous studies argued that during prolonged periods of low sea level stands, Megara Basin (NW Saronikos Gulf, Greece) becomes an isolated basin that produces thick beds of fine-grained aragonite until the reconnection with the open sea is re-established again.

The purpose of this thesis is to examine the conditions under which this carbonate factory flourished after the end of the LGM within Western Saronikos and determine the changes that went through till its termination.

Based on the results of this thesis, by the end of the LGM, Megara Basin was indeed an isolated aragonite-dominated marine basin, with no indications of river discharges. This hypothesis is supported by both the measured MS of all the retrieved cores and the terrigenous mineralogy of SAR39 that verify the absence of significant terrigenous input previous to Holocene. Moreover, bulk carbonate mineralogy and XRD estimates support the idea that Megara Basin was relatively shallow and supersaturated with respect to CaCO_3 , though it never experienced typical hypersaline conditions (e.g. forming gypsum)

Also, the data, which were derived from the marine sediment core SAR39 point to the brief “cold” HS1 Event that disrupted aragonite deposition to a minor level without however destroying the carbonate factory, followed shortly after by the warmer Bølling-Allerød interstadial that accelerated aragonite precipitation, reaching (80-90%). Finally, distribution of the carbonate minerals along the basin points out that reconnection of western Saronikos Gulf with the open sea was in fact delayed, not being reestablished before SL reached ~-82m.

CHAPTER 1. Introduction

As it is widely known due to numerous studies, **during the Last Glacial Maximum (LGM)** from 23 to 15.8 ka BP the sea level stood much lower than today therefore the shorelines then did not resemble their present form. Particularly, at the peak of the LGM, around 21-20 ka BP, the sea level reached -120m (*Yokoyama et al., 2000a*), resulting to the exposure of large land mass throughout the world. Such a land mass, as I will discuss below is the **N-S oriented ridge in Saronikos Gulf** that is responsible for the isolation of the **Megara Basin** up to early Holocene.

Regarding **Eastern Mediterranean Sea**, during the latest **lowstand** (21.5 ka BP) extensive shelf areas were exposed in the Aegean and Ionian seas. Most near-shore islands were connected with each other, forming bigger islands, like the extensive land plateau that was formed in the Cyclades sector (*Van Andel&Shackleton, 1982*) or in some cases connected with the mainland, like in the case of the Corfu Island in the Ionian Sea or the Northern Sporades islands, in the central Aegean Sea. Furthermore and most importantly for this thesis, a great part of the periphery of most gulfs (e.g. Pagasitikos, Evoikos and Saronikos) in the western Aegean Sea, was exposed, being their entrance shallower than 120 m, resulting to the formation of isolated lakes in their center (*Perissoratis&Van Andel, 1991; Lykousis&Anagnostou, 1994, Karageorgis et al. 2013*).

Soon after that point, a subsequent global melting followed, starting at about 19.6 ka BP and spanning for almost 12,000 years. The mean rates and the magnitude of relative sea-level elevation were reconstructed thanks to analysis of drowned reef-crest corals. Typically, marine transgression, during which sea level rises, differs from place to place, even though eustatic sea level change had to have been globally uniform, local geologic variables (e.g. coastal subsidence, tectonic uplift etc.) led to differences regarding the timing and the rate of relative seal level rise from place to place.

So far, only three **deglaciation curves** based on coral reef records have been accurately dated for times reaching the **Pleistocene-Holocene boundary**:

- in Barbados between 19 and 8 ka BP (*Fairbanks, 1989; Bard et al., 1990*)
- in Papua New Guinea between 13 and 6 ka BP (*Chappell&Polach, 1991; Edwards et al., 1993*), and
- in Tahiti between 13.8 and 3 ka BP (*Bard et al., 1996*).

However, according to these curves, the post-glacial sea level rise proceeds not at a steady pace rather than as **pulsed deglaciation**, with brief intervals of accelerated melting called the **meltwater pulses (Fig. 3)** and with **slow-stands (stillstands)** in between. They were first reported by *Fairbanks (1989)* who plotted age/depth data from cores of a reef sequence in Barbados. These sea-level jumps were truly astonishing, reaching as much as 15 m in short time, with rates of up to 60 mm yr⁻¹.

In conclusion, the last deglaciation was discontinuous, characterized by particularly sharp pulses of rapid rise alternating with periods of slow rise, but in other respects there were no reversals (*Fairbanks, 1989; Bard et al., 1990*).

There is an obvious control factor, for the magnitude and the rate of the meltwater pulses to correlate with: **the solar insolation**. Most of the changes (e.g. temperature, terrestrial fresh water input, wind-induced seawater mixing) are orbital-driven. For instance, the climatic evolution of the eastern Mediterranean region involves orbital-driven changes in humidity, where **cold and arid** conditions take turns with **warm and wetter conditions** up to the Holocene (*Tzedakis, 2004; Kuper&Kröpelin, 2006; Kotthoff et al., 2008*).

These **time gaps** between orbital-driven oscillations and meltwater pulses are most common. The slow transport of heat into the oceans and the slow ice volume response time, due to the thermal inertia of the large ice sheets, mean that long periods are required for the system to reach new climate equilibrium. The exact time delay between the deglacial oscillations and the ice sheet response depends on various factors.

The most defined of all the meltwater pulses were from when solar insolation reached its peak, demonstrating a full transition from glacial climates

to interglacial. These periods were called **terminations**. For instance, **Meltwater Pulse 1A**, one of the strongest and most rapid –glacial sea level benefactors began 14.11 ka BP, according to [Stanford et al. \(2011\)](#), precisely 500-600 years after the onset of **Bølling warming**, during **Last glacial–interglacial Termination I (MIS 2)**.

According to many researchers, these melt events even though were rather short, ranging from 10 to 10³ years ([Gornitz, 2009](#)), affected not only the sea level but also the temperature, the salinity of the oceans and subsequently the biogeochemical processes of the marine ecosystem ([Rohling&Hilgen, 1991](#); [Casford et al., 2003](#)).

For instance, during the LGM the global mean salinity was approximately 1‰ higher than today due to the lower global sea level. Especially in Mediterranean basin, in western region it was saltier by 1.9‰, while in eastern Mediterranean it was saltier by approximately 2.7‰ ([Thunell&Williams, 1989](#)) compared to today.

Regarding changes in deposition, a typical example is the formation of C_{org}-rich sediments. Episodes of increased temperature and humidity repeatedly led to the formation of sapropels (e.g. [Wehausen&Brumsack, 2000](#); [Calvert&Fontugne, 2001](#)), in deeper basins, usually with a time lag of about 3,000 years to the maxima of the northern hemisphere summer insolation. In fact, the trigger mechanism for the basin's repetitive transitions into sapropel formation is believed to be the amplification of the African summer monsoon by solar orbital forcing ([Rossignol-Strick et al., 1983](#); [Hilgen, 1991a](#); [Lourens et al., 1996](#)), during which time it is believed that monsoon freshwater runoff enhances productivity.

Timing (ka BP)	Rate of Sea Level Rise (mm/year)	Increase in level, m	Source
>19	-	10-15	<i>Yokoyama et al. (2000)</i>
19	>20	10m in <500 years	<i>Clark et al. (2004)</i>
19.6-18.8	12.5 (average)	10	<i>Hanebuth et al. (2009)</i>

Table 1. MELTWATER PULSE 1A₀

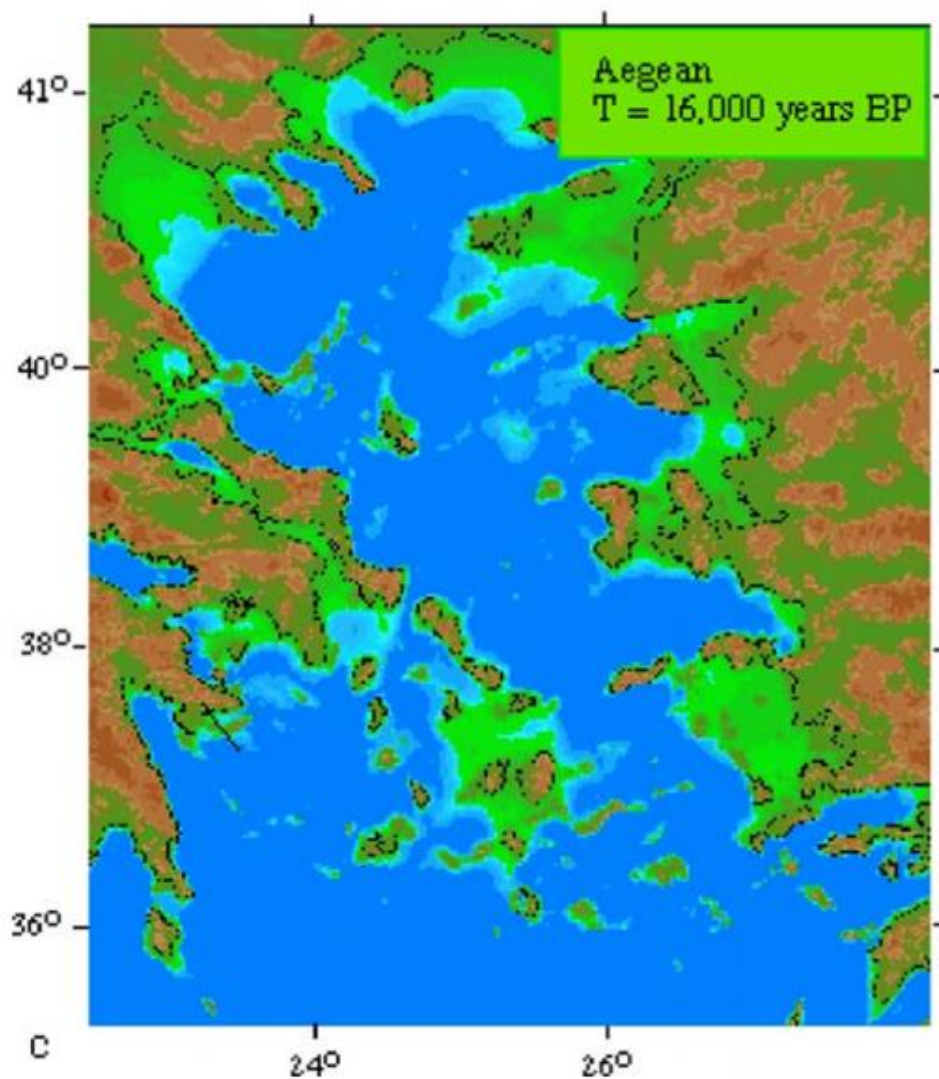


Fig. 1 Palaegeographic reconstruction of the Aegean Sea, during the slow-stand at about 16 ka BP (*Lambeck, & Chappell, 2001*)

The repetitive occurrence of deepwater sapropels, however is not the only indicator of climatic oscillations. Shallower basins in Eastern Mediterranean Sea

have also responded sensitively to orbital climate and hydrological changes too. **The precise mechanisms by which a shallow and isolate basin, such as the Megara Basin in western Saronic Gulf responds to this kind of changes, in order to reconstruct the palaeoenvironmental evolution of this setting till the end of the Quaternary is the main subject of our study**, but first we have to describe the evolution of the Eastern Mediterranean Sea by sorting out the main deglacial events that affected the region since the end of the LGM.

The first significant post-glacial upswing, even though not all sea level proxies record this event, is known as **Meltwater Pulse 1A₀ (MWP 1A₀)**. According to [Hanebuth et al. \(2009\)](#), sea level climbed at least 10 m within 800 years (12-13 mm yr⁻¹), while [Clark et al. \(2004\)](#) claim that the initial rise was even more rapid, amounting to about 15 m in perhaps 500 years (**Table 1**). Since this sudden event and up to 16 ka BP, the average increase rate of global sea level rise has been diminished significantly, reaching a point of only 3.3 mm yr⁻¹ (**Fig.1**)

As we already explained above, warming from LGM to today was not continuous. In between meltwater pulses, short intervals of relatively low SST occurred. The most common cold events during that period are the **Heinrich Stadial 1 (HS1) (Fig.2)**, that disrupts MWP 1A₀ and the Younger Dryas, which will discuss in detail later. Based on [Hemming \(2004\)](#)' results, HS1 dates at 16.8 ka BP. According to other authors, the climate responses of the eastern Mediterranean during HS1 are dated at 17.5 to 15.7 ka BP ([Grimm et al. 2015](#), [Ehrmann et al. 2007b](#), [Kotthoff et al. 2011](#)). There are various studies testifying the cold and dry affect of HS1 in low-latitudes (Gulf of Mexico: [Antonarakou et al. 2015](#); Western Mediterranean: [Cacho et al 1999](#); [Wansard et al. 2016](#)). Based on foraminiferal abundance data, these reduced surface salinities and temperatures and the increase in aridity during HS1 were also recorded in marine sediments from Aegean and Libyan Seas ([Kontakiotis, 2012](#)). Evidence of the affect the Heinrich events had on Eastern Mediterranean are rare, but not uncommon. Initially, the presence of the cold Heinrich event was suggested there, in order to explain high $\delta^{18}O$ values of speleothems in Israel. Later studies in both the SW Aegean ([Geraga et al. 2000](#)) and North Aegean ([Kotthoff et al](#)

2011) identified the impact of HS1 on the surface-water conditions in those areas, although by the time HS1 occurred the conditions were still relatively cold and dry (SST was around 15°C), therefore the HS1 event led to an additional minor decline in SST (1-3°C) in the Eastern Mediterranean region.

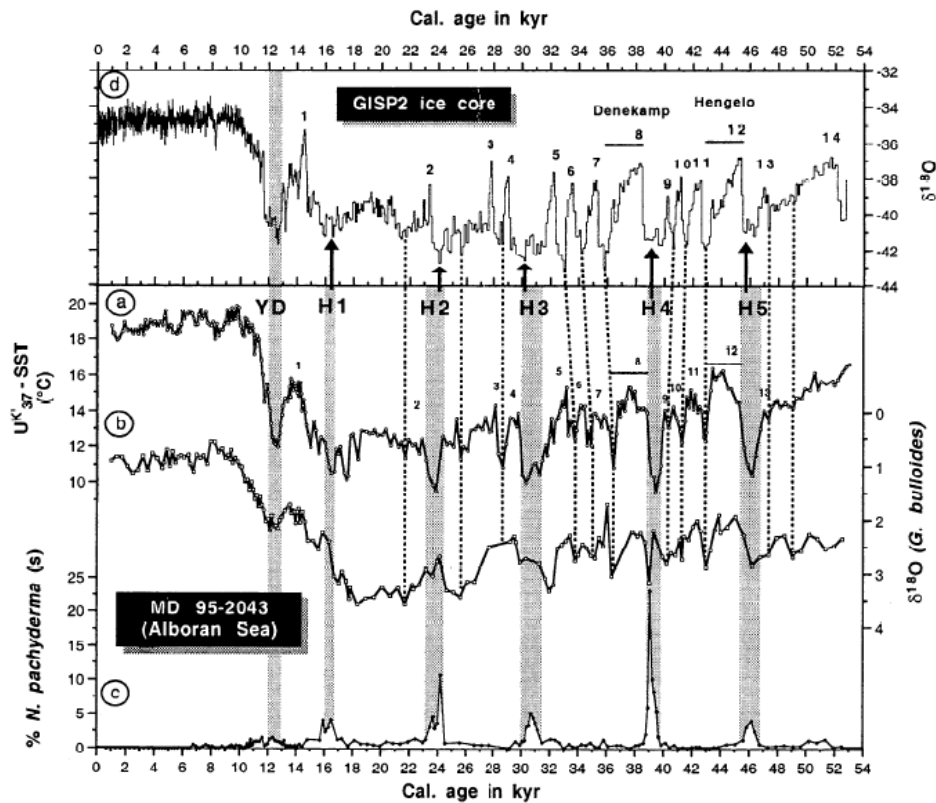


Fig. 2 (a) SST in the Alboran sea based on measurements of the relative composition of unsaturated C₃₇ alkenones, (b) δ¹⁸O in *G. bulloides* (c) Relative abundance (%) of *N. pachyderma* (s) and (d) δ¹⁸O record from an ice core. (Graph borrowed from *Cacho et al. 1999*)

Subsequently, the sea level uplift started to accelerate again, though the fastest rise is noted during the **Bølling-Allerød interstadial**. This warm interval was an abrupt event of rapid warming in the Northern Hemisphere that lasted from 14.7 to 12.9 ka BP. According to several researchers (e.g. *Stanford et al. 2011; Fairbanks. 1989; Bard et al., 1990a*) the **Meltwater pulse 1A (MWP 1A)**, closely follows the Bølling oscillation. Bølling oscillation occurred between 14.7 and 13.5 ka BP, while at 14.11 ka BP, according to *Stanford et al. (2011)*, began MWP 1A, with its peak at about 13.8 ka BP. During MWP 1A, sea level is estimated to have risen globally between 16-24 m (**Table 2**), in less than 1,000

years (*Fairbanks, 1989*) and at a rate of 26–53 mm yr⁻¹ (*Stanford et al. 2011; Hanebuth et al., 2000; Kienast et al., 2003*).

Site	Depth (m)	Adjacent Depth (m)	Magnitude (m)	Timing (ka BP)	Duration (years)	SL rise rate (mm/year)	References
Barbados	87 to 76-71	93 to 78-73	11-16	14.1-13.7	450	24-36	updated data <i>Blanchon&Shaw(1995); Toscano&Macintyre(2003); Peltier&Fairbanks(2006)</i>
Barbados	90 to 76-71	95 to 80-75	14-19	14.6-14.3	300	47-63	updated data <i>Blanchon&Shaw(1995); Toscano&Macintyre(2003); Peltier&Fairbanks(2006)</i>
Sunda Shelf	96-93 to 80		13-16	14.6-14.3	280	46-57	<i>Hanebuth et al (2000); Kienast et al. (2003)</i>
Barbados	96-76	96-76	20	14.3-14	300	65	re-evaluated data <i>Liu&Milliman (2004)</i>
Barbados			24	13	<1000	39 (max)	<i>Fairbanks (1989)</i>
Barbados				13.5		37	<i>Bard et al. (1990)</i>
				13.8-14.11		26 (max)	<i>Stanford et al. (2006); Stanford et al. (2011)</i>

Table 2. MELTWATER PULSE 1A

This high rate is one of the reasons MWP 1A is referred to as the ‘catastrophic rise event 1’ by *Blanchon&Shaw, 1995*, as most of the meltwater would correspond to massive seasonal melt-water inputs of continental ice to the oceans (i.e., ~50–40 mm y⁻¹ is roughly equivalent to an annual discharge of 16,000 km³).

In summary, in our study area, in eastern Mediterranean, large parts of the shallower Aegean seafloor were left exposed above sea level from LGM till the onset of the Bølling–Allerød period, when the sea level rise started to accelerate again. Traces of such **plateaus** in present day are only found by the form of islands today, such as the [i] **Cycladean plateau** (e.g. islands Andros, Mikonos, Paros, Tinos, Naxos and Ios), as well the [ii] **N-S oriented ridge in Saronikos Gulf** (islands Agkistri, Poros, Aegina, Salamis) that isolated the **Megara Basin** from the rest of the Aegean Sea. (**Fig. 1**)

Between the Bølling and Allerød interstadials, at about 13.5 ka BP, a cold brief event occurred, called the **Older Dryas** dropping the **Sea Surface Temperatures (SSTs)** as low as 13-14°C. According to *Liu&Milliman, 2004*

MWP 1A increased freshwater discharge to the North Atlantic enough to disturb thermohaline circulation and initiate the Older Dryas global cooling.

After that small gap, that lasted only 200 years, the Allerød oscillation raised significantly the SSTs, until the onset of the **Younger Dryas (YD)**, when the sea level rise slowed down again. YD was an extremely arid period, if not the most arid of the Late Pleistocene, as *RosignolStrick (1995)* suggested, with an average annual rainfall below 150mm (e.g. *Gvirtzman & Wieder, 2001; Bar-Matthews et al. 2003*) and distinctively cold compared to the Bølling–Allerød and the Holocene. Regarding the Mediterranean region, the Ionia Sea records a higher glacial-interglacial temperature change in comparison to Alboran Sea. For instance, SST in the Ionian Sea rose up to 21° C in the Allerød and declined again to 14°C during YD (*Emeis et al., 2000*). Generally, climate conditions during the HS1 and the YD are considered almost identical, the YD, however, occurred abruptly, interrupting a transition to much warmer and more humid conditions initiated during the Bølling/Allerød, while prior to HS1, conditions were still relatively cold. According to *Kotthoff et al. 2011*, this was the reason why mostly the YD seemed to have affected severely the marine ecosystem, with a temperature decline >6°C, whereas HS1 not as much, especially concerning foraminiferal assemblages.

On the other hand, according to several researchers, by the end of MWP 1A, at about 13 ka BP the sea level had already rose from -94 to -75m, while by the end of YD sea level stood at -58m. This 17 m rise in less than 1,000 years (YD lasted from 12.9 up to Holocene around 11.7 ka BP) is rather peculiar, considering the fact that the cold and dry YD is known for causing a temporary delay in sea level rise. The slow pace of deceleration left probably enough time for the sea level to rise even though its mean rate slowed down from 20 mm yr⁻¹ to 4 mm yr⁻¹, maintaining a stillstand up to perhaps 11.5 ka BP (*Edwards et al., 1993; Bard et al., 1996*).

Moreover, by the end of this relative stillstand in the sea rise, the exposed shelf in Eastern Mediterranean Sea was considerably diminished, Cyclades plateau was restricted to a smaller central area, most of the gulfs were already

overflowed by the advancing sea and **only few areas, where the barrier in their entrance was higher, still preserved their previous form.**

On the other hand, marine records of the YD are less conclusive, which is surprising. Even though there is an abundance of terrestrial proxies worldwide that record a clear climatic change during the YD, in Eastern Mediterranean, the marine record is not consistent with a clear climatic response. For instance, while in Western Mediterranean (e.g. [Kallel et al., 1997b;](#)) a shift towards lower SSTs and higher salinities is detected, **in the Red Sea this cooling is not accompanied by any change in salinity.**

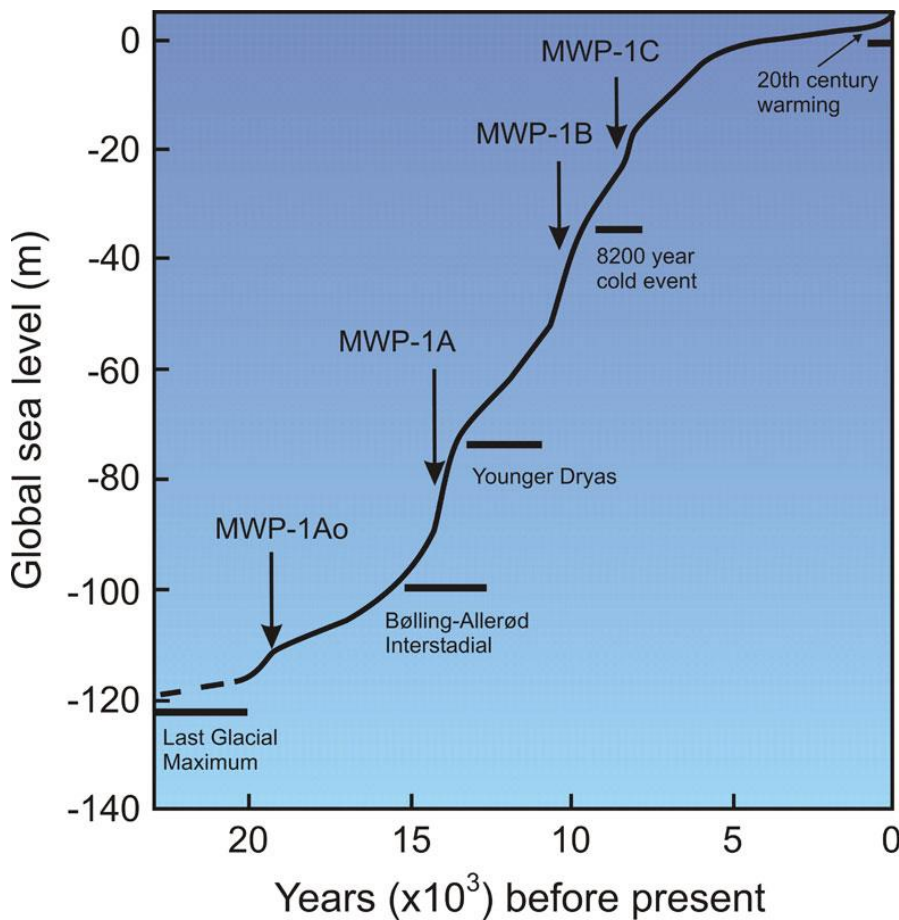


Fig. 3 Most significant deglacial events to global changes in sea level from 23 ka to the present ([Gornitz, 2009](#))

Site	Depth (m)	Adjacent Depth (m)	Magnitude (m)	Timing (ka BP)	Duration (years)	SL rise rate (mm/year)	References
Tahiti	66-59	65-59	7	11.5-11.3	215	28	recalculated from Bard et al. (1996)
Huon	32-25	53-46	7	11.1-	372	19	Edwards et al. (2003)

Pen				10.7			
				11.5		7.5	<i>Blanchon&Shaw (1995)</i>
Barbado	58-45	58-45	14 ± 2	11.5-	300	40	<i>Liu&Milliman (2004)</i>
s				11.2			
Barbado				11		25	<i>Bard et al. (1990)</i>
s							
Barbado			2	10.5		26	<i>Fairbanks (1989)</i>
s							
				10.9		19 (max)	<i>Stanford et al. (2011)</i>

Table 3. MELTWATER PULSE 1B

Finally, the YD is disrupted by a subsequent rapid North Atlantic warm event, known for introducing both the **Holocene** and the **Meltwater Pulse 1B (MWP 1B)**. The total temperature change during the transition to the ‘warm’ Holocene is estimated at about 10°C (*Emeis et al., 2003*). This rapid warm event at **Late Pleistocene-Early Holocene boundary** affected the Northern Hemisphere ice sheets significantly (e.g. *Fairbanks* estimated discharge rates of 9500 km³ yr⁻¹) with a time lag of approximately 400 years. Once however the warmth returned, rates of significantly rapid sea level rise are recorded e.g. 40 mm yr⁻¹, according to *Liu&Milliman (2004)*, who suggested that between 11.45 ka BP and 11.1 ka BP, in less than 300 years, sea level rose about 14 ±2m, from -58 to -45m (**Table 3**). According to *Lambeck and Chappell (2001)*, after applying a 5 m correction for isostatic uplift in Greece, in Amvrakikos gulf sea level reached 60 m at about 11.5 ka BP and 49 m at 10.6 ka BP.

Since then, there is considerable unresolved disagreement over the magnitude of the MWP 1B, as most of the data indicate a particularly decrease of sea-level rise (*Fairbanks, 1989; Bard et al. 2010; Stanford et al. 2011*) therefore for the rest of the post-Younger Dryas period, till about 8.8 ka BP, rates of sea-level rise averaged between 25 and 15.2 mm yr⁻¹. By the end of MWP 1B the sea level did not exceed -20m.

During the **Holocene Climate Optimum (HCO)**, which is estimated between 9 ka BP and 5 ka BP, global sea level exceeded the current sea level followed by a nearly uniform drop afterwards. This maximum Holocene highstand is evident in various sites, some of them recording a highstand of 1-2 m above the present

level, others 2.5 to 4 m higher. Temperatures were also 1-2° warmer than present (**Fig. 4**), SSTs reaching 16-19°C in Mediterranean basin (SSTs were constantly 2-3°C higher in eastern basins) (*Emeis et al., 2000*). This was called the **Holocene Transgression**. The high temperatures and the rise of the sea level above its current position during the Early to Mid-Holocene are of course consistent with higher insolation. Furthermore, the Northern Hemisphere monsoons had been intensified, due to the more humid climate over most of NE Africa (*Jolly et al., 1998*), resulting to an increased discharge of freshwater from the Nile into Eastern Mediterranean (*Rossignol-Strick, 1985; Rohling et al., 2002*) affecting therefore both thermohaline circulation and bottom-water oxygen and finally creating **Sapropel S₁** till 6.5 ka BP (*e.g. De Rijk et al., 1999; De Lange et al., 2008*)

However, both HCO and S₁ deposition were disrupted by a cold event, the **8.2 ka BP cooling** in North Atlantic (*Beget, 1983*) with characteristically lower SSTs and intensified storm activity (*e.g. Clarke&Rendell, 2009*) therefore causing another stillstand. This 8.2 ka BP cold event was a significant exception to general trends of the Holocene climatic optimum. It resulted from the catastrophic drainage of glacial lakes Agassiz and Ojibway around 8.47 ka BP. According to, however, many climate records, this abrupt event did not influenced on a local rather on a global level, probably because of the solar insolation decrease around 8.4-8.0 ka that enhanced this cold event. Indeed, the climatic conditions in middle and high latitudes in western Europe, east Asia, central America, Africa and Arabia were recorded cold and arid. Only in Eastern Europe and basically in the Mediterranean Basin (*Rohling et al., 2002; Triantaphyllou et al., 2009a, b*) the climate seemed to be a bit more humid, probably due to westerly wind changes and monsoon weakening. the responses of regional climate to the 8.2 ka BP event differed.

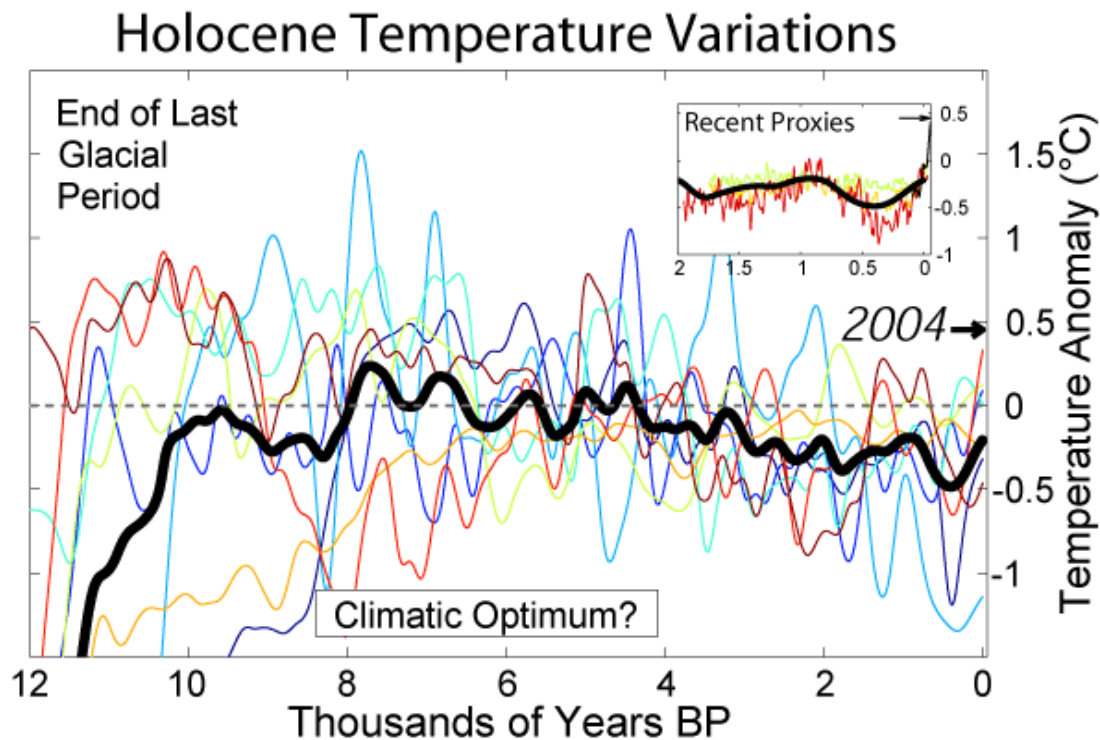


Fig. 4 Holocene Temperature Variations interpreted by ice cores, sediment cores and pollen analysis by [Robert A. Rohde](#) (dark blue: SST from Eastern Tropical Atlantic: [Zhao et al., 1995](#) blue: paleotemperature from Central Antarctica: [Petit et al., 1999](#) light blue: paleotemperature from Greenland: [Alley et al., 2000](#) green: SST from Kilimanjaro in Eastern Central Africa: [Thompson et al., 2002](#) yellow: SST from North Atlantic: [Lea et al., 2003](#), orange: Pollen distributions, interpreted temperature, Europe: [Davis et al., 2003](#), red: SST obtained from ice core from Central Antarctica: [EPICA community members, 2004](#)), dark red: SST from Western Tropical Pacific: [Stott et al., 2004](#)).

For instance, paleoceanographic data from the Aegean suggests that short cooling events during the Holocene, such as this might be associated with intense northerly winds superimposed on the tropical/sub-tropical influence on the regional hydrography and ecosystems ([Rohling et al., 2002b](#); [Casford et al., 2003](#); [Gogou et al., 2007](#)). These findings suggest that the NE Mediterranean climate was more variable during the last climate cycle than generally believed.

A

In the Eastern Mediterranean, this cold dry event has also left archaeological imprints, in many locations such as the Cyclops' Cave in the Northern Sporades, the Theopetra Cave in Thessaly, Sidari in Corfu island ([Berger&Guilaine, 2009](#)) and in a Neolithic age settlement near Knossos, in Crete ([Efstratiou et al., 2004](#))

Site	Depth (m)	Adjacent Depth (m)	Magnitude (m)	Timing (ka BP)	Duration (years)	SL rise rate (mm/year)	References
Caribbean	18 to 13-9	18 to 13-9	5-9	8-7.6	400	13-23	updated data <i>Toscano&MAcintyre(2003)</i> ; <i>Peltier&Fairbanks(2006)</i>
Caribbean			6.5	7.6			<i>Blanchon&Shaw (1995)</i>
	11	11		8.26-7.68	580	34-44	<i>Tooley (1989)</i>
Mississippi Delta			1.2	8-8.17 to 8.25-8.42		4.9 (average)	<i>Tornqvist et al. (2004)</i>
Chesapeake Bay, USA			6	7.6-8.2	<500	12	<i>Cronin et al. (2007)</i>
Swedish Baltic Sea	3.0 to 7.2	3.0 to 7.2	4.5	7.6		10	<i>Yu et al. (2007)</i>

Table 4. MELTWATER PULSE 1C

According to discoveries of drowned reefs from Caribbean, Grand Cayman, Florida and the Gulf of Carpentaria in Australia (*Blanchon et al., 2002, Banks et al., 2007, Harris et al., 2008*), the onset of the 8.2 cold event is closely followed by a relatively minor meltwater pulse, **the Meltwater Pulse 1C (MWP 1C)**, which lasted until 7.6 ka BP (*Tornqvist et al. 2004; Blanchon&Shaw, 1995; Barber et al., 1999; Carlson et al., 2008*). When lakes Ojibway and Agassiz suddenly drained into Atlantic Ocean, a massive torrent of around 100,000 km³ was unleashed lifting the global sea level. Sea level rose 5 to 9 m with a mean rate of 40mm yr⁻¹ (*Blanchon&Shaw, 1995; Cronin et al. 2007*) and in less than 580 years (*Tooley, 1989*) the sea level reached -11 m (**Table 4**). Most of the glacial melting ended around 7-6 ka BP when sea surface almost approached present-day levels. However, Antarctic deglaciation did not cease at 6 ka BP but continued slowly since then, adding a further 2-3 m to the equivalent sea level rise till 3 ka BP (*Nakada&Lambeck, 1989; Lambeck, 2002*). So by that time sea level rose up to -3 m. Late Holocene sea-level rise has a rather small magnitude (< 1 m) occurring between about 4 to 2 ka BP, therefore is more

distinctive by the unloading of the crust in sites with ice sheets rather than by the loading of the meltwater.

Also, there are significant differences between the Holocene high-stand amplitudes as presented in bays and gulfs and as presented in open coastlines. For instance, in Western Saronic, according to geomorphological (e.g. submerged tidal notches incised on the carbonate basement and beachrocks formed in the intertidal zone) and archaeological indicators, such as the ancient harbor in Kechries, Epidaurus and on Aegina island, as well the extended coastal buildings and constructions in Agios Vlassis, Psifta and Palaiokastro-Methana, and Vagionia on Poros island (*Kolaiti et al., 2015*) prior to the latest sea transgression that led to the modern sea level in West Saronic, there was a long period of sea level stability. This stillstand lasted at least 2,200 years, from the Middle Bronze Age to the Late Roman period which means that by that time sea level remained at -3m.

CHAPTER 2. Geodynamic Setting

During the Late Plio–Pleistocene, two WNW–ESE striking, large-scale extensional fault zones crosscut mainland Greece which gradually bend eastward into a NNW–SSE direction. The one in the north resulted to the Gulf of Amvrakikos that was connected with the Sperchios half-graben and the Evoikos Gulf (*Mariolakos 1976; Clews 1989; Poulimenos&Doutsos 1996; Kranis&Papanikolaou 2001; Goldsworthy et al. 2002*). The other in the south, on the other hand, was the fault zone that was responsible for the formation of the Gulf of Corinth (*Doutsos&Piper 1990; Armijo et al. 1996; Sorel 2000*), which was connected in the east through the Isthmus of Corinth with Saronikos Gulf. Particularly, the Isthmus of Corinth and Saronikos Gulf were already subjected to extension since the Early Pliocene (*Collier and Dart 1991; Van Hinsbergen et al. 2004; 2006*).

This Basin probably originated as a Tertiary detachment that has been reactivated since Late Miocene- Early Pliocene with a slight anticlockwise rotation towards a NNE–SSW strike (*Dietrich et al., 1993*).

In general, the basin of Saronikos Gulf is a highly complex neotectonic basin, representing both the northwestern edge of the modern Hellenic Volcanic Arc (*Makris et al, 2004; Papanikolaou et al, 1988; Dietrich et al, 1993*), as well the tectonic boundary that separates the Cycladic blueschist belt to the southeast from the Paleozoic to Mesozoic platform carbonates of the Sub-Pelagonian Zone to the west.

Region	Basin	Orientation	Depth	Geodynamic setting	Maximum thickness	Mean Rate of Sedimentation
SW	Epidauros	WNW-ESE	>400m Deep basin	WNW-ESE marginal faults with big throw	250-500m	5cm to 10 cm /1,000 years
NW	Megara	E-W	<250m Shallow basin		>500m	10cm/ 1,000years
SE	South-Eastern basin	WNW-ESE	Shallow Horsts and grabens	E-W, ENE-WSW to N-S faults with small throw		
Centre	Central ridge	N-S	graben	NNE-SSW faults		5cm /1,000 years

Table 5. Saronic Gulf

The neotectonic extensional regime of the area is connected with the thinning of the crust to 20 km in the basin of Saronikos (*Kolaiti et al. 2016; Drakatos et al, 2005*) and the Plio-Quaternary volcanic arc activity, which is distinguished into two major phases (*Pe, 1973, Pe-Piper et al, 1983, Dietrich et al, 1988, Dietrich et al, 1993, Seymour, 1996 and Morris, 2000*). The first phase is represented by the Pliocenic volcanic outcrops of the Loutraki-Sousaki area, Aegina and south of Poros island (*Fytikas et al, 1986*), while the volcanic centre in the peninsula of Methana belongs to the second phase of Pleistocene

([Gaitanakis&Dietrich, 1995](#); [Fytikas et al., 1986](#)). The most recent volcanic activity is dated in 230 BC at the NW side of the peninsula of Methana and was described by Strabo ([Makris et. al, 2004](#); [Stothers&Rampino, 1983](#)).

Saronikos Gulf is a neotectonic basin, divided by a very shallow north-south-oriented platform into a western and an eastern part. So, accordingly there are three well -defined regions:

The southeastern basin that includes Plio-Pleistocene volcanics that correspond to the northwest end of the active South Aegean Volcanic Arc. A detailed seismostratigraphy by [Anastasakis et al. 2006](#) underlines the resemblance of the volcanic outcrops in the area with those near Milos ([Anastasakis&Piper, 2005](#)). The seafloor of the southeast Saronic Gulf has generally smoother topography having northwest-southeast faults of relatively small throws with an alternation of horsts and grabens oriented WNW-ESE ([Papanikolaou et al., 1988](#)).

A N-S oriented submarine plateau (Salamis basin or palaeolake of Kifissos), located in the centre of the Basin, which is distinctively flat and shallow (**Fig. 6**), rising well above the level of the ambient seabed. The margins of this underwater ridge are located between -100 and -130m, while its mean depth is between -70 to -80 meters and even has parts that emerge above the current sea-level, shaping into the islands Agkistri, Poros, Aegina, Salamis and the peninsula of Methana. According to [Foutrakis, 2016 \(Fig.5\)](#) the connection between Salamis basin and Megara Basin, in the northwest, would be at -92 m, while the lowest point for the seawater to enter from the East would be at -80-82m. [Drakatos et al., 2005](#) attributes the occurrence of this ridge, separating the western part from the southeastern Saronikos, to the existence of a rupture zone, with a fault throw >400m that trends NNE-SSW, which seems to be the offshore extension of a large thrust belt on the adjacent onshore areas.

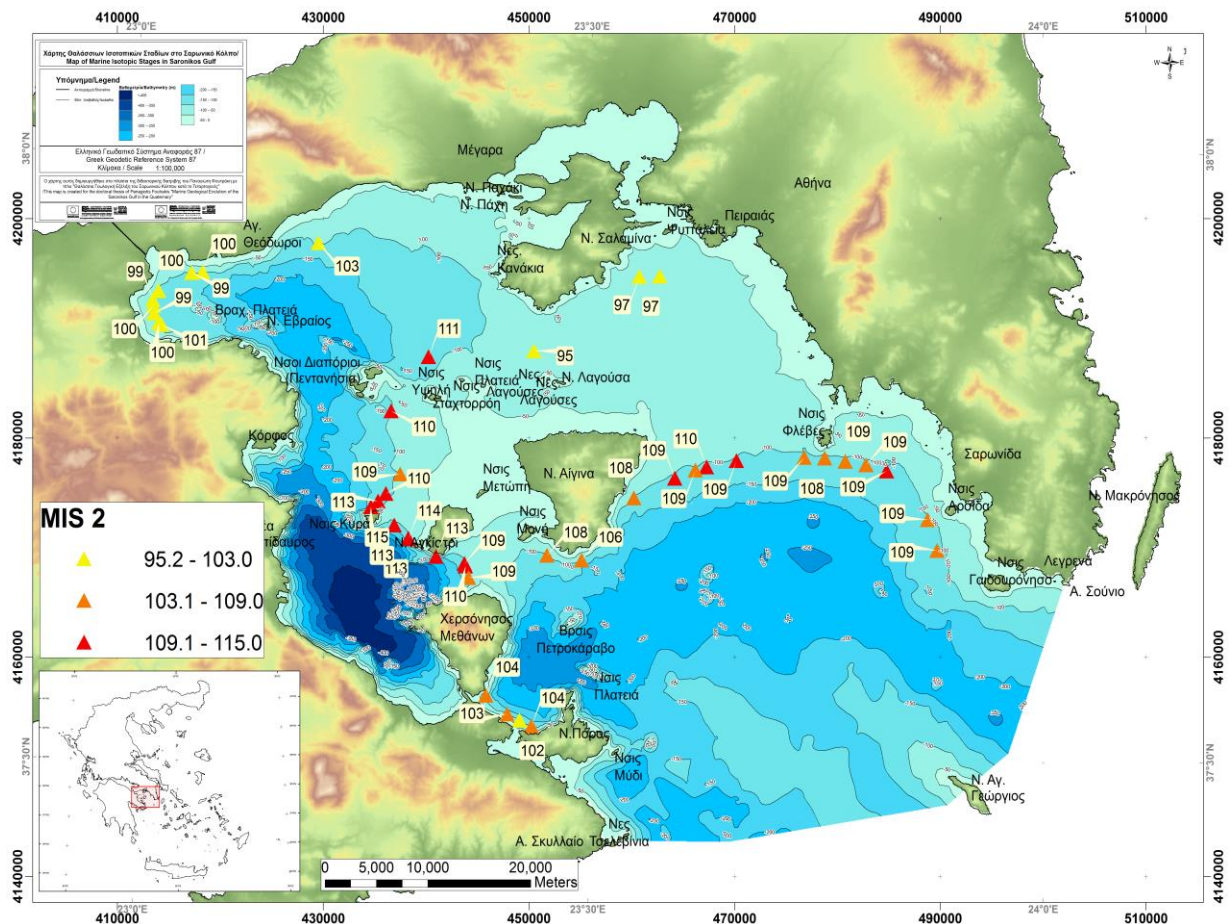


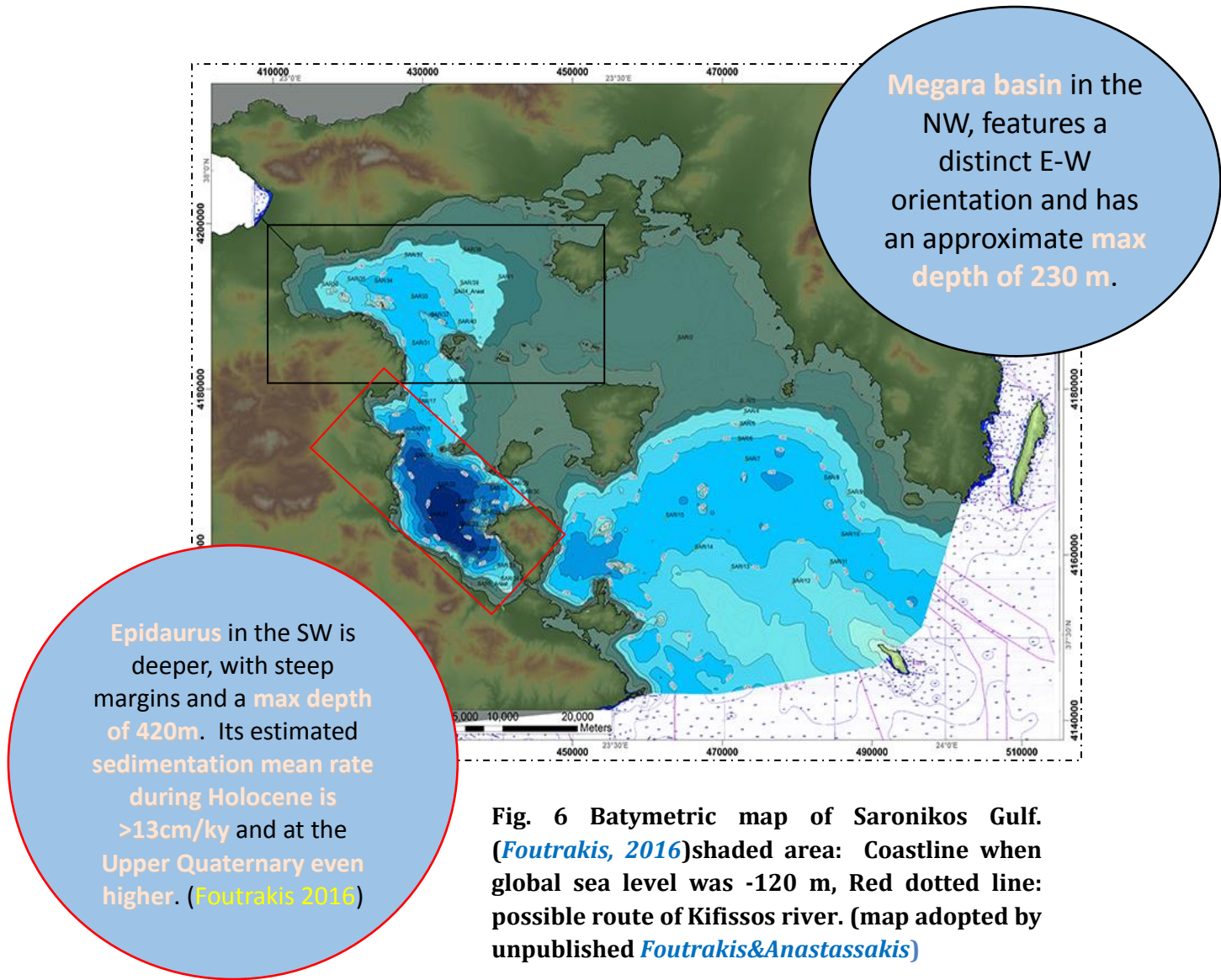
Fig. 5 Sea levels based on clinofoms (*Foutrakis, 2016*)

This plateau is also referred in literature as the palaeolake of Kifissos, due to the fact that the neotectonic activity during early-middle Pleistocene led to the formation of the Kifissos river. Kifissos is a river that flows through the Athens plain and discharges today in eastern Saronic, with its mouth located today in the Faliro Bay. Since Middle Pleistocene the Athens Plain is very similar to its present form and Kifissos river is still the main fluvial system of the hydrological basin of Athens. However when global sea level stood at -120m, the drainage network of Kifissos river extended above the emerging N-S ridge of Saronikos Gulf and there are contradictive theories regarding the old position of its mouth(**Fig. 7**)

The western part of the Gulf consists of two distinct basins:

the Megara basin in the north, featuring a distinct E-W orientation and is determined by a series of active E-W, ENE-WSW to N-S fault zones, with an approximate maximum depth of 230 m ([Makris et al, 2004](#)), smooth angles (>4%) and a maximum thickness of quaternary deposits that exceeds 500m. Finally, regarding the isostatic effects in western Saronic, according to a set of three uplifted marine cliffs, with the highest containing dated corals at 25-35 m, and of a raised biogenic notch at 2 m, the upper Pleistocene to Holocene uplift rate of the Megara Basin is estimated at about 0.3 mm yr⁻¹, as the whole basin is being uplifted and tilted south-eastwards on top of the footwall of the active major normal fault that bounds the southeastern margin of the Alkyonides Gulf, offshore of Alepohori ([Collier et al. 1992](#))

b) the deeper southwestern basin of Epidauros, that is oriented WNW-ESE, with sharp steep margins and a maximum depth of approximately 420m. The maximum thickness of the quaternary deposits is between 250 and 500m, therefore the sedimentation mean velocities during this period was believed to be at about 5 to 10 cm/1,000 years in the Epidauros basin ([Papanikolaou et al. 1988](#)), while recent studies supported that the estimated sedimentation mean rate in Epidauros basin, during Holocene is >13cm/ky and at the Upper Quaternary was even higher. ([Foutrakis 2016](#))



Also the WNW–ESE marginal extensional faults at the southwestern margin of Epidaurus Basin have a throw of approximately 350 m, therefore forming a rather symmetric tectonic graben with significant volcanic outcrops within the eastern region of the basin. (Papanikolaou et al., 1988 and Drakatos et al., 2005).

Even though Epidaurus and Megara Basin differ significantly, especially regarding their depth, they share a common history. As we mentioned before, Saronikos Gulf was well affected by the sea level changes since LGM. It is known, based on the isobaths, that the N-S submarine plateau, in the center of Saronikos Gulf, that represents a great part of the gulf, was once exposed, with Aegina and Salamina Island to be connected with the land (Mariolakos& Theocharis, 2001). This plateau for a long time represented a shallow barrier between

western Saronikos and open sea. It behaved as a sill, isolating western Saronikos Gulf and both Megara and Epidaurus basins were palaeolakes, while at the same time this sill was a bridge of land that

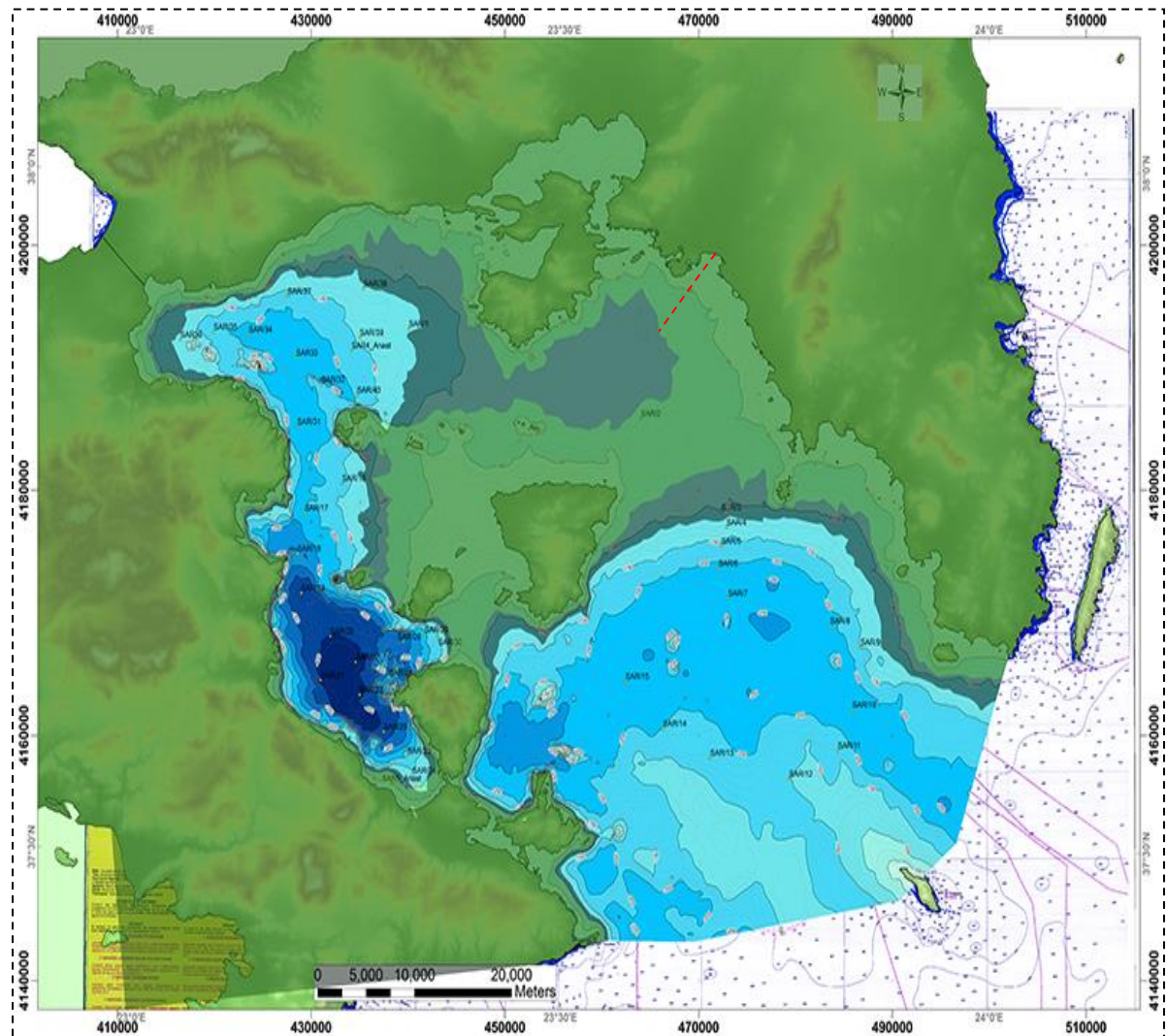


Fig. 7 Megara Basin remains isolated. Coastline when global sea level was -90 m, Red dotted line: possible route of Kifissos river. (map modified: adopted by [Foutrakis, 2016](#))

,connected Attica and Peloponnesus. (Fig. 6). Furthermore Epidaurus and Megara Basin were always connected. This means that by the time sea level rose enough, the most direct route for the seawater to enter Epidaurus Basin was through the Megara Basin, since the lowest point for the sea to reconnect with western Saronikos would be through Salamina-Aegina strait at -92m.

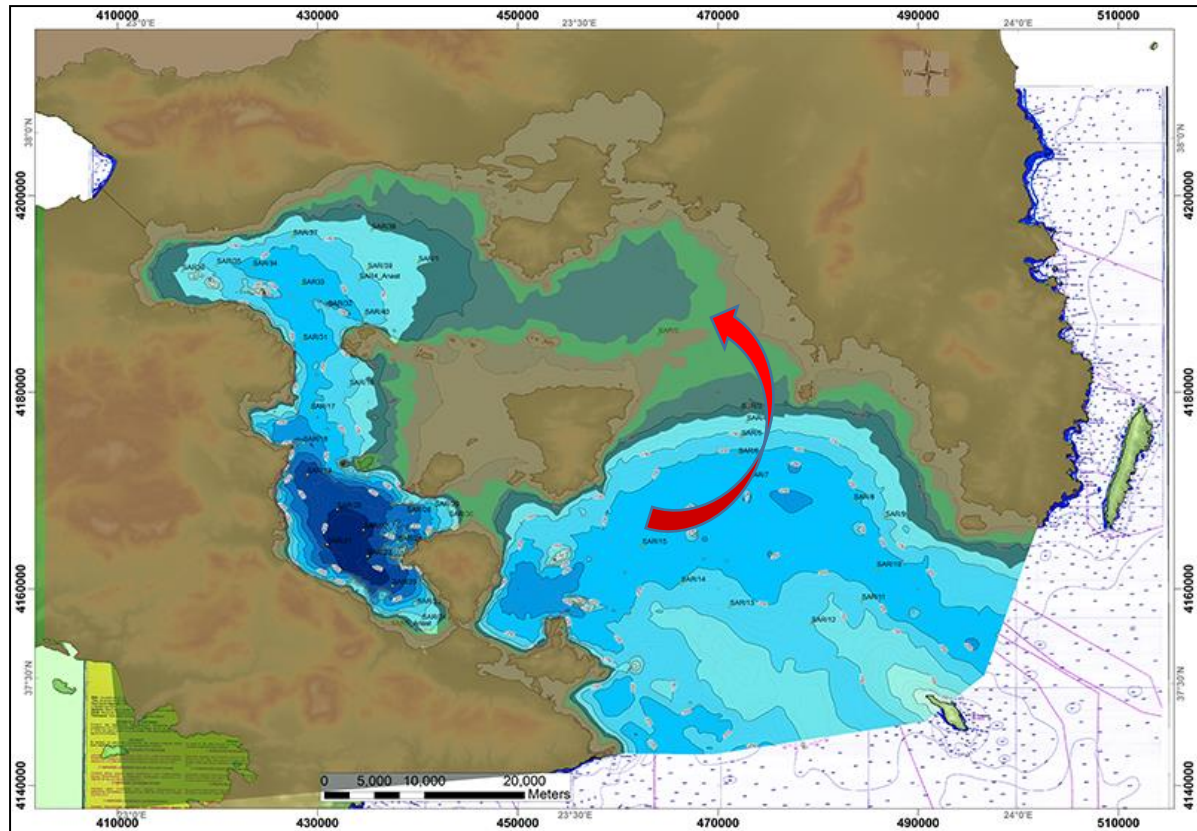


Fig. 8 Shaded area: Coastline when global sea level was -75 m (map modified: adopted by [Foutrakis, 2016](#))

Conclusively, this might mean that by the time the sea level stood at -92m western Saronikos would progressively reconnect with the open sea, but again based on the isobaths this might not be the case, since the lowest point for the water to enter Salamis Basin would be at -80-82m. This complex system of the three basins connected to each other, that obliges the seawater to follow a specific path (**Fig.8**) in order to reach the western Saronikos, indicates that reconnection with Eastern Mediterranean might in fact had been established much later, than supposed.

On the other hand, [Lycousis et al. 1993](#) support the claim that the reconnection with the open sea was established earlier, before 14 ka BP. This claim is based on the absence of aragonite coupled with sand phases recorded in the cores that were retrieved from the shallower depths representing a rise of the sea and the presence of *Mytilus galoprovincialis* (typical of 30m depth) in the interval of 110-140m within one core. Another proof for the reconnection of

Saronikos Gulf with the open sea is formation of a sapropel layer within one of the cores he collected.

CHAPTER 3. Carbonate Chemistry

Calcium carbonate polymorphs are widespread minerals throughout nature, occurring either as the main constituents of sedimentary rocks or as inorganic components in the skeletons and tissues of many mineralizing organisms, mainly marine invertebrates of various phyla.

Aragonite is one of the most common calcium carbonate crystalline phases in natural systems, usually of biogenic origin, as many mineralizing organisms selectively produce aragonite, via the process of biomineralization, but it also precipitates inorganically from seawater by favorable chemical abiotic processes ([Flügel, 2004](#)).

In many sedimentary environments aragonite is precipitated rather than calcite. However, **calcite** is considered to be the most abundant carbonate mineral, as the appearance and persistence of aragonite are highly sensitive to ambient conditions therefore it is expected for aragonite to eventually revert to the more stable calcite, which has the same chemical formula but different crystal structure.

It is common for aragonite to be riddled with strontium and barium atoms. Apart from Sr^{2+} and Ba^{+2} , some SO_4^{2-} sulfate ions can replace the carbonate ions too. On the other hand, calcite's structure usually accommodates substitution of Mg^{2+} for Ca^{2+} . Depending on Mg^{2+} content, calcite ranges between **high-Mg calcite** (>4 mol%) in marine environments, coupled with aragonite very often, and **low-Mg calcite** in meteoric water.

Furthermore, the factors that determine whether aragonite or high -Mg calcite will precipitate are less clearly defined. Kinetically aragonite is favored over high-Mg calcite in shallow waters when **i) seawater Mg^{2+} and SO_4^{2-} contents are relatively higher than usual** (both ions act as **kinetic inhibitors**

and serve to delay the growth of calcite) **ii) at lower PO_4^{3-} concentrations, and c) with increasing temperature.**

Thus, the processes leading to the formation and preservation of calcium carbonate polymorphs in natural environments have been of considerable interest among researchers, while many of them still debate about the origin and control factors of carbonate mineral precipitation, mostly regarding aragonite mud.

Control factors

For a long time scientists debated about the factors controlling the precipitation of calcium carbonate minerals in natural environments, as well for the role of Mg^{2+} ion into calcite. For instance, a novel experimental approach showed that calcium carbonate mineralogy and textural differences between calcium carbonate mineral phases depend highly on the presence of sulfate and magnesium ions, as well on the Mg:Ca ratio in solution composition and the saturation state (Ω) with respect to CaCO_3 . There are of course many other factors that affect inorganic precipitation of calcium carbonate from seawater, such as terrigenous input, salinity and carbon dioxide levels (pCO_2). Two of the most likely controlling variables on the compositions of recent marine carbonate cements are concerned to be by most the temperature and the degree of carbonate mineral supersaturation (CO_3^{2-} ion concentration) of seawater.

Nevertheless, all of these factors influence the polymorph mineralogy of CaCO_3 and the inorganic precipitation from seawater-based solutions (*Bischoff & Fyfe, 1968; Walter, 1986; Burton & Walter, 1991; Tucker et al., 1992; Morse et al., 1997; Ries et al., 2008*) and will be examined.

3.1 PRESENCE OF IONS

Sulfate (SO_4^{2-}) in solution

Holds back precipitation of both calcite and aragonite due to surface adsorption. However inhibition is greater for calcite than for aragonite,

according to [Walter, 1986](#) therefore if seawater is rich in sulfate, then it tends to favor precipitation of aragonite.

Phosphate (PO_4^{2-}) in solution

Discourage precipitation of both calcite and aragonite and even though inhibition is greater for aragonite than for calcite ([Walter, 1986](#)) usually phosphate is consumed in seawater by organisms that photosynthesize, therefore small proportions make it irrelevant in seawater.

Mg^{2+} in solution

Prevents precipitation of calcite at concentrations as low as 5% of those in seawater ([Bernier, 1975](#)), via adsorption of hydrated Mg^{2+} on calcite surface, while it has no effect on aragonite, therefore much Mg^{2+} in modern seawater favors precipitation of aragonite. Mg component will be discussed further.

Fe^{2+} and Mn^{2+} in solution

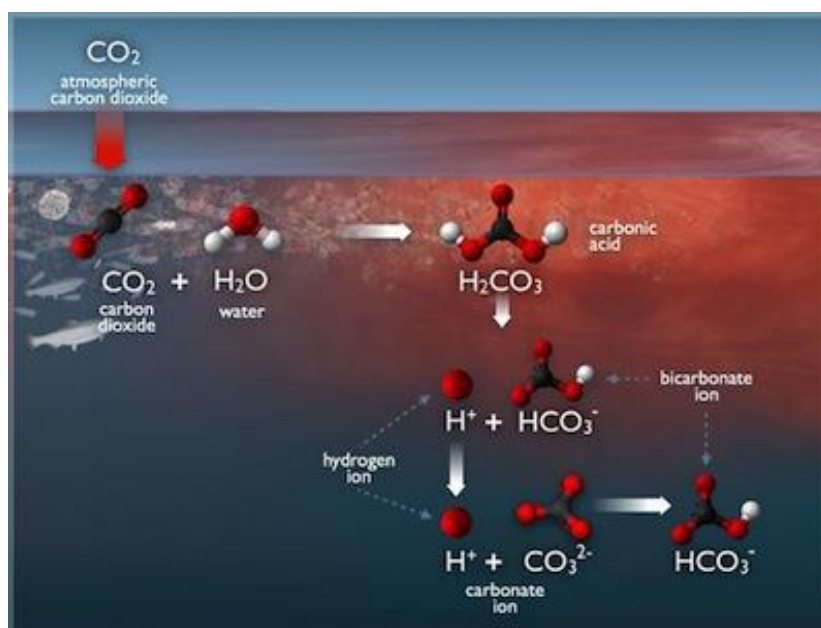


Fig. 9 CO_2 exchange and the chemical reactions of the dissolved CO_2 with the other solutes

The presence of Fe^{2+} and Mn^{2+} into the solution tends to slow down the carbonate precipitation rate ([Meyer, 1984; Dromgoole and Walter, 1990a, b](#)). Both Fe^{2+} and Mn^{2+} are sensitive to the oxidation state. Especially Fe^{2+} has proven experimentally to oxidize to Fe^{3+} rapidly in alkaline solutions even in the

presence of very low concentrations of O₂ (anoxic waters) , while both elements can be oxidized by UV radiation.

3.2 PARTIAL PRESSURE OF CARBON DIOXIDE (pCO₂)

Partial pressure of carbon dioxide, pCO₂, determines the world’s oceans readily exchange of CO₂ with the atmosphere. pCO₂ defines to what extent atmospheric CO₂ dissolves into water and the chemical reactions of the dissolved CO₂ with the other solutes. Carbonate ions (CO₃²⁻) represent one of the three forms in which carbon dioxide occurs in sea water. The other two forms are **bicarbonate ions (HCO₃⁻)** and **carbonic acid (H₂CO₃)** (Fig. 9). Furthermore, DIC (Dissolved inorganic carbon) is a key parameter when making measurements related to the pH of natural aqueous systems. CO₂ concentrations increase in seawater when CO₂ concentrations in atmosphere increase and more CO₂ is absorbed from sea surface (Table 6)

Production of CO ₂	Consumption of CO ₂
decomposition of organic matter	photosynthesis
precipitation of Calcium Carbonate	Dissolution of calcium carbonate
Low water temperature	High water temperature

Table 6. Production/ Consumption of CO₂

Due to decomposition of organic matter. Water column pCO₂ measurements provide a relative measure of the **trophic status** as there is a delicate balance between CO₂ production (during decomposition) and CO₂ consumption (by **photosynthesis**). Photosynthesis is mostly confined to the surface waters of the ocean (< 200 m or so) where sunlight reaches. Below that depth falling organic matter gets decomposed by bacteria, resulting to the production of CO₂. Moreover the seasonal variation of photosynthetic capacity affects both pCO₂ and the pH of seawater, accordingly.

Due to precipitation of Calcium Carbonate



The opposite reaction would be of course dissolution:



When water temperature decreases (*Copin-Montegut, 1988*). Additionally when the water temperature increases, there is a tendency for CO₂ to be released back into the atmosphere

pCO₂ vs. Mg:Ca

When pCO₂ levels are low, aragonite and high-Mg calcite are supposed to be favored, while, as pCO₂ increases, Mg²⁺ content decreases, therefore promoting calcite to precipitate instead, until it reaches a point where aragonite does not precipitate at all (*Tucker et al., 1992*). Besides, it is widely known that during Phanerozoic relatively low levels of atmospheric pCO₂ have produced “**aragonite seas**,” whereas relatively high levels were responsible for “**calcite seas**” (*Wilkinson and Algeo, 1989; Mackenzie and Morse, 1992*).

On the other hand, *Burton&Walter, 1991's* experiments showed contradicting results. According to them in present-day seawater, (Mg:Ca mole ratio = 5.17), variations in temperature from 5 to 45 °C, coupled with changes in pCO₂ from 10⁻¹ to 10^{-4.5} atm, produce Mg-calcite compositions ranging from 6 to 18 mol% MgCO₃. However, even though pCO₂ is unquestionably a significant influence on the MgCO₃ content of precipitated calcite from seawater, it cannot dictate whether calcite or aragonite precipitates from seawater.

Leeder, 2011 also supported this theory. He too suggested that changing pCO₂ (for fixed degrees of supersaturation) has little effect upon the rate of calcite or aragonite precipitation, while *Plummer et al., 1988* proved that pCO₂ is not as viable control as many think. For instance, in present-day seawater (S = 35 ppm, 1 atm, at 25°C, normal alkalinity), the boundary for aragonite-calcite transition is between of 2,600 and 3,500 ppm (*Morse et al., 1997*), meaning that only for a narrow range of pCO₂, seawater will become undersaturated with respect to aragonite and at the same time supersaturated with respect to calcite, but in order to happen that such high levels of pCO₂ would probably cause the

dissolution of the aragonitic shells of the organisms immediately after their secretion.

Calcite and aragonite precipitation is kinetically inhibited by numerous dissolved ions. Chief amongst these ions is Mg^{2+} . Concerning Mg^{2+} ions, their dissolved presence in supersaturated seawater favors the precipitation of $CaCO_3$ as aragonite instead of calcite (*Deleuze et al. 1997*). Specifically, dissolved Mg^{2+} tends to severely hold back calcite precipitation, while aragonite remains unaffected. Furthermore, *Berner (1975)* found that only calcite crystallization is inhibited by dissolved Mg^{2+} , while variable studies (*Reddy&Wang, 1980; Mucci&Morse, 1983b*) have proven that calcite growth rate decreases with increasing dissolved Mg concentration. Therefore, it has long been recognized that changes in the Mg:Ca ratio of seawater cause low-magnesium calcite to precipitate instead of aragonite and vice versa. Both the data for natural saline lakes (*Müller et al., 1972*) and experimental results support this relationship (*Füchtbauer&Hardie, 1976, 1980*). Based on the nucleation fields that were determined experimentally, at 25 °C, modern low-latitude shallow seas have a molar Mg:Ca ratio of 5.2, therefore aragonite and high-Mg calcite are the precipitates (*Tucker et al., 1992*), even though only aragonite is usually preferred to nucleate. Concurrent nucleation of calcite and aragonite occurs for a broad span of supersaturations near Mg:Ca= 2, for modern seawater ionic strength and atmospheric pCO_2 , meaning that Mg:Ca around 2 is basically the boundary between calcite precipitation field from the aragonite ± high-Mg calcite precipitation field (**Fig. 11,12**). For instance, near surface meteoric water has a molar Mg:Ca ratio of 0.5 and so low-Mg calcite is the normal precipitate there.

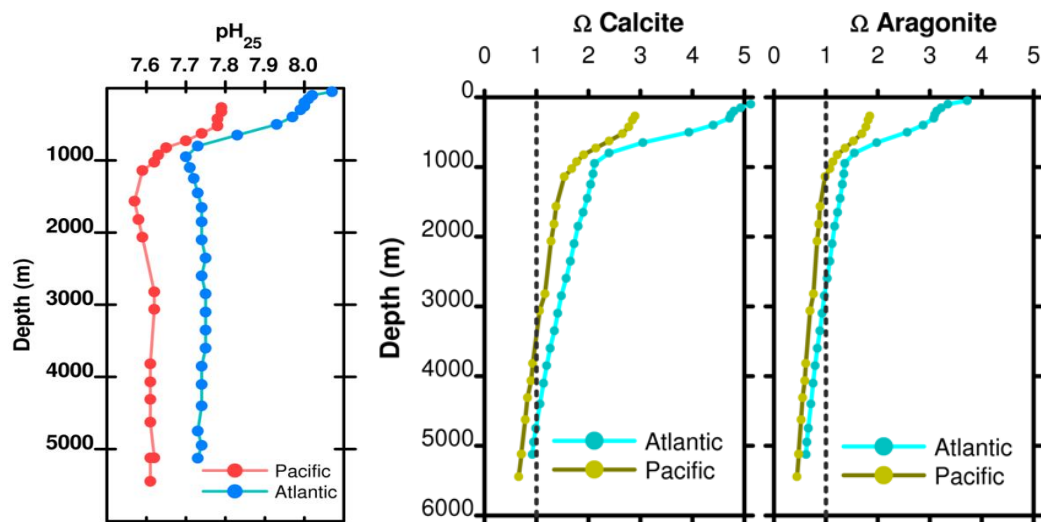


Fig. 10 (left) pH (at 25 deg C) as a function of depth in the Atlantic and Pacific oceans. (right) Depth profile of Ω for calcite and aragonite as a function of ocean basin. Also the depth at which the dotted line crosses the $\Omega=1$ gives the depth below which aragonite and calcite dissolve

Mg:Ca ratio vs. Saturation State: 12 mole% $MgCO_3$ has a similar stability to aragonite while calcite solubility increases with increasing Mg^{2+} content. So, with increasing solution Mg:Ca ratio (e.g. increased incorporation of Mg^{2+} in the calcite lattice), progressively higher degree of supersaturation is demanded for calcite to precipitate, as calcite growth rates decrease while aragonite growth rates stay constant, therefore the latter becomes the dominant mineral phase in environments with high Mg:Ca ratio (e.g. saline water) and low supersaturations. Furthermore, *V De Choudens-Sánchez et al., 2009* proved experimentally that despite decreased calcite growth rate, the percentage of $MgCO_3$ in calcite increases with increasing solution Mg:Ca ratio.

Mg:Ca ratio vs. Temperature: The transition between the aragonite and the calcite + aragonite precipitation fields is controlled by the Mg:Ca ratio at which the $CaCO_3$ polymorph has precipitated from seawater, but as a function of temperature. Experimental data indicate a dramatic change in the critical Mg:Ca ratio over a relatively small temperature range. For example, in normal seawater with a Mg:Ca ratio of 5:1, the critical temperature is 6 ± 3 °C, meaning that aragonite forms at temperatures higher than 6°C, while calcites precipitate at temperatures <6°C, under the same conditions. At a temperature of 25 °C,

however, Mg:Ca must be less than $1:4 \pm 0.1$ for calcite to form, meaning that the warmer the conditions the more difficult for calcite to precipitate. (*Morse et al., 1997*) Regarding our study area this information is crucial, knowing from fact that the well-mixed water column of in eastern Mediterranean has a mean temperature above $>12.5^{\circ}\text{C}$, which means that aragonite is favored presently. (*Klein et al., 1999*)

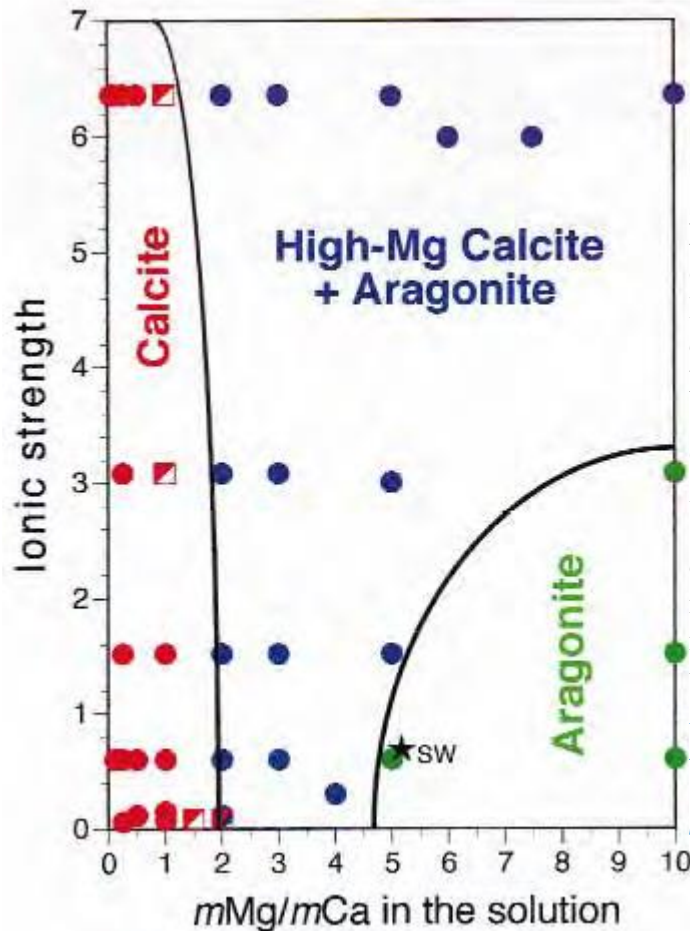


Fig. 11. Experimentally determined nucleation fields of low-Mg calcite with MgCO_3 content < 6 mol% (red), high-Mg calcite + aragonite (blue), and aragonite (green) in $\text{MgCl}_2\text{-CaCl}_2\text{-Na}_2\text{CO}_3\text{-H}_2\text{O}$ solutions at 28°C , atmospheric pCO_2 and 1 atm total pressure. MgCO_3 content of high-Mg calcite increases systematically with increase in the Mg:Ca ratio in the aqueous solution (data of [Füchtbauer & Hardie, 1976, 1980](#)). Black star SW: modern seawater. (Diagram borrowed by [Stanley & Hardie, 1999](#))

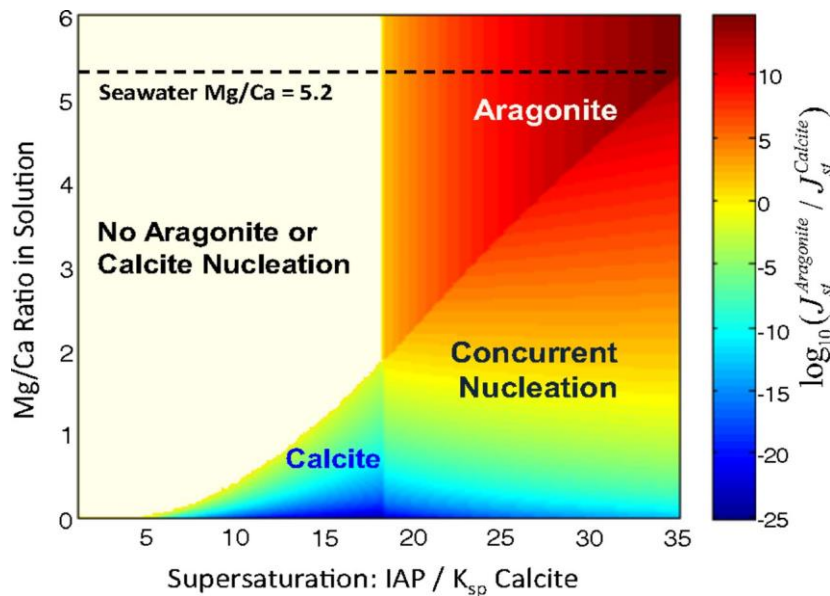


Fig. 12 Kinetic phase diagram of the relative nucleation rate between calcite and aragonite (color-coded) as a function of solution Mg:Ca ratio and the supersaturation. For Mg: Ca = 5.2 (present seawater) only aragonite is preferred to nucleate. Concurrent nucleation of calcite and aragonite occurs for a broad span of supersaturations near Mg:Ca= 2. ([Sun et al. 2015](#))

Mg:Ca ratio vs. Salinity: Salinity displays a positive correlation with Mg:Ca ratios, though shows only about half as much influence as temperature, which explains why Mg:Ca ratios are frequently used for reconstructing SSTs while foraminiferal stable oxygen isotope ratios, are preferred as paleosalinity proxy.

Salinity in some systems can account for about 25% of the variation in Mg:Ca ratios, with 32% explained by temperature, Although the temperature effect is more important than the salinity effect, **a change of 4 salinity units is equivalent to a 1 °C bias on Mg:Ca-based temperatures** therefore its effect on Mg incorporation is considered minor.

3.4 SATURATION STATE (Ω)

As we mentioned before, seawater, in normal conditions is undersaturated with respect to all evaporitic minerals and the fact that during evaporation gypsum should precipitate before halite (*Leeder, 20011*), although the saturation state, Ω , is not the only inorganic factor controlling the precipitation of aragonite from seawater.

At present, most of the open surface waters of the oceans are supersaturated with respect to CaCO_3 , except at high latitudes where surface seawater temperatures are decreased, (**Fig. 13**), so there must be at least a broad inorganic control on precipitation of CaCO_3 from seawater. Also, even though surface seawater is distinctly supersaturated with respect to aragonite, calcite and dolomite, only the former seems to precipitate directly from seawater (excluding porewater). On the other hand, seawater, in normal conditions, is usually undersaturated with respect to all evaporitic minerals. Especially halite is even more undersaturated than gypsum or anhydrite, which means that if evaporation occurs **gypsum will precipitate before halite.** (*Leeder, 2011*)

<u>Mineral</u>	<u>K</u>	<u>IAP</u>	<u>IAP/K</u>
Calcite	4.39x 10 ⁻⁹	1.35x10 ⁻⁸	3.4
Aragonite	6.3 x 10 ⁻⁹	1.35x10 ⁻⁸	2.1
Dolomite	10 ⁻¹⁷	10 ⁻¹⁵	100

Table 7 Solubility products (K) and ion activity products(IAP) for carbonate minerals in surface seawater at 25°C. Note that surface seawater is supersaturated with respect to all these carbonate minerals (Leeder, 2011)

Saturation state, Ω governs both chemical precipitation (and dissolution) of calcium carbonate as well biochemical precipitation. Even though, carbonate-secreting marine organisms can form CaCO₃ even from water that is not saturated, CaCO₃ precipitation flourish when water is saturated. The saturation state of a precipitating solution with respect to a given mineral is simply the ratio of the ion activity or concentration product to the thermodynamic or stoichiometric solubility product, K_{sp} .

Regarding the solubility of calcium carbonate in the sea, at standard P and T, aragonite is concerned to be more soluble than calcite. Also, 3 factors are taken into account (Trask, 1937):

- (1) the concentration of calcium**, which at any given depth depends almost entirely upon salinity, because S represents the concentration of the total solids, so if the salinity changes, then it follows that of the concentration of all the salts.
- (2) the apparent solubility product constant, (K_{sp})**. The apparent solubility product constant is influenced by several factors, including temperature and salinity. **It increases with rise in salinity and decreases with increase in temperature, and**
- (3) the concentration of carbonate**. The concentration of carbonate, in all three forms (carbonate, bicarbonate, or carbonic acid), depends upon a large number of variables and is by far the most influential factor in the deposition of calcium carbonate. Furthermore, the two apparent dissociation constants, K_1' and K_2' , similar to the apparent solubility product constant of calcium carbonate,

K_{sp} are affected by external conditions, such as temperature, salinity, and the activity of the ions in the solution.

Accordingly, the calculation of the saturation state of the seawater with respect to carbonate minerals is the ratio of calcium carbonate ion activity products to the stoichiometric solubility constants of calcite or aragonite, as determined by *Mucci (1983)* in seawater at various salinities. Furthermore, *Mucci (1983)* calculated the apparent solubility product (K_{sp}) of aragonite from temperature and salinity based on this equation.

$$\Omega_{calc} = \frac{[Ca^{2+}][CO_3^{2-}]}{K_c}$$

(*Mucci, 1983*)

$$\Omega_{arag} = \frac{[Ca^{2+}][CO_3^{2-}]}{K_a}$$

,where K_c and K_a is the apparent stoichiometric solubility product of calcite and aragonite, respectively, in seawater at a given salinity at 25°C and 1 atm total pressure. Subsequently, inorganic precipitation increases likely and/or rapid as Ω increases further above 1.0, and dissolution increases likely and/or rapid as Ω decreases further below 1.0.

Ω increases above 1	precipitation increases
Ω decreases below 1	dissolution increases

This assumption is based on the fact that if $\Omega = 1$, the solution is saturated, meaning that the solid and solution are in equilibrium, when $\Omega > 1$, the solution is supersaturated. and precipitation should occur, while if $\Omega < 1$, the solution is undersaturated and mineral dissolution should occur. The estimated K_c and K_a are relatively close. K_a ranging between 10 and 6.19 and K_c between 10 and 6.37. This means that the range of calcite supersaturation states that yields

simultaneous aragonite undersaturation is narrow ($1 < \Omega_{\text{calc}} < 1.5$), and generally requires that seawater be near undersaturation with respect to calcite too.

According to *Jiang et al. 2015*, Ω_{arag} was highest in the surface mixed layer and surface Ω_{arag} in open oceans was always supersaturated, ranging between 2 and 4.2, with the exception of polar areas where Ω_{arag} decreases below 1.5.

Saturation state (Ω) vs. Temperature: Temperature affects K_{sp} and therefore Ω too. The temperature of seawater affects the solubility of calcium carbonate in the water in various ways, because of its influence on

- (a) the solubility of free carbon dioxide in the seawater,
- (b) the apparent solubility product constant, K_{sp}
- (c) the two apparent dissociation constants of carbonic acid, K_1' and K_2' , and
- (d) the H^+ concentration.

Millero, 1996 provides a series of long equations for calculating K_{sp} for both aragonite and calcite. For instance the K_{arag} has gone from 1 at 25 °C to 0.91 at 40 °C to 0.55 at 80 °C. Likewise for calcite, the relative K_{calc} has changed from 1 to 0.96 to 0.73 over this temperature range, showing that temperature displays a negative correlation with K_{sp} and since when the latter decreases, saturation state should increase. Conclusively the higher the T, the higher Ω is, the more likely precipitation will take place.

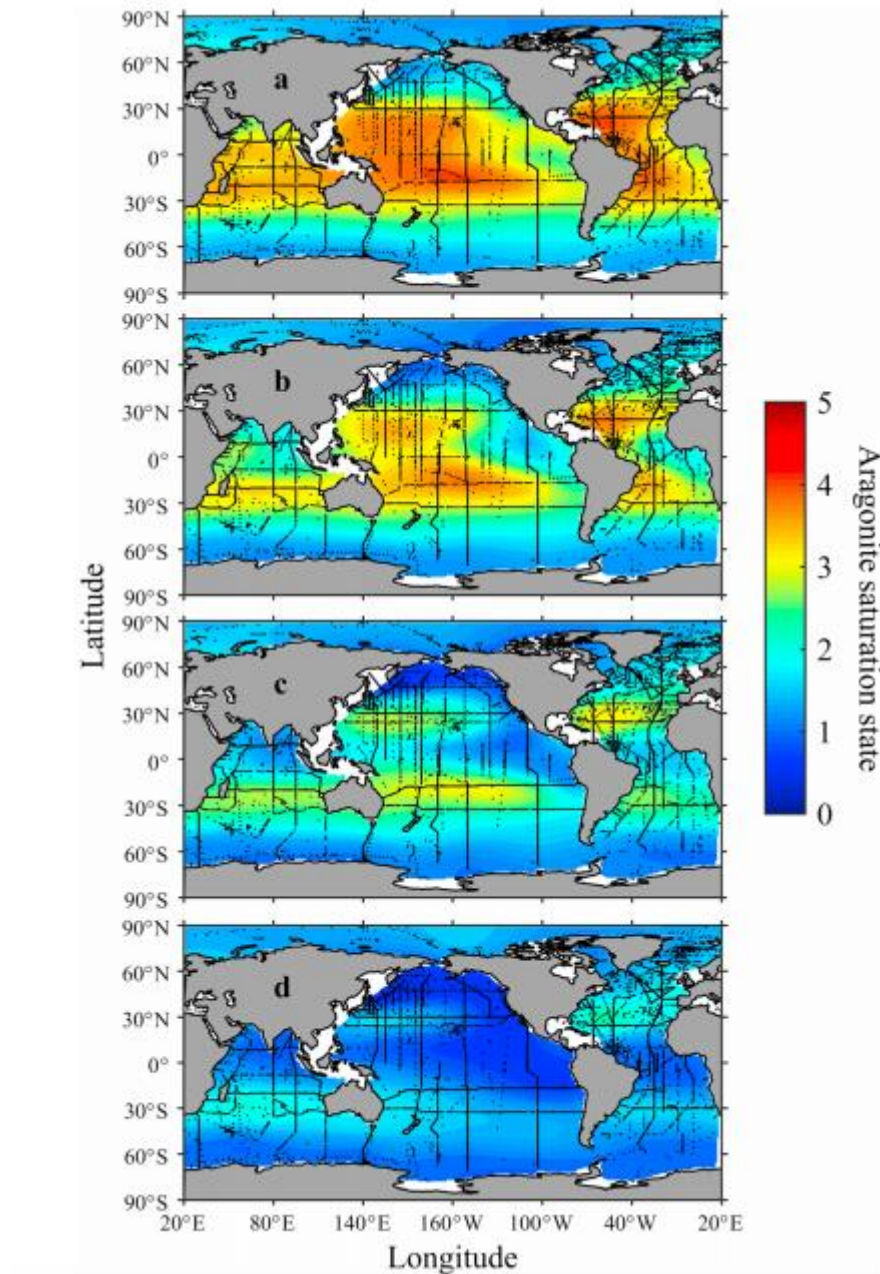


Fig. 13. Spatial distributions of aragonite saturation state (Ω_{arag}) today at depth levels of (a) 50 m, (b) 100 m, (c) 200 m, and (d) 500 m in the global oceans. Colors show gridded values based on Data Interpolating Variational Analysis (DIVA). Black dots show the sampling stations.

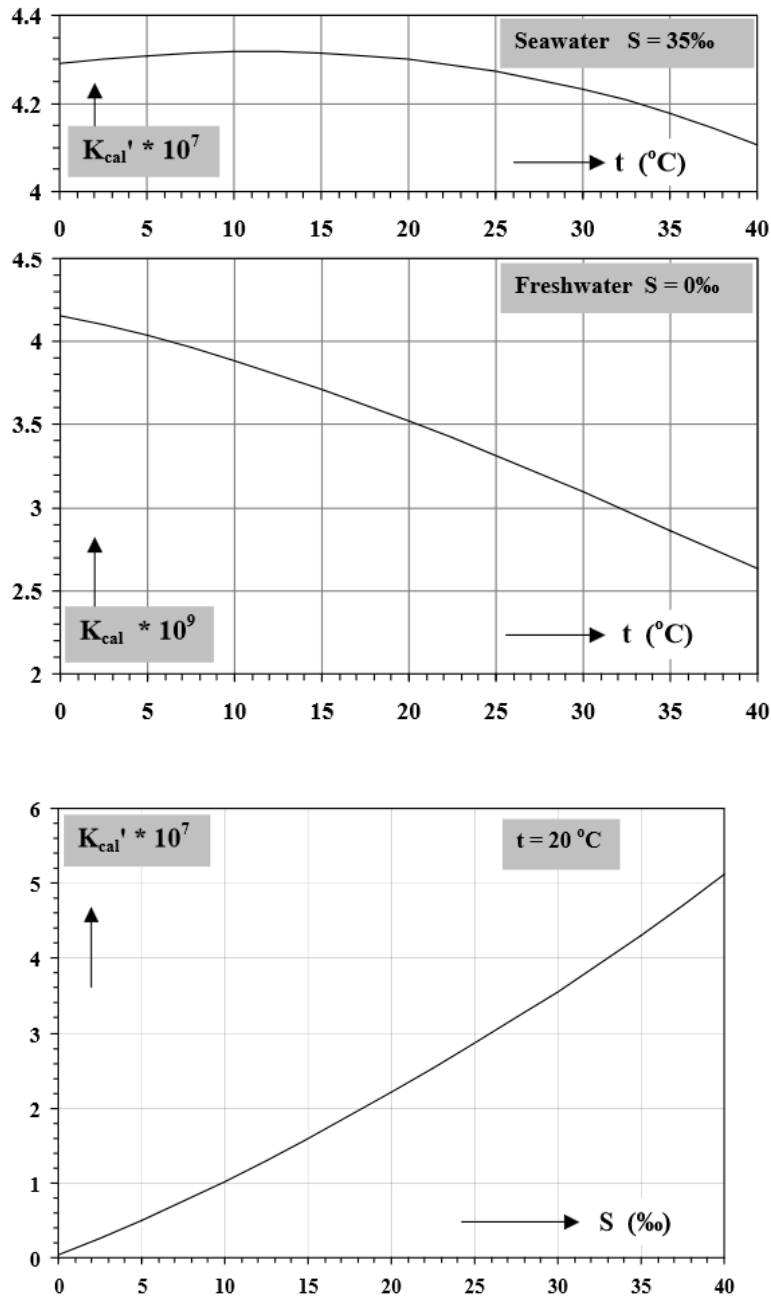


Fig. 14 The solubility product of calcite ($CaCO_3$) depending on the water temperature and salinity during precipitation (values according to *Mucci, 1983*). For instance, at $S=35$ and 1 atmosphere pressure, the K_{sp} decreases slightly as the temperature rises

Saturation state (Ω) vs. Salinity:

Salinity has a more complex effect on the saturation state of calcite and aragonite, causing both increases in K_{sp} values and in $[Ca^{2+}]$ concentrations with rise in salinity, favoring at the end the precipitation of calcium carbonate. In

conclusion, both the total alkalinity (TA) and CaCO_3 saturation state Ω increase with salinity, which is contradictive with the fact that even though temperature displays always a negative relationship with K_{sp} , as discussed before, salinity shows a positive relationship with both K_c and K_a . For example, the increasing solubility of CaCO_3 with salinity suggests that organisms in more marine environments should have difficulty depositing shell material if this factor was the only one influencing shell formation. Therefore, even though higher salinity can cause increased solubility, there are many other factors that interact in this system to influence the shell deposition of marine or even estuarine organisms. The salinity of seawater affects the solubility of calcium carbonate in the water because of its relations to:

- (1) the solubility of free carbon dioxide in the water,
- (2) the constants, K_1' and K_2' and the K_{sp} (**Fig.14,15**)
- (3) the hydrogen-ion concentration, and
- (4) the quantity of calcium and excess base in the water.

Ω_{arag} was calculated by *van Heuven et al., 2009* based on *Mucci's* equation. $[\text{Ca}^{2+}]$ in seawater was assumed to be conservative with salinity by *Millero, 1995*

$$[\text{Ca}^{2+}] = 293.86 S$$

where the unit of $[\text{Ca}^{2+}]$ is $\mu\text{mol kg}^{-1}$, and S is salinity. $[\text{CO}_3^{2-}]$ was calculated from in situ temperature, pressure, salinity, dissolved inorganic carbon (DIC), total alkalinity (TA), silicate and phosphate with the dissociation constants for carbonic acid, potassium bisulfate, boric acid and the total borate concentration equations.

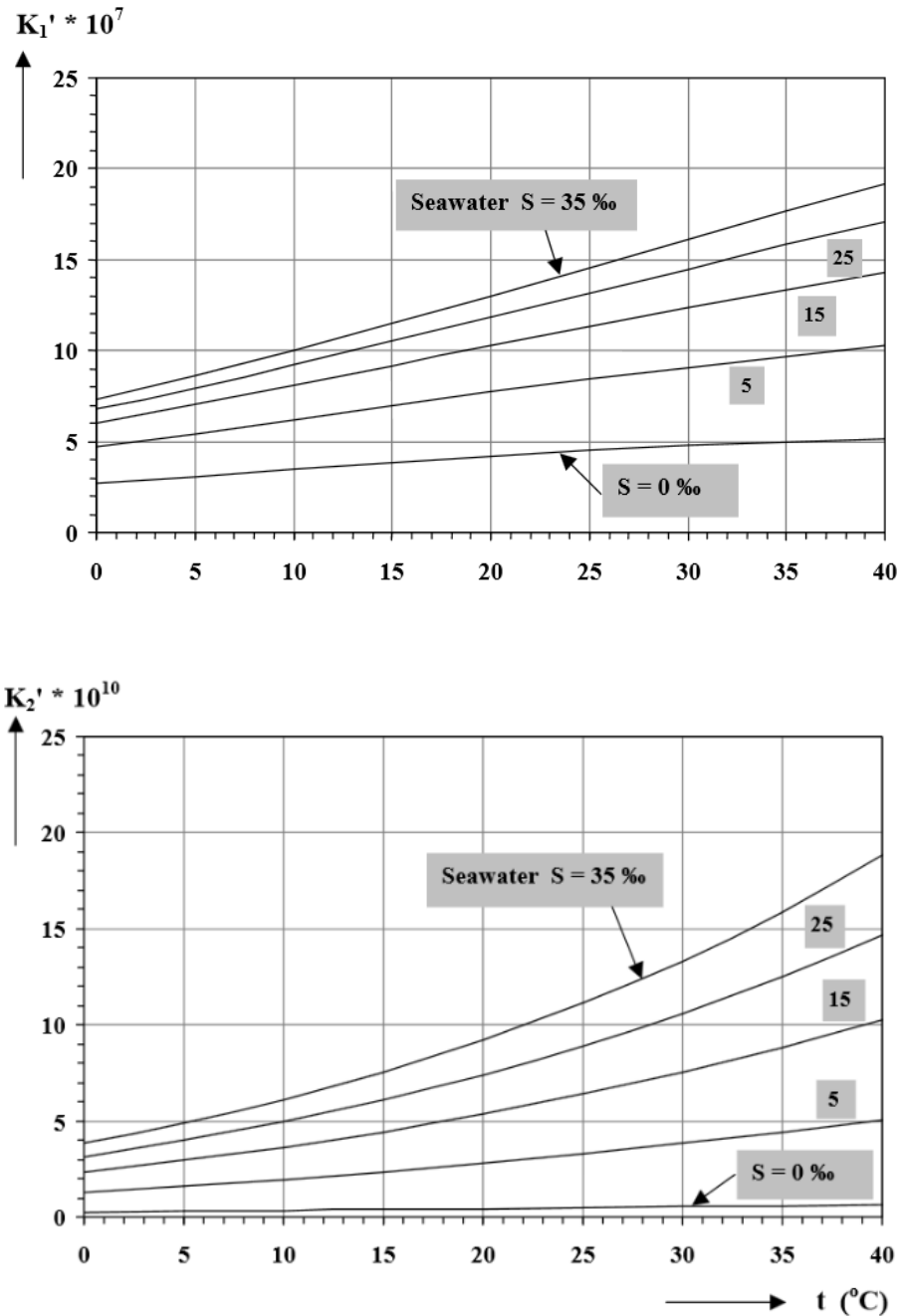


Fig. 15 Graph above: The acidity constants for the first dissociation of carbonic acid in freshwater and seawater as a function of the water temperature at salinities of 0, 5, 15, 25, and 35‰. Second Graph: The acidity constants for the second dissociation of carbonic acid in seawater as a function of the water temperature at salinities of 0, 5, 15, 25, and 35‰. The values are according to [Millero&Roy\(1997\)](#). The marine values are equal those reported by [Mehrbach et al. \(1973\)](#) as discussed by [Dickson&Millero \(1987\)](#) ([Source:https://ay1415.moodle.wisc.edu/prod/pluginfile.php/172623/mod_resource/content/5/Carbonate%20System%20Chemistry.pdf](https://ay1415.moodle.wisc.edu/prod/pluginfile.php/172623/mod_resource/content/5/Carbonate%20System%20Chemistry.pdf))

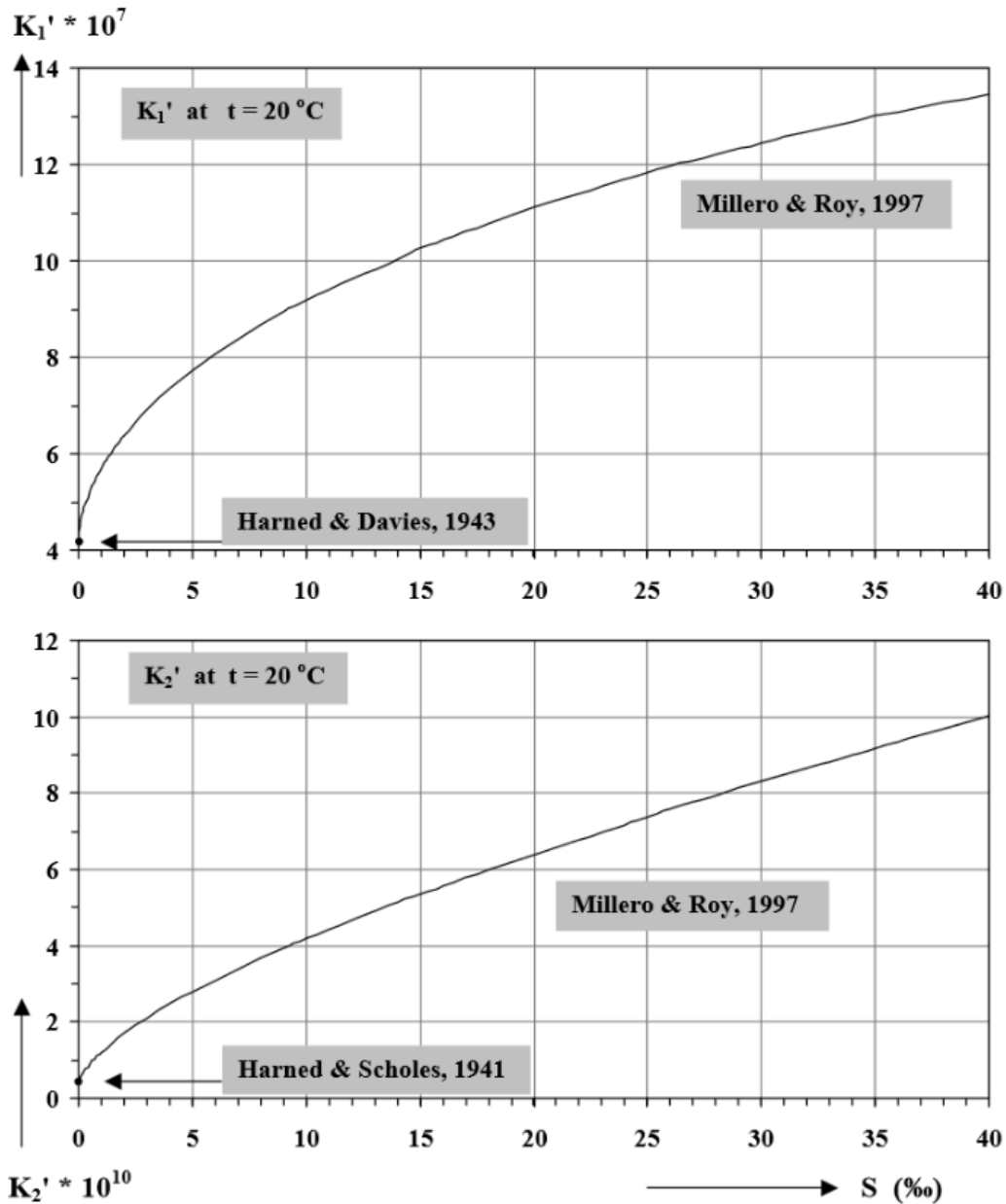


Fig.16 Values for the first and second dissociation constants of dissolved carbonic acid as a function of the salinity (Millero&Roy, 1997). The values are valid for a water temperature of 20°C. Available dissociation constants of carbonic acid, K_1, K_2 , as a functions of salinity (Source: https://ay14-15.moodle.wisc.edu/prod/pluginfile.php/172623/mod_resource/content/5/Carbonate%20System%20Chemistry.pdf)

Moreover, laboratory experiments allowed scientists to separate a direct salinity effect from a possible independent impact through differences in the calcite saturation state of the seawater (Ω).

3.5 TEMPERATURE

According to many researchers, temperature is the most likely controlling factor on the compositions of recent marine carbonate cements. This was well presented in previous chapters where was discussed temperature's great impact on both solubility and Mg: Ca ratio. Temperature also affects the growth of living organisms, which in turn affect the deposition of CaCO_3 . Moreover, due to its effect on evaporation, temperature obviously influences the salinity of the water too. Finally, temperature changes with depth, as it is known. All these effects, some major other minor depend of course from the environment.

Carbonate minerals precipitate in various sedimentary environments. However, the deposition rate of CaCO_3 is favored in warm, shallow basins than in the deep ocean. Also shallow-water carbonate-rich sediments are mostly confined today to the subtropic and tropic climatic zones, as the sea surface temperature in high latitudes tends to be lower.

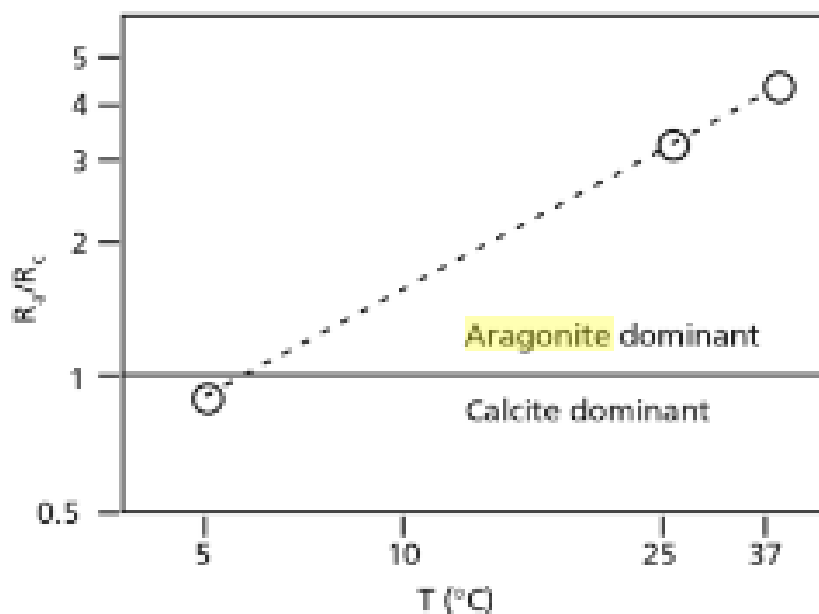


Fig. 17 Relative precipitation rates of aragonite vs. calcite (R_a/R_c), as a function of temperature in seawater five times supersaturated with respect to calcite (After [Burton&Walter, 1987](#))

Burton et al. 1987 carried out laboratory experiments to investigate the relative growth rates of calcite, high-Mg calcite, and aragonite in seawater as functions of both temperature (5, 25, and 37 °C) and of carbonate ion concentration (2.5 to 15 times supersaturated with respect to calcite). According to their results, **the precipitation rates of aragonite relative to those of calcite increase strongly with increasing temperature** while there is a minor effect by the changes in saturation state.

Specifically, even though at 5 °C, calcite precipitation rates are nearly equivalent to those of aragonite ($R_a/R_c \approx 1$), regardless of the degree of saturation, at both 25° and 37 °C (**Fig. 17**) aragonite precipitation rates are much more rapid than those of calcite, except at very low saturation states. On the other hand, calcite compositions vary from less than 5 mol% MgCO₃ at 5 °C to 14 mol% MgCO₃ at 37 °C, according to **Burton&Walter, 1987**. These results suggest that the well-documented shift toward precipitation of lower mol% Mg-calcite and the decrease in abundance of aragonite cements with increasing depth and latitude can be attributed mostly to lower temperatures, whereas higher temperature in low-latitude warm (and usually shallow) seawater favors precipitation of aragonite.

3.6 SALINITY

Salinity's distribution was already discussed. In summary, salinity represents the concentration of the total solids, so if the salinity changes, then the concentration of calcium changes accordingly. Salinity as mentioned previously displays also a positive correlation with Mg:Ca ratios, though its effect is considered minor, while it has a positive correlation with the apparent solubility product constant, (K_{sp}) too. Due to the detailed discussion regarding the relations between the control factors, we will display now various modern analogues of typical saline environments.

Salinity in saline water (e.g. seawater, salt lakes) ranges from 30 to 50 ppt (permille or parts per thousand or ‰). For example, the average seawater has a salinity of 34.7 ppt. Typically, Mediterranean sea has 38 ppt. Both the Red Sea and the Persian Gulf are higher saline regions (**Rochford, 1964**). The salinity of

their water masses is about 40-41 ppt, while there are limited areas (sabkhas) in the Persian Gulf, where salinity exceeds 50 ppt (*John et al. 1990*). Salinity in brine water, e.g. brine podsm tends to exceed 50 ppt (**Table 8**). Brines are known for providing the ingredients required for the production of evaporate minerals such as aragonite and gypsum in the lakes (*Starinsky, 1974; Neev and Emery, 1967; Stein et al. ,1997; Hazan et al. , 2005*) A typical example of hypersaline area is the Dead Sea.

Brackish Water	Saline Water	Brine Water
5-30 ppt	30-50 ppt	>50 ppt
Baltic Sea (8 ppt)	Mediterranean Sea (38 ppt)	Dead Sea
Black Sea (18 ppt)	Red Sea (40 ppt)	
Caspian Sea	Great Bahamas Banks (36 to 46.5 ppt)	

Table 8 Salinities of Modern Environments

High salinities are supposed to be the result of extremely high evaporation, insignificant rainfall, low river flow and restricted exchange with the open ocean.

In a classic evaporite sequence, the first endogen precipitates are carbonates (from waters with a minimum salinity of 0.12g/kg), which are then followed by the calcium sulfates - anhydrite and gypsum - at high salinities (*Wenk and Bulakh, 2004*).

Evaporation though is not an easy process. *Usiglio, 1849 (Fig.18)* in fact pointed out that, in order for gypsum to precipitate, only 20% of the initial water volume should survive within the basin. Falsely though, most of the times if not always hypersaline conditions are linked with the formation of aragonite alone, instead of gypsum. It has recently been claimed, however, that the mechanism for aragonite precipitation is much more complex. The Dead Sea, which is a famous modern analogue (*Friedman 1993, 1994*) of abiotic chemical

precipitation, known for forming massive aragonite deposits in the form of varves, since late Pleistocene, is an interesting exception, being a Ca-chloride hypersaline lake whose **aragonite**

Evaporation Sequence of Seawater

Volume of water remaining	Evaporite Precipitated	
50%	<ul style="list-style-type: none"> ➤ At this point, minor carbonates begin to form. ➤ A little iron oxide and some aragonite are precipitated. ➤ Minor quantities of carbonate minerals (Calcite and dolomite) form. 	a) Calcite (CaCO ₃): <ul style="list-style-type: none"> ✓ Precipitates if < 50% of seawater is removed. ✓ Only accounts for a small % of the total solids The first phase
20%	Gypsum precipitates: Gypsum (<42°C) or Anhydrite (>42°C).	b) Gypsum: <ul style="list-style-type: none"> ✓ Precipitates if 80-90% of seawater has been removed ✓ Solution is denser
10%	Rock salt (halite) precipitates	c) Halite: <ul style="list-style-type: none"> ✓ Precipitates if 86-94% of original seawater has been removed ✓ Brine (solution) is very dense ✓ The deposition of salt beds provides the source for about three-fourths of all salt used.
5%	<ul style="list-style-type: none"> ➤ Mg & K salts precipitate ➤ Precipitation of various <i>magnesium sulfates and chlorides</i>, and finally to <i>NaBr and KCl</i>. ➤ Potassium and magnesium salts (kainite, carnallite, sylvite) 	d) Potassic salts: <ul style="list-style-type: none"> ✓ Precipitate if > 94 % of original seawater has been removed ✓ So: ionic strength (potential) of evaporating seawater has a strong control over minerals that form. ✓ After the deposition of common salt, chlorides and sulfates of magnesium and potassium are the other chief salts deposited. The potassium minerals result from evaporation carried almost to completion and, therefore, only rarely are they deposited.

↑ Decreasing order of solubility
↓ Increasing Evaporation Rates

Fig.18 Usiglio Model (1849)(Evaporation Sequence of seawater)

deposition is affected not by evaporation rather than by flooding. Specifically, instead of summer evaporation and warming of surface water (whiting events), the true trigger mechanism for massive aragonite inorganic mixing of a small percent of the Ca²⁺-rich brine with a lot of runoff freshwater of high bicarbonate (HCO₃⁻) content. This mixing of these two solutions, the one supplying with Ca²⁺, the other with HCO₃⁻ in 1:9 ratio, during winter flooding, implies according to *Barkan et al. (2001)* that it is possible for other saline environments to produce much more aragonite during humid conditions rather

than arid. This promotion of aragonite precipitation during wetter climate was suggested from *Gavrielli et al., 2006*, as well. The general conclusion was once again that during wetter conditions, the large amounts of fresh water that filled the basin, diluted the surface water, and led to development of long term stratification (meromixis) and eventually to deposition of thick sequences of laminated aragonite.

Another typical example of stratification is the Baltic Sea. The enclosed sea receives so much freshwater from the adjacent lands that the surface water is brackish, with an average salinity of about 8 ppt, while the saline water is left at the bottom, with limited mixing between them due to the lack of tides and storms. Similarly, in the Black Sea the surface water is also brackish, with an average salinity of 17- 18 ppt, while an inflow of deep anoxic saline water occurs from the Mediterranean Sea.

Thomson et al., 2004 supported as well that an analogous conjunctions of two different water bodies, may promote aragonite precipitation in less saline and more open aquatic systems. For instance, Eastern Mediterranean salinities are much lower than those of the Dead Sea, but according to their hypothesis, sapropel formation is not the only product directly linked to monsoonal-driven surface ocean production. The production hypothesis suggests that the very fine CaCO₃ whittings, (mainly aragonite) occur at the base of the fresher surficial layer, possibly through the picoplankton biomineralization (*Thomson et al., 2004; Robbins&Blackwelder, 1992*). This mechanism has already been proposed after all to explain whittings, observed in the water column over shallow subtropical carbonate banks.

Coastal waters, carbonate banks, lagoons etc. are typical cases of environments where seawater ionic concentration deviates from typical ocean values. In summary, salinity distribution in a basin is basically a function of three physical processes: **(1) water exchange, (2) evaporation rate and (3) input of fresh water**. Comparison of qualitative physical parameters of modern analogues of carbonate factories such as **the Bahamas Banks, the Belize lagoon and the Persian Gulf**. (Table 9) provides an alternative way of a deeper

understanding of these controlling processes that determine the resulting sedimentary assemblages in dynamic carbonate producing systems. For instance, according to **Table 9**, salinity distribution in Persian Gulf results mostly from a high evaporation rate in an arid region, while both the Bahamas and the Belize lagoon reflect a humid climate, even though only the latter is strongly influenced by an influx of freshwater. In an offshore archipelago such as the Bahamas Banks rainfall is the only source of fresh water (*Eberly et al. 2010*)

Attribute/Parameter	Bahamas	Belize	Persian Gulf
Tectonic Setting	Passive Continental Margin	Strike-Slip Setting	Convergent Basin
Morphology	Flat Platforms With Sharp Shelf Edges	Lagoon Bound On W By Continent And On E By Shelf Edge, Barrier Reef And Offshore Atolls	Restricted Epi-Continental Sea Within Foreland Basin Ramp Setting
Climate	Subtropical	Tropical	Subtropical
Marine Influence	Fully Marine	Marine And Continental	Continental
Humidity (Rain: Evaporation Ratio)	Humid	Humid	Arid
Temperature	Warm And Stable	Warm And Mostly Stable	Hot In Summer; Highly Variable With Large Range
Salinity	Normal To Locally High	Low To Normal	Very High To Approaching Normal At Entrance (Strait)
Restriction Effects	Locally High Salinity In Large Platform Interior	Lowered Salinity In Shelf Lagoon	Very High Salinities And Large Temperature Fluctuations
Reefs	Barrier And Patch Reefs	Extensive Barrier (Shelf Edge) Reef And Lagoonal Patch Reefs, Pinnacles	Patch Reefs (No Shelf Edge) = No Barrier Reefs
Terrigenous Input	No	Yes	Yes
Evaporite/Dolomite Precipitation	No	No	Yes

Table 9. Typical carbonate factories

All three areas have the distinctive characteristic of forming whittings (areas of milky water where aragonite precipitates in the water column). In all of them, the surface waters should be supersaturated with respect to both aragonite and calcite, even though, in cases like the Bahamas Banks only the former seems to precipitate directly from seawater. For instance, in the Bahamas the carbonate mud consists mostly of aragonite and to a minor extent of high Mg-calcite ([Morse et al. 2003](#)), in contrast to areas with fresh water input like Belize where aragonite and high-Mg calcite are accompanied by low-Mg calcite precipitation. Furthermore, the lime mud in Belize lagoon is 70 to 90% high-Mg calcite containing 9-10 mole % MgCO₃. ([Reid et al. 1992](#)). On the other hand, in the Persian Gulf, which is a typical higher saline area, the mud is composed predominantly of aragonite, while the precipitation of high-Mg calcite occurs only in the northern part where a source of fresh water exists.

Even in the Great Bahamas Banks, that are thought to be typical saline environment, evaporites are considered ephemeral to absent. Gypsum is usually formed seasonally only on tidal flats like those at Andros Island. Specifically Andros Island has a mean annual rainfall >120mm, meaning that gypsum appears during the dry period but dilutes when the weather becomes more humid therefore is not preserved for the geologic record, in contrast to Persian Gulf where the mean rainfall is <10mm and therefore gypsum is common.

3.7 O₂

Aragonite is considered to be more soluble than calcite ([Walter&Burton, 1990; Patterson&Walter, 1994](#)) Aragonite dissolves at a higher pH than calcite (pH 7.8; [Tynan & Opdyke 2011](#))) and is less likely to be preserved in the rock record. For example it has been estimated that 50% of all carbonate sediments are geologically preserved but only 10% of aragonitic grains escape dissolution ([Ku et al. 1999; James et al. 2005](#)). This preferential dissolution has implications for our understanding of carbonate productivity.

The length of carbonate precipitation is different in anoxic and slightly oxidizing environments, than it is from typical oxidizing environments. *Sumner and Grotzinger (1996a, b)*. Carbonate deposition is affected by changes in the oxidation state of seawater. For instance, oxic breakdown of organic material produces acid, which dissolves some carbonates, while anoxic conditions produce bicarbonate, resulting in enhanced preservation of carbonates (*De Lange et al., 1989*).

The carbonic acid reacts with calcium to form calcium carbonate, increasing alkalinity. The precipitation reaction may be summarized as



Oxidation of buried organic matter either due to decomposition by aerobic metabolisms or sulphate reduction can also alter both the pH and alkalinity of pore waters and subsequently influence the diagenesis of carbonate minerals.

O₂ vs Early diagenesis

The saturation state of the pore waters, depending on pH, alkalinity and pCO₂, can be described as mainly affected by three elements:

- **The oxidation of organic matter** and its reaction bi-products that influence calcium carbonate saturation state, by releasing/consuming chemical compounds that interact with the carbonate system (*Tribble, 1993; Morse&Mackenzie, 1990*)
- **The degree of openness of the system** (e.g. openness of the system determines the effect of sulphate reduction) (*Sanders 2003; Melim et al. 2002*) and
- The degree to which FeS (or other minerals) act as a sink for dissolved sulphide produced during **sulphate reduction** (*Tribble 1993; Perry&Taylor, 2006*)

Oxic respiration may generate small amounts of acidity and can be described by the following reaction:



However the upper centimetres of the sediment column are generally open and interacting with the supersaturated seawaters above. So, reaction products from aerobic oxidation alone are unlikely to build up to significant levels in order to cause aragonite dissolution in pore waters. Sulphate reduction is another important anaerobic organic matter oxidation process in carbonate sediments:



All marine sediments contain layered bacterial reduction zones. Oxygen can only diffuse into the first centimetre of sediment from the overlying water column (*Ku et al. 1999*), and respiring bacteria quickly create anoxic conditions unless there is a continuous supply of oxygen. In a marine environment bacterial sulphate (SO_4^{2-}) reduction occurs very close to the sediment-water interface as the bacteria utilize seawater sulphate and produce hydrogen sulphide (H_2S) (*Ku et al. 1999; Sanders 2003; Wheeley et al. 2008*) as a metabolic bi-product

Modern Analogues of post-depositional diagenetic formation of aragonite within different environments

1. Aragonite Content within S1 sapropels in Eastern Mediterranean

Thomsons et al. 1995, 2003 found a high proportion of aragonite with high F. profunda reported within all recent eastern Mediterranean sapropels S1, based on XRD analysis and bulk sediment Sr/Ca ratios. They proposed that the aragonite that occurs along the presence of sulphides in the S1 units demonstrates that anoxic conditions must have been established in pore waters at shallow depth very soon after sediment deposition. Furthermore XRD analysis revealed that aragonite increased from 5 wt % in the marls above the sapropel to 15 wt % in the sapropel

2. Aragonite mineral within sediments collected from anoxic brine-filled Poseidon Basin, eastern Mediterranean

Based on a piston core the average carbonate content is slightly higher in the sapropelic sediments from the anoxic brine-filled Poseidon Basin in eastern Mediterranean than it is in the top sediments ([Rutten et al. 1999](#)).

Basically this study indicated that carbonates are preserved better in brine sapropels compared to sediments deposited in a 'normal' eastern Mediterranean environment with 'normal' sapropels. Nevertheless enhanced preservation of aragonite during periods of anoxic conditions is again demonstrated ([De Lange et al., 1989](#)).

3. **Aragonite preserved under anoxic conditions within sediments from lake Iznik, Turkey**

4. According to [Roesser et al. 2015](#) who studied the fresh to brackish lake Iznik, aragonite and calcite preservation in sediments from there are also related to bottom lake oxygenation and water column depth, as the repeated periods of stratification and therefore the enhanced sulphate reduction seems to be responsible for aragonite preservation

5. **Preservation model for the aragonitic shells of the ammonites within The Blue Lias Formation at Lyme Regis (Dorset, UK) ([Jordan et al. 2015](#))**

The abundance of large ammonites is highly uncommon as they are originally composed of aragonite and such fossils tend to dissolve. In order to have survived dissolution [Jordan et al. 2015](#) suggested that the oxygen concentrations in the overlying water column had to be low during deposition. The preservational model presented here implies that diagenetic loss of aragonite will be greatest in those areas where dysoxic-anoxic sediment lies beneath an waterbody rich in O₂ but least where both the sediment and the overlying water are oxygen depleted..

CHAPTER 4. Results

Methods.

- ❑ The Department of Historical Geology-Palaeontology (EKPA, Greece) recovered 6 different long cores from the NW Saronikos Gulf (SAR1, SAR4, SAR34, SAR36, SAR38 and SAR39) at distinctive water depths (**Fig. 19, Table 10**)
- ❑ All 6 cores were scanned for Magnetic Susceptibility (MS)
- ❑ Four long cores (SAR4, SAR36, SAR38 and SAR39) were logged and their carbonate contents were continuously determined, at 1-2cm resolution
- ❑ Selected samples from SAR4, SAR36 and SAR39 were studied about their XRD bulk and carbonate mineralogy.
- ❑ SAR39 was studied about its terrigenous mineralogy.
- ❑ SEM was also employed and an AMS radiocarbon dating was conducted at 196-198cm of SAR39

Core Name	Depth (m)	Core Length (cm)	Latitude	Longitude
SAR1	124	110	37°53'2.79"N	23°19'7.39"E
SAR4	182	318	37°52'4.00"N	23°14'6.60"E
SAR34	230	263	37°52'43.18"N	23° 7'50.34"E
SAR36	123	247	37°52'27.55"N	23° 3'1.80"E
SAR38	124	262	37°54'47.90"N	23°15'49.26"E
SAR39	140	260	37°52'38.32"N	23°15'39.96"E

Table 10. Info of the long cores retrieved from NW Saronikos Gulf



Fig.19 Long cores' locations within Megara Basin

4.1 MAGNETIC SUSCEPTIBILITY

Methodology

The Bartington MS2 instrument measures the MS with the help of a sensor that consists of a very high thermal stability oscillator for which a wound inductor is the principle frequency-determining component. MS2C is a sensor specifically designed for the measurement of continuous sections of core and provides MS values either in CGS or in SI and in ranges $\times 1 \times 0.1$, though the measured values need to be corrected, therefore the mean of an air measurement before and after the sample is subtracted from the sample measurement:

The equation for correcting MS is:

$$R_k = R_1 - R_2 / 2$$

where:

R₁, measured sample. R₂, measured air and R_k, the corrected value.

The measurements for the present study were conducted in CGS system at 0.1 range (Bartington Instruments Ltd., 1995) with a resolution of 1 cm.

Results

In this chapter, we present the results of down core variations in magnetic susceptibility (MS) of six piston cores (SAR1, SAR16, SAR34, SAR36, SAR38 and SAR39) retrieved from the Megara Basin of western Saronic Gulf (**Fig. 20**), with the exception of SAR16 that was collected southern of the Megara Basin, near Aegina island. MS was measured using a Bartington Model MS-2 core scanning sensor with search loop, a common method for whole-core logging. The results are reported in $\times 10^{-6}$ SI units. According to Bartington, the accuracy of this method is 5%.

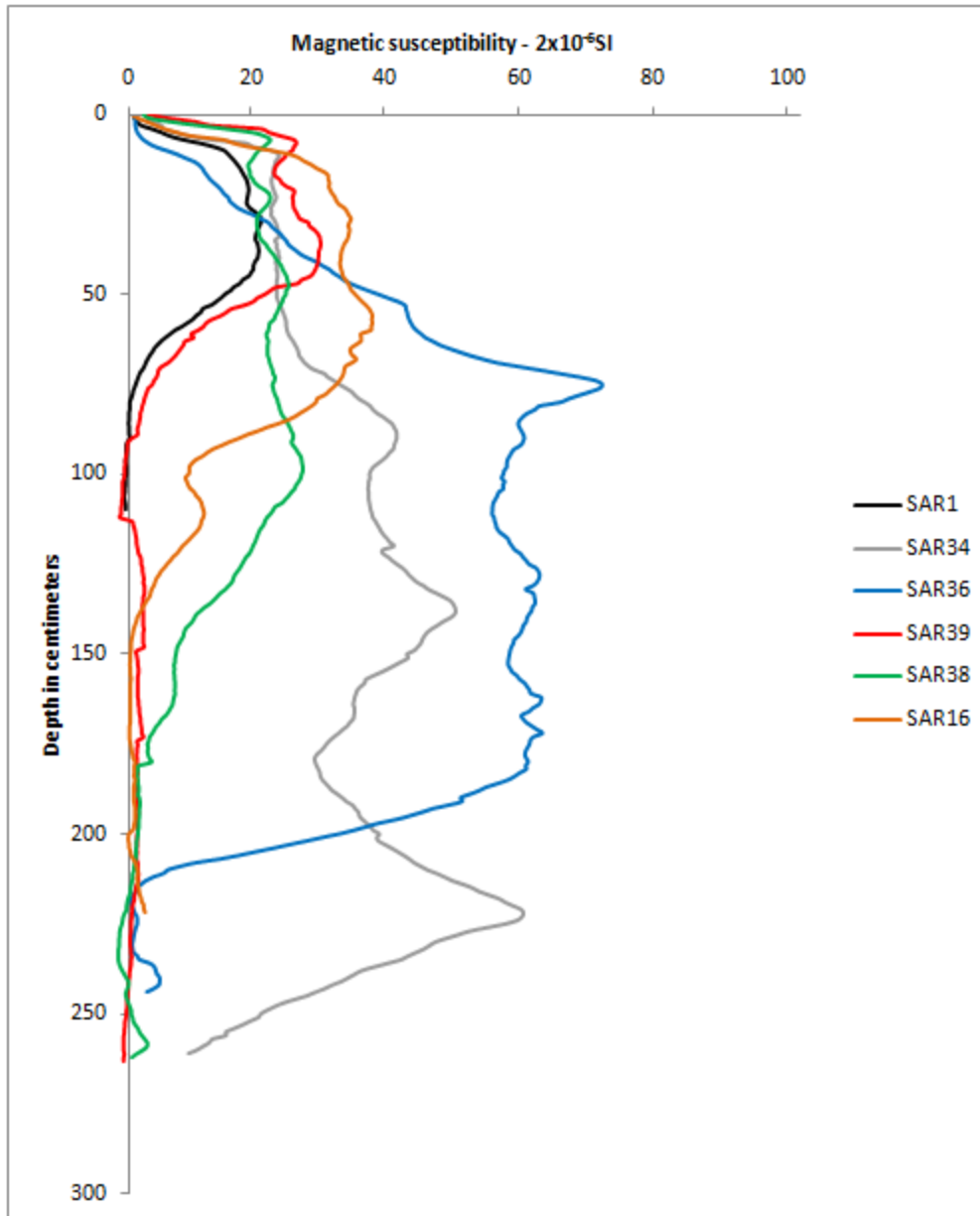


Fig 20 MS variations of the piston cores from Saronikos Gulf

Susceptibility values in all piston cores ranged from few tens of 10^{-6} to less than 0.1×10^{-6} (or even negative) SI units. There is a category of magnetism referred to as diamagnetism, where the magnetic field interacts with the orbital motion of electrons to produce weak and negative values of magnetic susceptibility. (Table 11.) Materials that fall into this group include many minerals which do not contain iron, like quartz and calcium carbonate. These readings are acceptable for the usually low magnetic susceptibility carbonate

sediments. Based on the MS low estimates, the endogenic processes are the primal depositional mechanism in the Megara basin the last 17,000 years.

Type of material	Magnetic Susceptibility
Ferromagnetic	Strong positive susceptibility e.g. pure iron, nickel, chromium
Ferrimagnetic	Strong positive susceptibility e.g. some iron oxides and sulphides (magnetite, maghemite, pyrrhotite, greigite)
Canted antiferromagnetic	Moderate positive susceptibility e.g. some iron oxides (hematite, goethite)
Paramagnetic	Weak positive susceptibility e.g. Many Fe-containing minerals and salts (biotite, olivine, ferrous sulphate)
Diamagnetic	Weak negative susceptibility e.g. water, organic matter, plastics, quartz, feldspars, calcium carbonate

Table 11. Classification of minerals based on their MS

Magnetic susceptibility is usually an indicator of the presence of allogenic sediments. Variations in magnetic properties in the piston cores could also reflect differences in magnetic properties of the source areas of detrital clastic material. **In comparison to the entire core, almost always only the upper parts of all the cores collected from the Megara Basin are characterized by relatively high MS values. This restriction of the highest values of MS within the upper parts of the cores and therefore their consistence within the most recent sediments reflects the hydrologic and chemical evolution of the Megara Basin from a shallow basin with no river discharges (rich in carbonate supply) to a normal marine environment with significant terrigenous supply.**

This statement is supported by XRD results as well. Sediments deposited last consist of representative detrital minerals such as quartz and plagioclase.

Along with them moderate amounts of low-Mg calcite were found. Some if not all of the low-Mg calcite deposited during that time probably is of biogenic origin, while the rest may also be of detrital origin, derived mainly from carbonate rocks in the surrounded area.

So all the cores reflect a later detrital influx. However the size of it differs from core to core. In some cores seems weaker in other areas stronger. For instance SAR34 and SAR36 record the highest MS values among all cores and have persisting high MS values along the first 200 and 230cm, accordingly, even though SAR36 was retrieved near the western shores of Megara Basin while SAR34 was collected from a much greater depth.

On the other hand SAR1 and SAR39 that were collected 5.22 km away from each other seem to to have a similar trend, be ridden of magnetic mineral after the first 50cm. From the data it is apparent that there is significant variation regarding the length of persistence of the MS, reflecting the different depositional rates as well the various sources of detrital material.

The following decreases in MS across the oldest sections are coupled with a TIC increase (**Fig.21**), indicating a transition to chemical precipitation, which is also reflected in the non-magnetic authigenic minerals found in the sediments, comprised mostly by a great amount of the mineral aragonite as well.

So, prior to the arrival of the siliclastics recorded in the upper section of the cores either the allogenic input was minimal or sediments became progressively enriched in endogenic carbonate at the expense of terrigenous material. Furthermore, high TIC and low MS values may also be the result of high productivity and low oxygen bottom levels, due to the consumption of O₂ via decomposition of the sinking organic matter. The lack of O₂ on the Megara Basin bottom would have prevented iron and titanium from oxidizing and forming magnetic hematite and ilmenite. In a way *Lykousis et al. 1993* who collected 14 piston cores from Saronikos Gulf support this claim too, as they noticed that within aragonite-dominated sequence the benthic-dominated communities are limited.

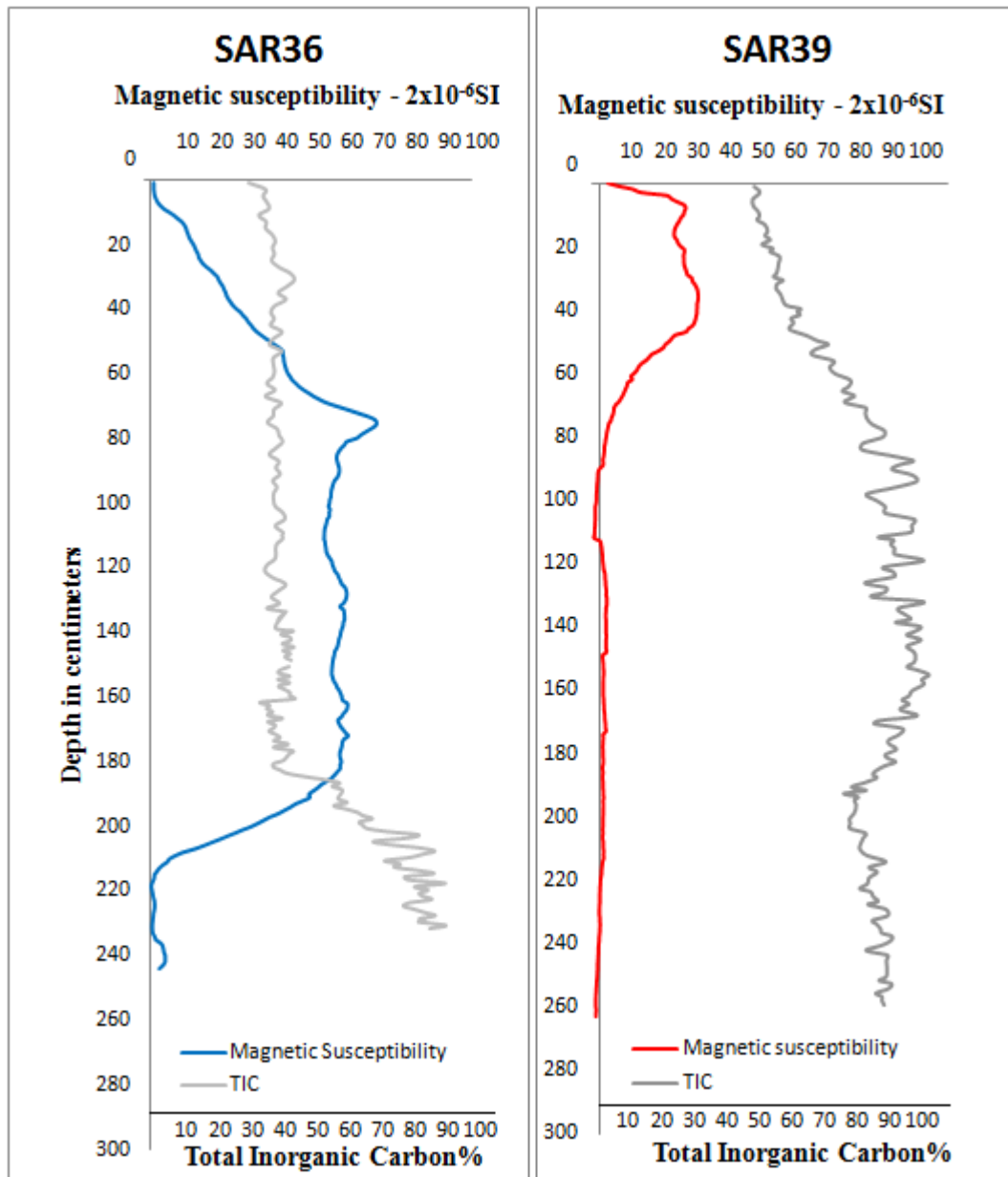


Fig. 21 Downcore trends illustrating the inverse relationship of TIC to MS within cores SAR36 and SAR39

4.2 DESCRIPTION OF LITHOLOGIC UNITS

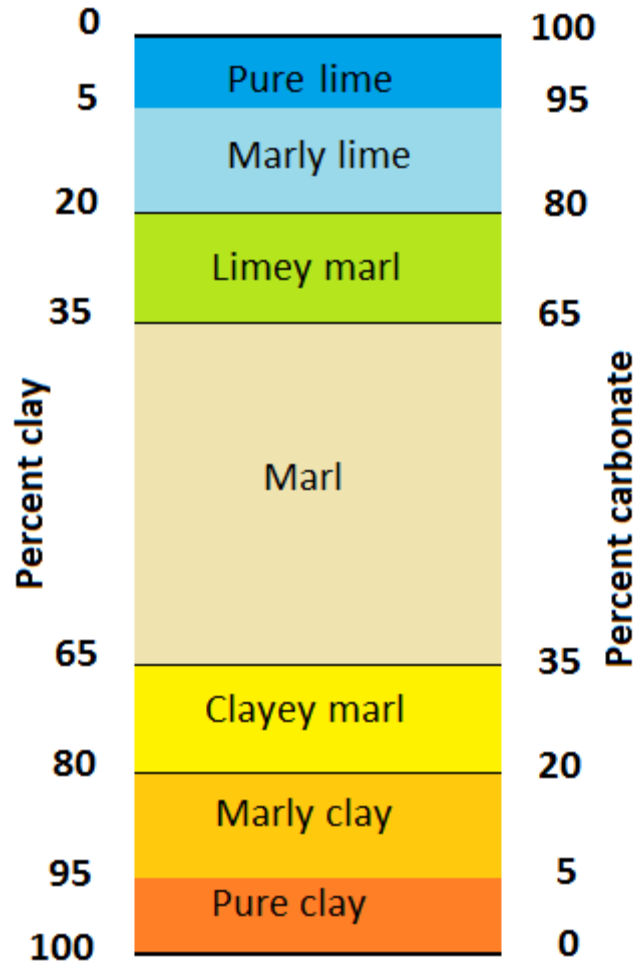


Fig. 22 Classification of carbonate-clay mixtures (modified after Barth et al., 1939)

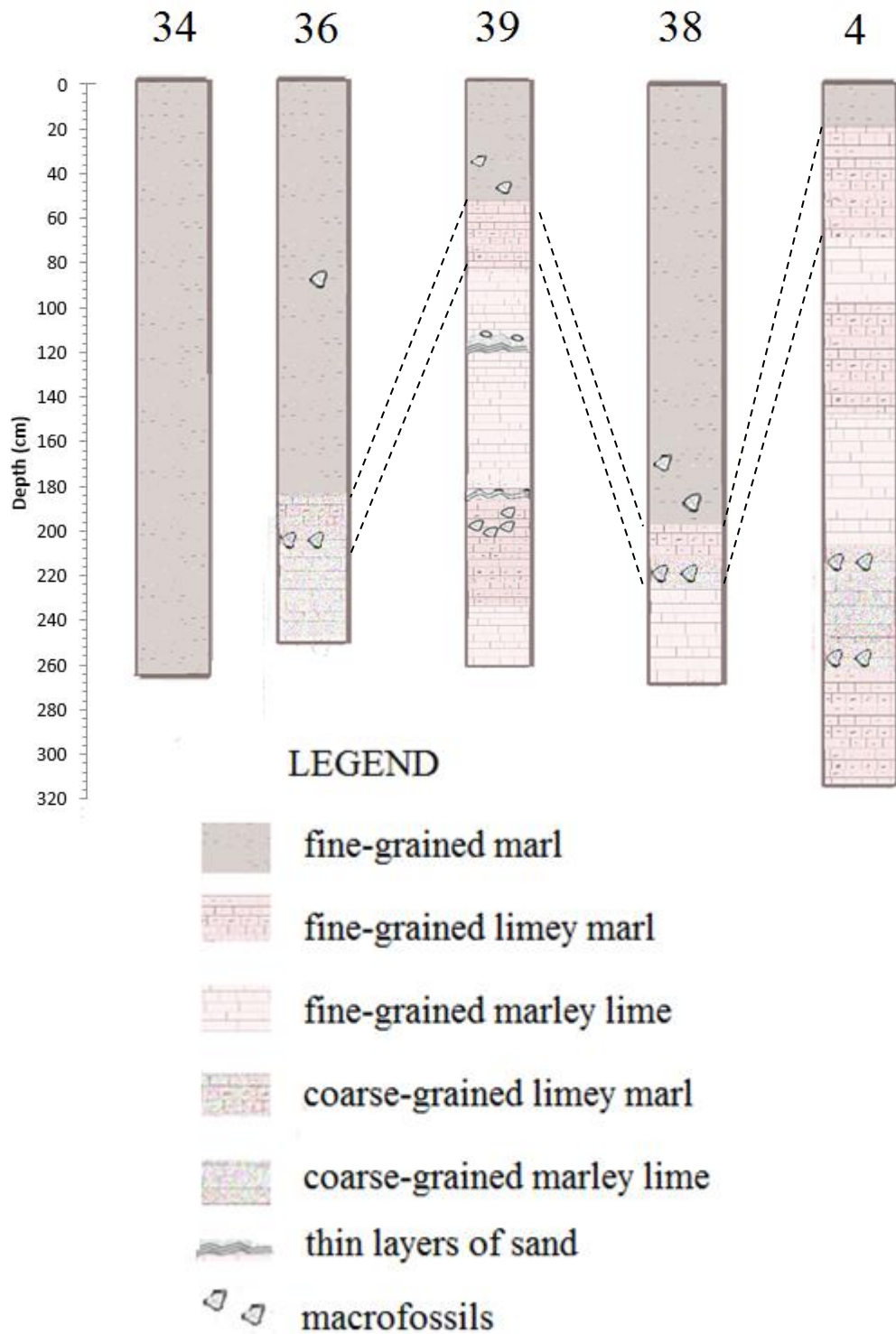
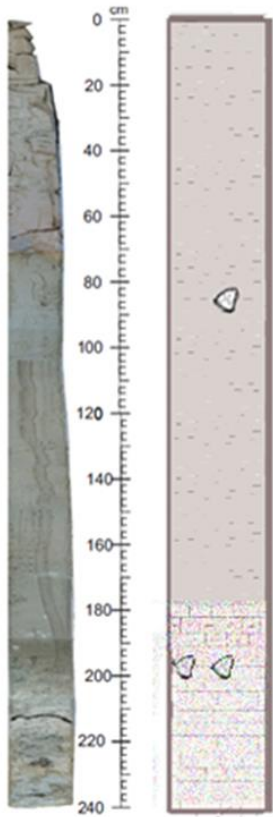


Fig23 Plots with the primary facies of the long cores based on their carbonate-clay composition

SAR36

LITHOFACIES



Facies I (0-180cm): fine grained marl

T Facies II (180-216cm): mostly coarse grained limey marl with macrofossils

Facies III (216-239cm): heavily bioturbated coarse grained marley lime

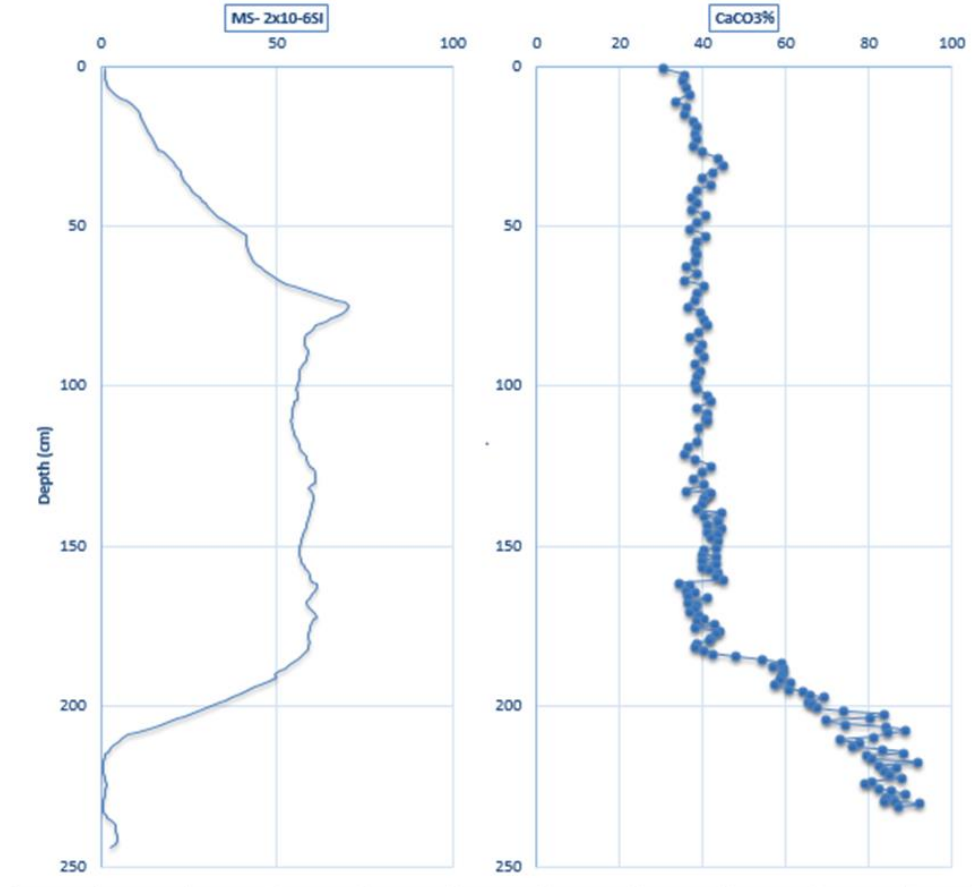


Fig.24a SAR36 facies based on carbonate-clay mixture

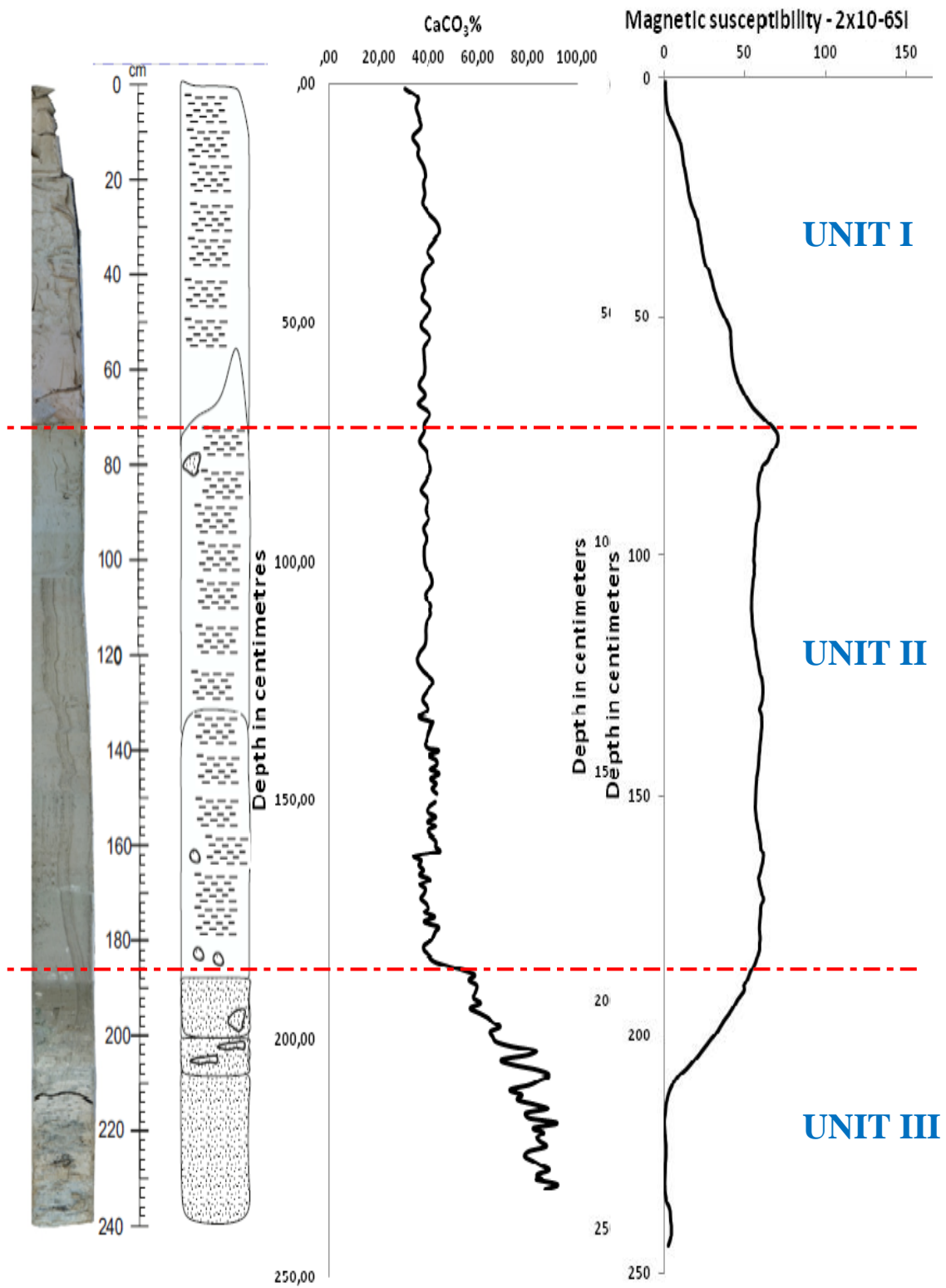


Fig.24b SAR36 subunits based on carbonate content-MS relationship

CORE I.D.		
Name of the core	SAR36	
Latitude	lat 37,87432	lat 37.52'27.5520"N
Longitude	long 23,0505	long 23.3'1.8"E
Core Length	247cm	
Bottom Depth	123m	

Table 12 SAR36 Info

Detailed Description:

Unit I

Interval: 0 cm, to 70 cm

Depth: 123-193 mbsf (meters below seafloor)

Unit I (123-193 mbsf) is characterized as grayish yellow clay (Hue 2.5Y 7/2, according to standard soil color charts). Its carbonate values (clayey marl to marl, 30-45 wt%) are relatively low, while magnetic susceptibility seems to increase up to 70 (2×10^{-6} SI)

Unit II

Interval: 70 cm, to 189 cm

Depth: 193-312 mbsf

Unit II (193-312 mbsf) is basically light grey clay (Hue 7.5Y 7/2). However inside its lower section (285-288 mbsf and 308-312 mbsf) we find lighter-colored sand nodules (Hue 7.5Y 8/2 light gray). These nodules represent the final remnants of a more calcareous-rich depositional environment, as we will see. Nevertheless, both magnetic susceptibility and CaCO₃ content remains relatively constant through this interval.

Unit III

Interval: 189 cm to 239 cm

Depth: 312-362 mbsf

Unit III is entirely bioturbated coarse-grained sand, rich in bivalves and calcareous algae, demonstrating a totally different environment. Also colors of

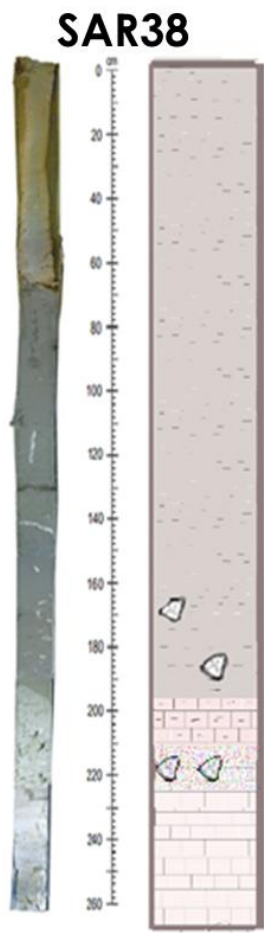
this interval seem paler (Hue 7.5Y 8/2 light gray) Obviously, CaCO_3 % shows a sharp increase, exceeding 90% at the lowest part of the core (from marl to pure lime) while at the same time magnetic susceptibility is diminished.

Comments: It seems that the long core retrieved nearest the western shores of Megara Basin sustains more allogenic characteristics (Unit I and II) than usual till the depth of -312mbsf where a transition to typical carbonate authigenic minerals (Unit III) is observed. Most of the core is dominated by clays only the interval 189 to 239 cm (Unit III) seem to record significant carbonate deposition. Furthermore this section does not resemble the typical aragonite-dominated sequence the other cores record, rather than a transitional deposit correlating with marine transgression, being consisted mostly by highly bioturbated coarse-grained marl.



Fig.25 Photos of SAR36 (a. nodules within marl (facies I), b. transitional facies II, c. heavily bioturbated marley lime)





LITHOFACIES

Facies I (0-198cm): brown gray to grayish olive fine grained marl with some nodules. The bottom of the layer is rich in Turitellas.

T.Facies II (198-225cm): fine grained limey marl to coarse-grained marley lime, rich in Turitellas

Facies III (225-261cm): fine grained pure lime

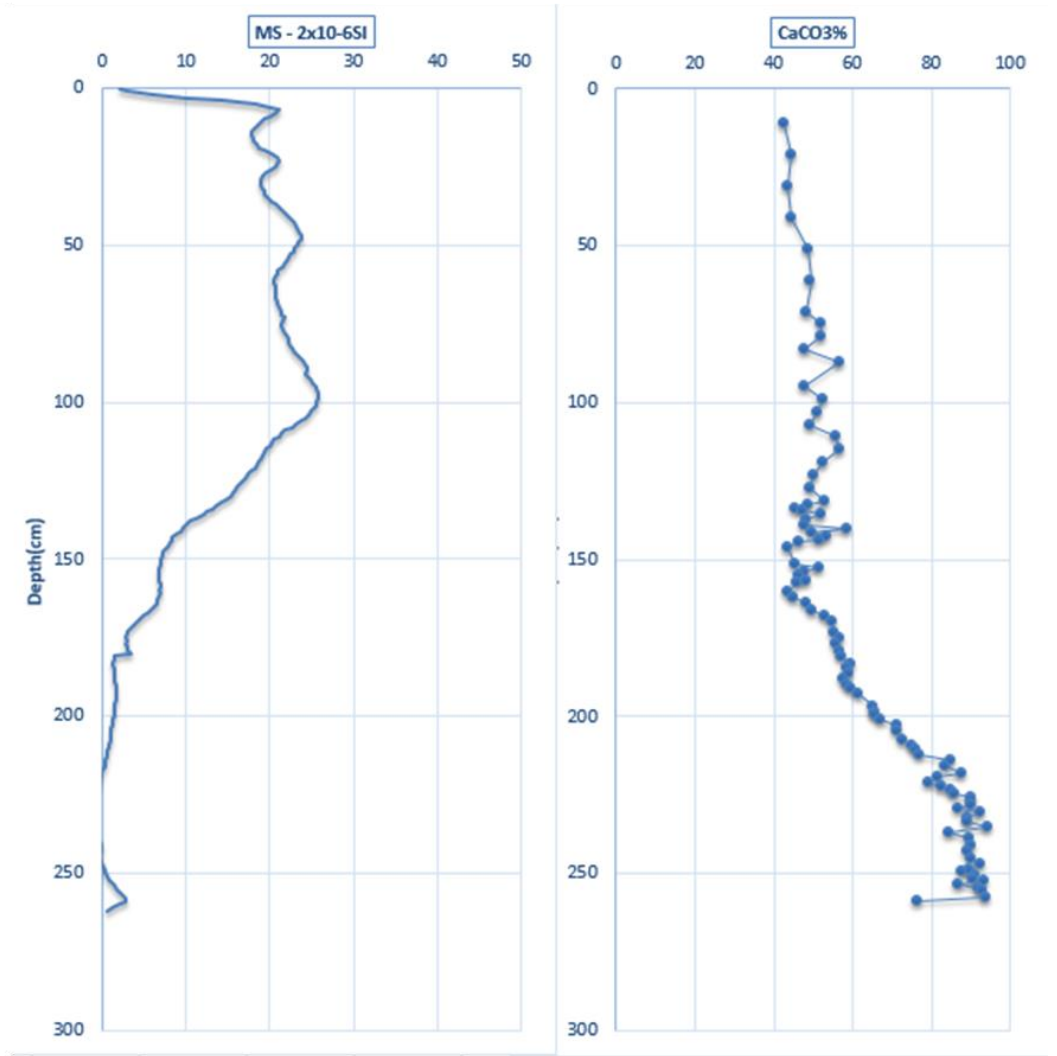


Fig.26a SAR36 facies based on carbonate-clay mixture

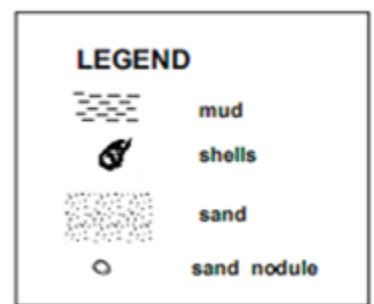
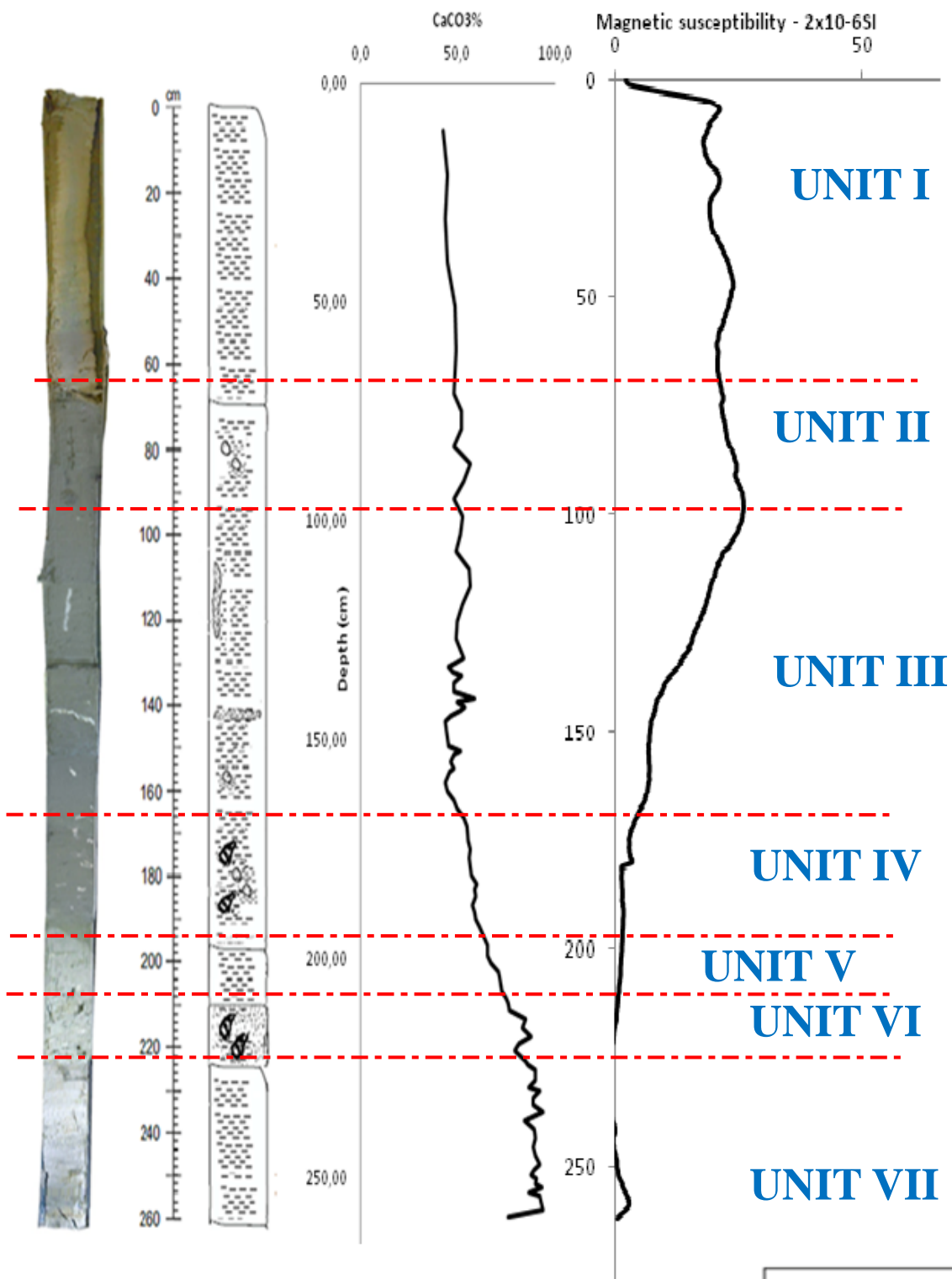


Fig.26b SAR38 subunits based on carbonate content-MS relationship

CORE I.D.	
Name of the core	SAR38
Latitude	lat 37°54'47.90"N
Longitude	long 23°15'49.26"E
Core Length	262cm
Bottom Depth	124m

Table 13 SAR38 Info

Detailed Description:

Unit I/ Interval: 0 cm to 70 cm/ Depth: 124-194 mbsf

Unit I (124-194 mbsf) is characterized as yellowish brown clay (Hue 2.5Y 5/4). Its carbonate values are around (marl) 42-51 wt%, while magnetic susceptibility seems to increase up to 20-23 (2×10^{-6} SI)

Unit II/ Interval: 70cm to 100 cm/ Depth: 194-224 mbsf

Unit II seems to sustain the same carbonate and magnetic susceptibility values, even though the color changes. Unit II has a grayish olive color (Hue 7.5Y 5/2). Also inside the clay are found CaCO_3 -rich sand modules.

Unit III/ Interval: 100cm to 165 cm/ Depth: 224-289 mbsf

Unit III differs from Unit II only on the fact that magnetic susceptibility seems to decrease in a steady pace.

Unit IV/ Interval: 165cm to 198 cm/ Depth: 289-322 mbsf

Unit IV seems to be the extension of Unit III with the only difference that this interval is rich in fossils, such as Turitellas, while also an increase of the CaCO_3 content up to 65% (marl) is observed. Magnetic susceptibility has at this point insignificant values

Unit V/ Interval: 198 cm to 210 cm/ Depth: 322-334 mbsf

Unit V demonstrates a transition. It is characterized as light olive gray clay (Hue 2.5GY 7/1). CaCO_3 continues to increase, reaching 77%(limey lime) while magnetic susceptibility is totally diminished.

Unit VI/ Interval: 210 cm to 225 cm/ Depth: 334-349 mbsf

Unit VI is light olive gray sand (Hue 2.5 GY 7/1) rich in Turitellas. Up to this point CaCO₃ has reached 90% (marley lime) while magnetic susceptibility remains irrelevant.

Unit VII/ Interval: 225 cm to 261 cm/ Depth: 349-385 mbsf

This last interval differs both in grain size, being clay rather than sand and color being paler (Gue 7.5Y 8/2). This light gray clay demonstrates also a peculiar minor increase in magnetic susceptibility even though it maintains its high CaCO₃ values (>90%) (pure lime)

Comments: Two Turitellas-dominated benthic communities are recorded within Unit IV and Unit VI, with the latter being within the only interval represented by a mud phase, supporting the statement that aragonite starts to decrease with the introduction of new water masses into Megara basin, due to significant rise of the sea level. These marine gastropod mollusks seem to be gathered only in the transitional phase based on their absence from the most recent sediments, as the reconnection of the Megara Basin with the open sea had already been established by that time.

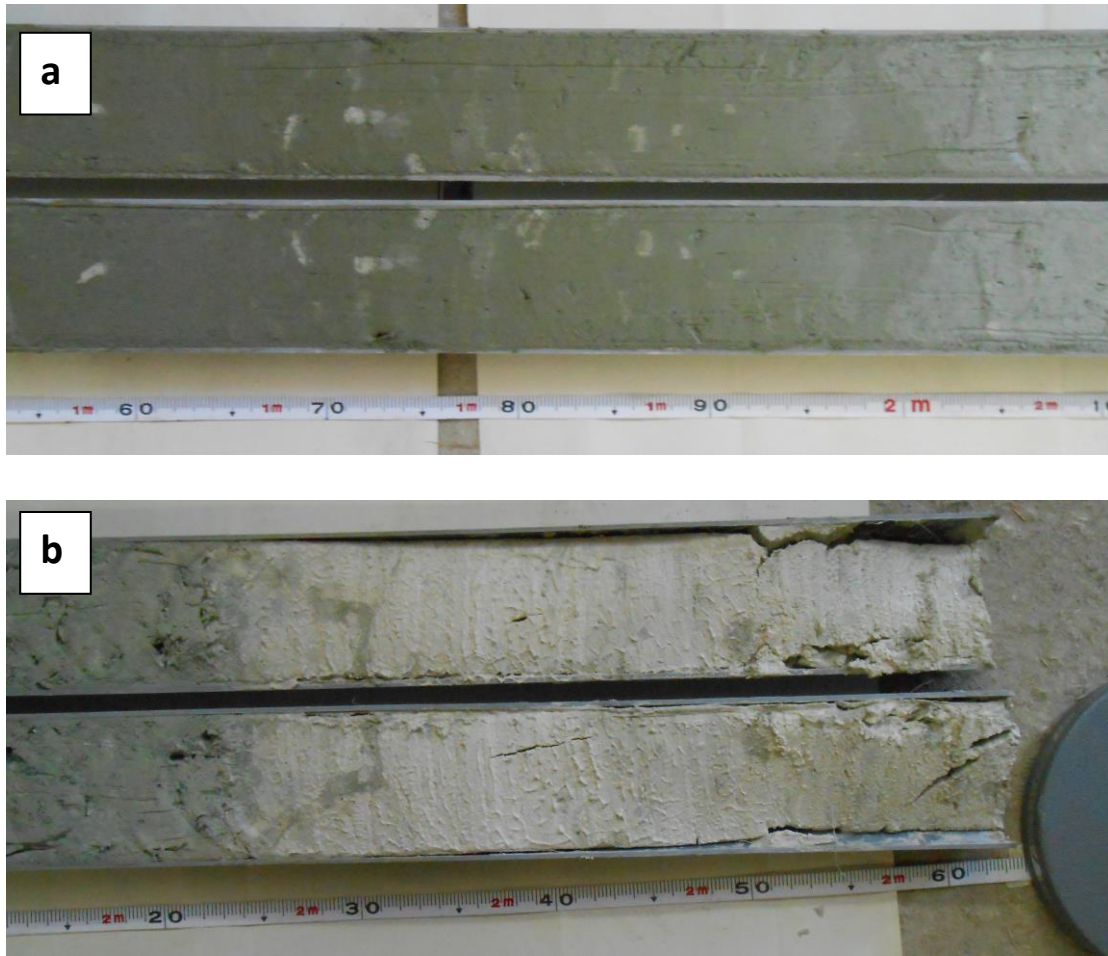


Fig.27 photos of SAR38 (a. facies I-facies II b. facies II-facies III)

SAR39

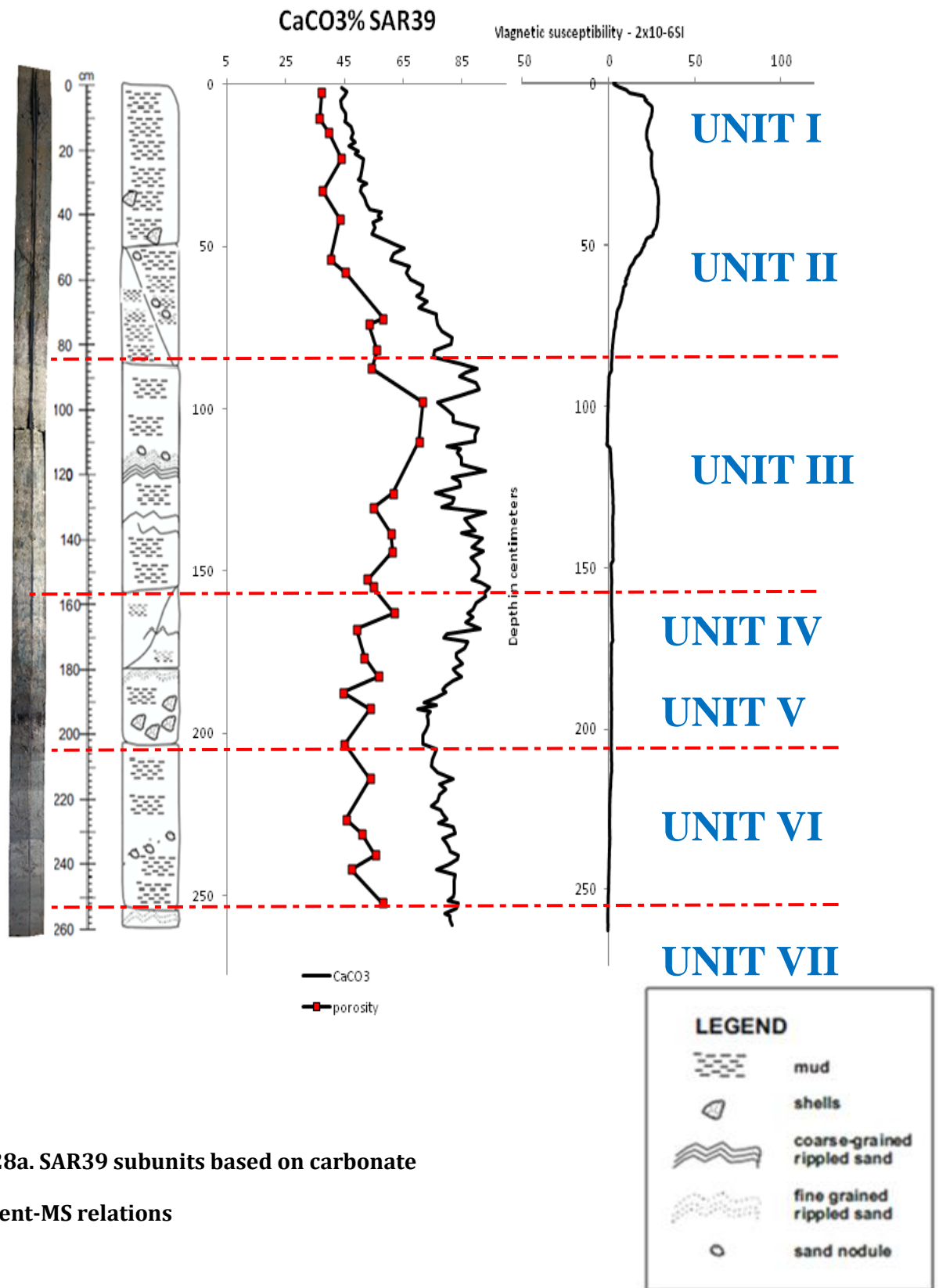


Fig.28a. SAR39 subunits based on carbonate content-MS relations

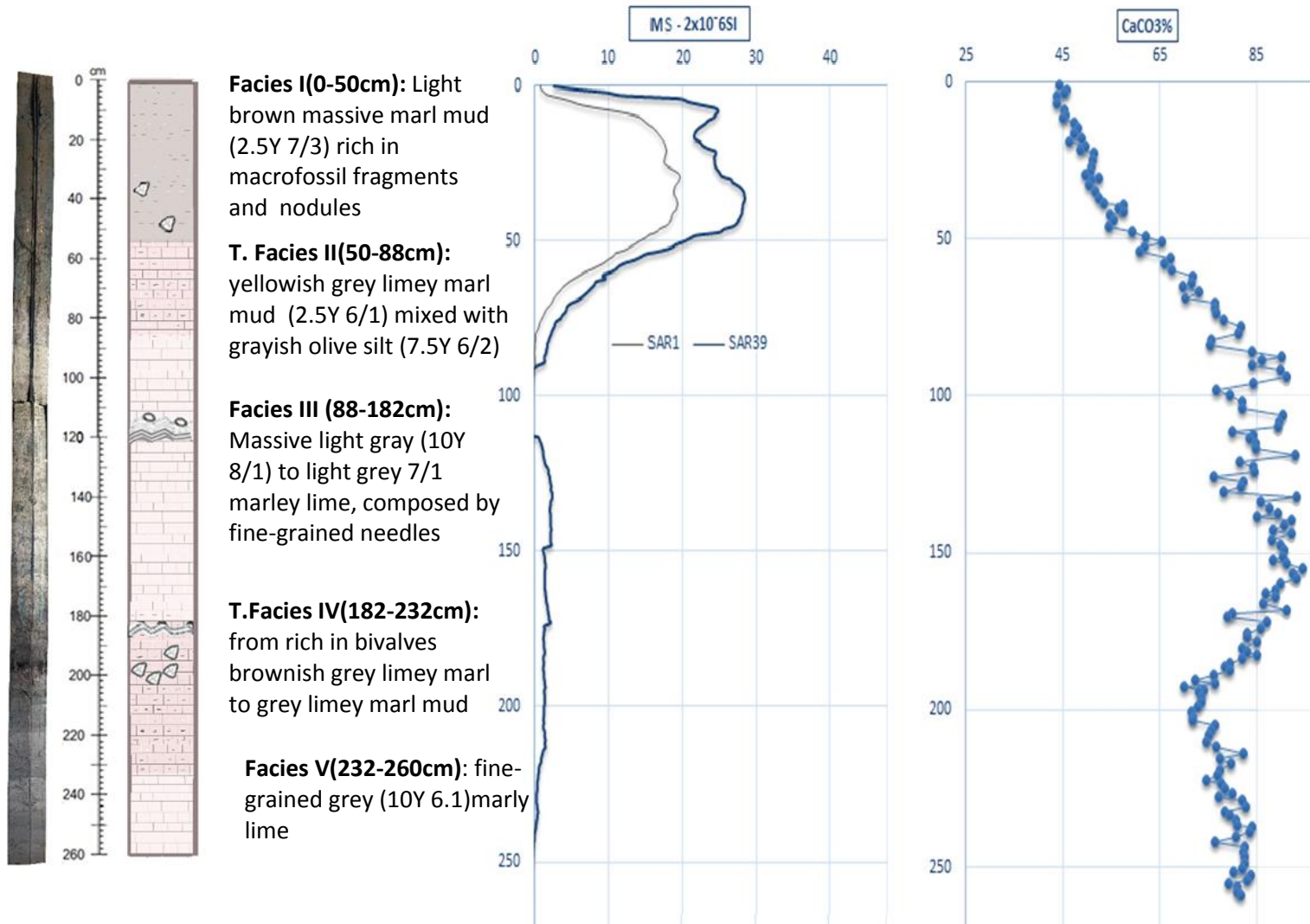


Fig.28b SAR39 facies based on carbonate-clay mixture

CORE I.D.	
Name of the core	SAR39
Latitude	lat 37,87731/ long 23,2611
Longitude	lat 37.52'38"N / long 23.15'40"E
Core Length	260cm
Bottom Depth	140m

Table 14. SAR39 Info

Detailed Description of SAR39

Unit I/ Interval: 0 cm, to 50 cm/ Depth: 140-190 mbsf

Unit I (140-190 mbsf) is characterized by light colors (2.5Y 7/3) and consistently high carbonate values (marl 45-65 wt%) that are directly related to the high content of macrofossil fragments. The unit is also characterized by low magnetic susceptibility values (2×10^{-6} to 30×10^{-6} SI).

Unit II/ Interval: 50 cm, to 85 cm/ Depth: 190-225 mbsf

Unit II (190-225 mbsf) is characterized by a mixture of yellowish grey mud (2.5Y 6/1) and grayish olive silt (7.5Y 6/2). Sand nodules are also observed within the latter. The unit is also characterized by a sharp decrease of magnetic susceptibility values from 20×10^{-6} to 1×10^{-6} SI while at the same time carbonate values increase from 65 to 85 wt% limey marl to marley lime).

Unit III/ Interval: 85 cm, to 158 cm/ Depth: 225-298 mbsf

Unit III (225-298 mbsf) is light gray marley lime mud (10Y 8/1) due to its consistently high carbonate values (85-95% marley lime to pure lime). **Thin layers of sand coupled with nodules are also observed.** Magnetic susceptibility is diminished and remains that way through all the rest of the core

Unit IV/ Interval: 158 cm, to 192 cm/ Depth: 298- 332mbsf

Unit IV (298-332 mbsf) is characterized by a mixture of light grey 7/1 lime and brownish grey 10YR 6/1 mud. The latter corresponds to the layer bellow. Carbonate content seems to start to decrease again (from lime to limey marl). No magnetic minerals are observed. Again near the lowest point **a thin layer of sand is observed**

Unit V/ Interval: 192 cm, to 203 cm/ Depth: 332-343 mbsf

Unit V (332-343 mbsf) is characterized by a distinguished brownish grey 10YR 6/1 limey marl, rich in bivalves of the genus *Chlamys*. No change in carbon content or MS is observed.

Unit VI/ Interval: 203 cm, to 252 cm/ Depth: 343-392 mbsf

Unit VI (343-392 mbsf) is characterized by grey 10Y 6/1 mud. Some sand nodules are found. Carbonate content seems to increase again, as the paler color of this layer indicates (from limey marl to marley lime)

Unit VII/ Interval: 252 cm, to 260 cm/ Depth: 392-400 mbsf

Unit VII (392-400 mbsf) is characterized by light brownish grey 5Y 7/2 sand. Carbon content remains high (85%), while magnetic minerals remain absent.

Comments:

Most of the sediment is mud with the exception of the 135-120cm interval and the 180cm-170cm where thin beds of sand were observed, coupled with carbonate content changes. Moreover from the 135 cm depth to the 120cm occurs a transition from coarse-grained to fine-grained sand (marine transgression), while in the deeper interval the opposite phenomenon is observed (marine regression?). Basically these two intervals define the limits of the aragonite-dominated sequence. Sand facies represent environmental changes e.g. rise of the sea level ([Lykousis et al. 1993](#)). Furthermore the bottom layer is also consisted of coarse-grained sand. SAR39 is the only piston core that records two transitional facies if not three (including last section) making him the most well documented core, regarding the evolution of the Megara Basin. Also, regarding the fossils in the SAR39 most impressive is the presence of medium-sized bivalves (>2cm) of the genus *Chlamys*, observed in brownish-grey mud, at depths between 180 and 203cm. One of the specimens was dated, by using C^{14} at approximately 16.935 ka \pm 50 yrs. Finally, porosity seems to be consistent at all times to the TIC trend.



Fig.29 Photos of SAR39 a.calcite-dominated sequence b. upper aragonite sequence c.d. thin layers of sand show possible marine transgression e. transitional facies (brownish) between the two aragonite sequences

SAR4

LITHOFACIES

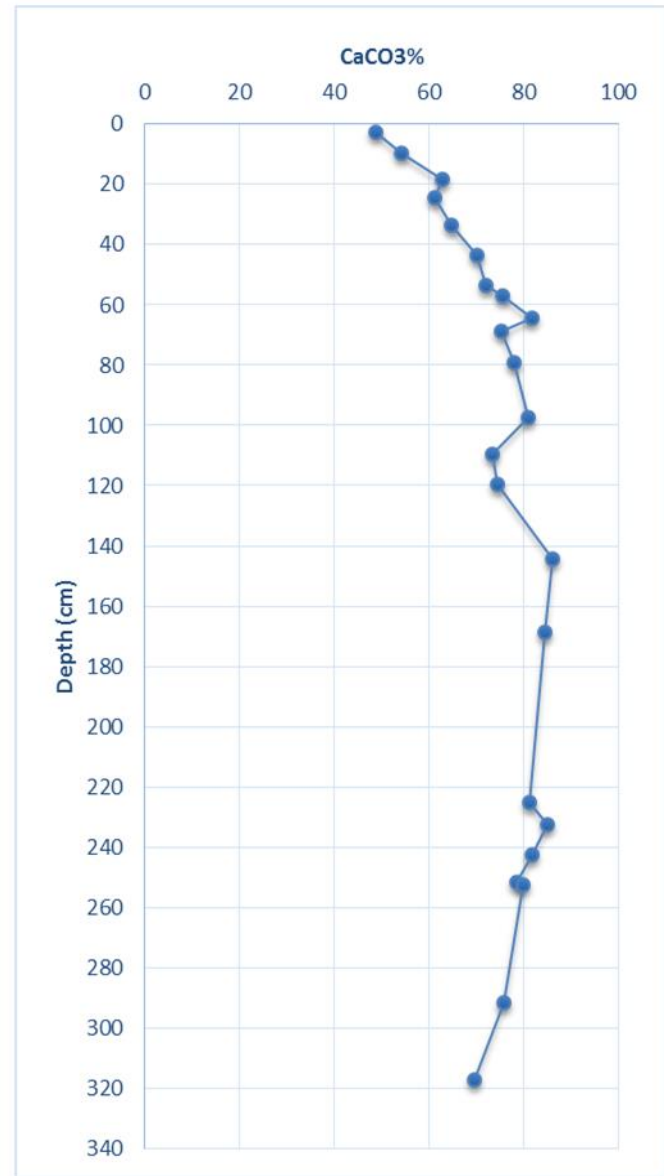
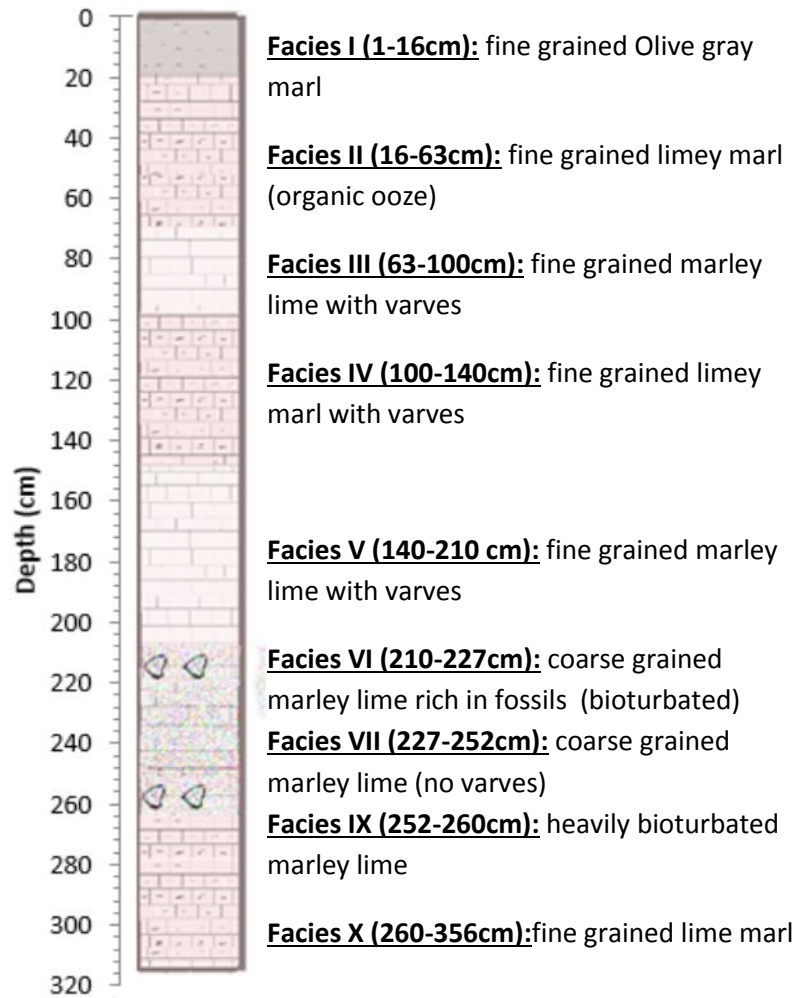


Fig.30 SAR4 facies based on carbonate-clay mixture

CORE I.D.	
Name of the core	SAR4
Latitude	lat 37°52'04"
Longitude	long 23°14'6.6"
Core Length	318cm
Bottom Depth	182m

Table 15. SAR4 Info

Detailed Description of SAR4

Unit I/ Interval 0-16cm/ Depth: 182-198mbsf

Olive gray marl 10Y 4/2 (48-54%)

Unit II/ Interval 16-63cm/ Depth: 198-245mbsf

organic ooze 7.5 GY 7/1-6/1 (light greenish gray to greenish gray) marl (55-75%)

Unit III/ Interval 63-227cm/ Depth: 245-409mbsf

Limey marl to marley lime 75-85%) varved interval alteration of 5GY 6/1 (olive gray) and 7.5 GY 8/1 (ligh greenish gray)

1 to 2.5 mm unit varves less

210-227 hype bioturbated at 162 to 202cm

Unit IV/ Interval 227-252cm/ Depth: 409-434 mbsf

Marley lime 81-84%) coarse-grained no varves 5 GY 8/1 to 7/1 (light gray to light olive gray)

Unit V/ Interval 252-260 mbsf

Heavily bioturbated 2.5 GY 8/1 light gray (Limey marl 79%)

Unit VI/ Interval 260-312 mbsf

Varving black stain

Limey marl 76%) 2.5 GY 7/1 (light olive gray) and 5GY 7/1

Unit VII/ Interval 312-322 mbsf

Limey marl (70%) Black stain 10BG 7/1-6/1 light bluish gray

Unit VIII/ Interval 322-356 mbsf

Limey marl (70%) 5BG 7/1 (light bluish gray) – 10BG 7/1 (light bluish gray)

Comments: Sadly most of the data about this core (photos of the core, log, MS values, a great amount of samples) are lost. Apart from this detailed description and the estimations of the carbonate content of few survived sumples no other

info is preserved. The choice of using these data was simply due to the fact that SAR4 and SAR39 were retrieved very close to each other.

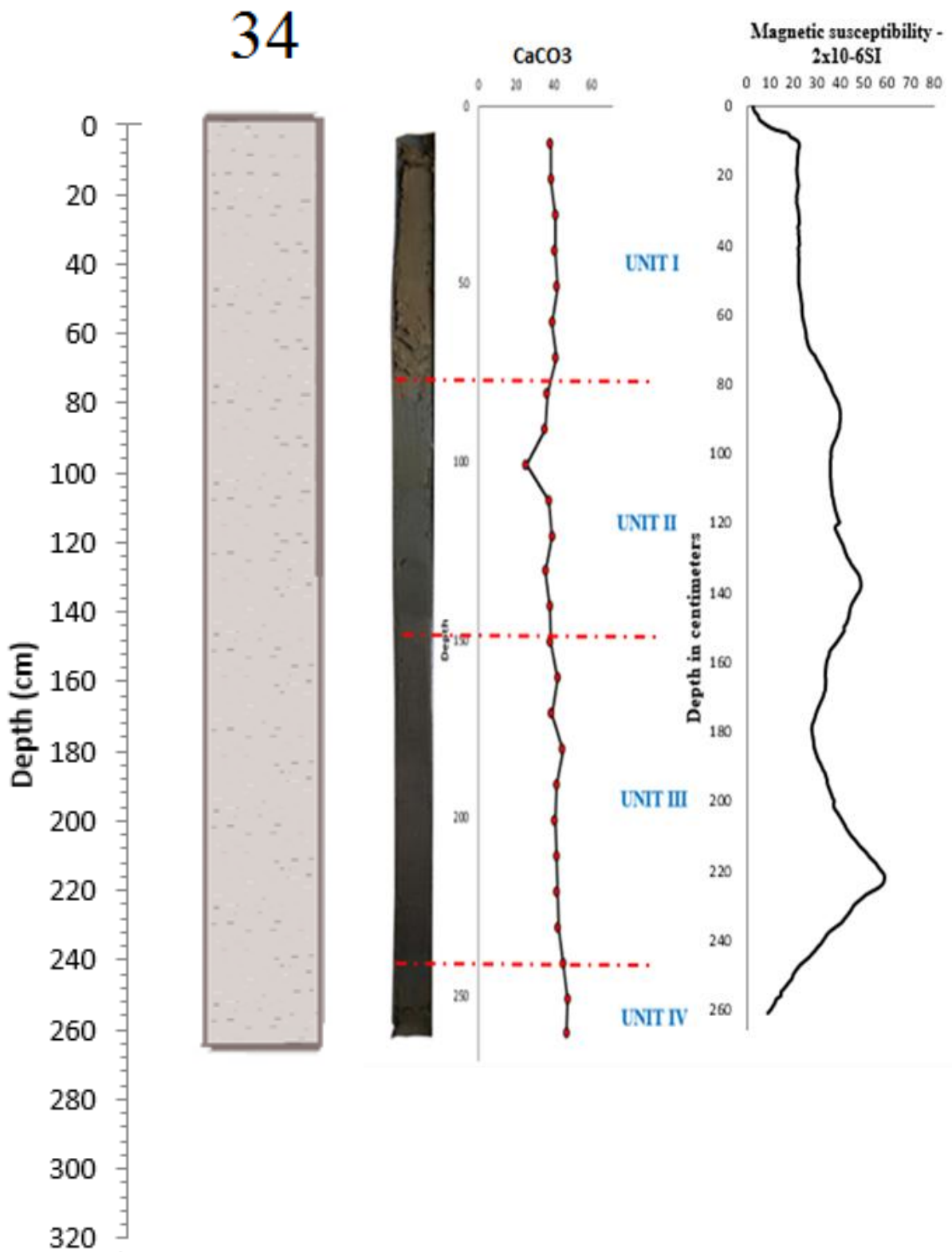


Fig. 31 SAR34 based on carbonate content-MS relationship (one facies, marl is present, SAR34 represents typical marine environment)

CORE I.D.	
Name of the core	SAR34
Latitude	lat 37,87866
Longitude	long 23,13065
Core Length	263cm
Bottom Depth	230m

Table 16. SAR34 Info

Detailed Description of SAR34

Unit I/ Interval 0-71cm/ Depth: 230- 301mbsf

Yellowish Brown marl 10YR 5/4

Unit II/ Interval 71-150cm/ Depth: 301-380 mbsf

Grayish olive marl 7.5Y 4/2. At 100cm carbonate content decreases sharply (25%) and then increases again.

Unit III/ Interval 150-246cm/ Depth: 380-476 mbsf

Grayish olive marl 7.5Y 4/2. Organic matter in discontinuous patches is present. MS values reach their highest point and then start to decrease.

Unit IV/ Interval 246-263cm/ Depth: 476-493 mbsf

Grayish yellow brown marl 10YR 5/2, An unconformity is present. MS values reach their lowest point. Carbonate content remains constant.

Comments: Regarding core SAR34 there is not much to mention. This core did not reach any transitional deposit to any carbonate facies. The whole core is basically one marl layer (40-50%). Regardless the visual homogeneity of the core we classified it into 4 Unit based on color. Other than that both the carbonate content and the MS values seem relatively constant with the exception of a decrease of the latter near the bottom layer. Also an unconformity observed in the lowest layer might indicate that the piston core might just missed the transitional deposit.

4.3 XRD ANALYSES

Methodology

X-ray powder diffraction is a rapid analytical technique primarily used for phase identification of a crystalline material and can provide information on unit cell dimensions. The method is based on constructive interference of monochromatic X-rays and a crystalline sample that is finely ground and homogenized (avoiding the orientation of the particles, as possible).

These diffracted X-rays are then detected, processed and counted. Conversion of the diffraction peaks to d-spacing allows identification of the mineral because each mineral has a set of unique d-spacings. Typically this is achieved by comparison of d-spacing with standard reference patterns.

The evaluation of the exported diagrams is then conducted computationally by X'Pert Highscore Plus Panalytical, softwares and graphically according to the calibration curves.

36 powdered samples from the long-piston core SAR39, 22 from the SAR4 and 20 samples from the SAR36 were prepared and analyzed on a SIEMENS D5000 X-ray diffractometer, which lies in the X-Ray Diffraction Unit of the Laboratory of Economic Geology and Geochemistry, (Department of Geology and Geoenvironment), NKUA. (Fig.24). All samples were scanned two times. XRD was carried out using CuK α radiation on unoriented powder specimens. Since no oriented powder specimens were run, no attempt has been made to quantify clay minerals, they were only recorded.

All samples were scanned from 5° to 36° 2 θ and from 25° to 34° 2 θ . Identification of minerals and determination of their abundances was based on peak height and peak area relative to the displacement of the (101) quartz reflection at approximately 26.669° 2 θ . The position of the d₍₁₀₄₎ calcite peak was determined at 29.45°±0.02 2 θ , the d₍₁₀₄₎ dolomite peak position at >30.79° 2 θ , and the two aragonite peaks at 26.22° and 27.22° 2 θ , respectively. The (112) high-magnesium calcites were defined as having 2 θ values >29.7 °The

MgCO₃-content of the Mg-calcite and the composition of the dolomite were determined by the shift of the (104) peak of calcite and of dolomite, respectively using the position of the (101) peak of quartz as an internal standard.



Fig. 32 SIEMENS D5000 X-ray diffractometer

For the determination of total inorganic carbon samples were dried (40°C) and ground to a size of less than 40 µm. The most important species of carbon are inorganic carbon (TIC), organic carbon (TOC) and sometimes black carbon (EC). In all international standards the TIC determination is performed by acidification and detection of the resulting CO₂. However, this method has certain disadvantages. For instance, some carbonates offer strong resistance against acid digestion like Magnesite (MgCO₃) or Dolomite (CaMg(CO₃)₂). Furthermore, not only the mineral influences the digestion of the carbonates with acid, organic

matter also may have an impact. The most common acid to remove the TIC is HCl. HCl is a non-oxidising acid and destruction of organic matter by HCl is not likely, although not impossible.

The proportions of carbonate minerals were calculated using the total TIC determined by high precision manometer after HCl treatment. The precision of this method is $\pm 5\%$ by weight.

For the determination of total carbonate and for x-ray diffraction analysis samples were dried (40°C) and ground to a size of less than $40\ \mu\text{m}$

X-ray analysis was made with unoriented powder specimens with a scanning speed of $1^{\circ} 20/\text{min}$; when Mg-calcite ($>4\ \text{mol-}\%$ MgCO_3) was present, scanning speed was reduced to $1/2^{\circ} 20/\text{min}$ to obtain better resolution.

The ratios of aragonite, calcite, and Mgcalcite were determined by measuring peak areas of the different carbonate minerals and calculated using calibration curves published elsewhere (*Müller and Müller, 1967; Müller, 1969*) (**Fig33**). The calcite-dolomite ratio was determined after the method described by *Tennant and Berger (1957)* (**Fig.26**)

The proportions of carbonate minerals were calculated using the inorganic carbon determined by the LECO-method and by the ratios obtained by X-ray diffraction. The precision of this method is $\pm 5\%$ by weight. The MgCO_3 -content of the Mg-calcite and the composition of the dolomite were determined by the shift of the (104) peak of calcite and of dolomite, respectively (*Goldsmith and Graf, 1958; Füchtbauer and Goldschmidt, 1965*) using the position of the (101) peak of quartz as an internal standard. Many samples contain both stoichiometric dolomite (Ca_50Mg_50) and Ca-dolomite (usually $\text{Ca}^{\wedge}\text{Mg}^{\wedge}$), the latter being more frequent and abundant. The proportions of quartz, K-feldspar, plagioclase, gypsum, anhydrite, and pyrite were estimated by their peak heights assigning arbitrary symbols for their abundance.

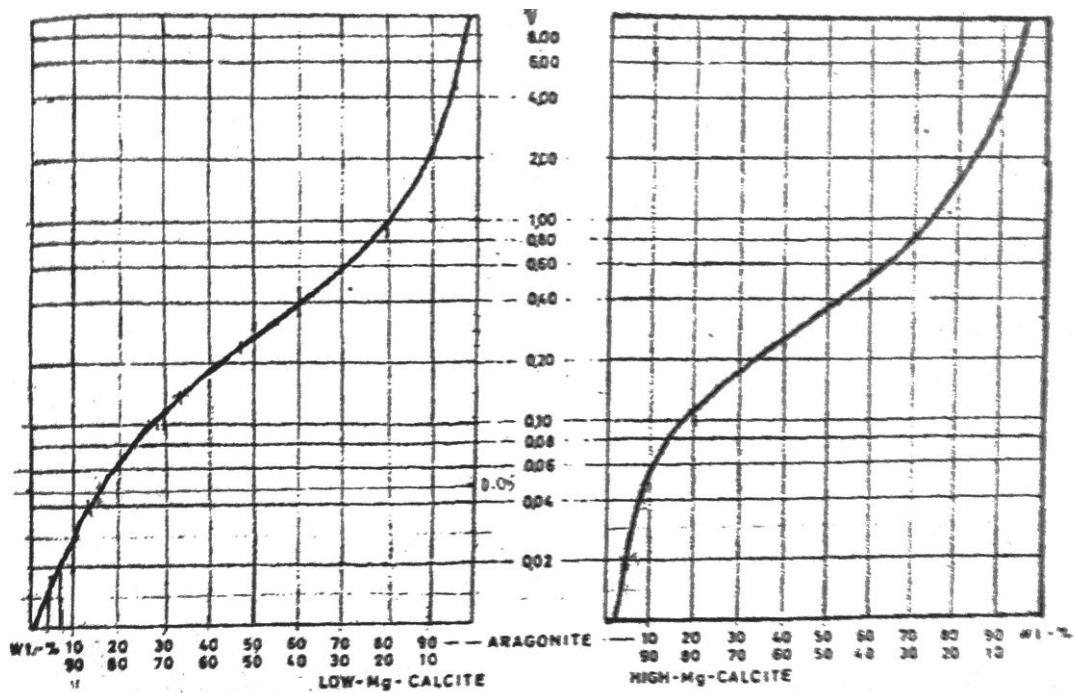


Fig. 33 Calibration curves for the determination of relative percentages of aragonite and calcite i.e. aragonite and high-magnesian calcite (Obtained from Muller and Muller, 1967).

The ratios of aragonite, calcite, and Mg-calcite were determined by measuring peak areas of the different carbonate minerals and calculated using calibration curves published elsewhere (Müller and Müller, 1967; Müller, 1969).

Relative % Aragonite was determined by using calibration curves for

$$\frac{\text{Peak Area of Aragonite}}{\text{Peak Area of low - Mg Calcite}} \quad (\text{Müller \& Müller, 1967; Müller, 1969})$$

Relative % low - Mg Calcite = 1 - Relative % Aragonite

$$\text{Ratio} \frac{\text{Aragonite}}{\text{low - Mg Calcite}} = \frac{\text{Relative \% Aragonite}}{\text{Relative \% low - Mg Calcite}}$$

$$\frac{\text{Peak Area of Aragonite}}{\text{Peak Area of high - Mg Calcite}}$$

Relative % high – Mg Calcite = 1 – Relative % Aragonite

$$\text{Ratio} \frac{\text{Aragonite}}{\text{high – Mg Calcite}} = \frac{\text{Relative \% Aragonite}}{\text{Relative \% high – Mg Calcite}}$$

The calcite-dolomite ratio was determined after the method described by *Tennant and Berger (1957)*.

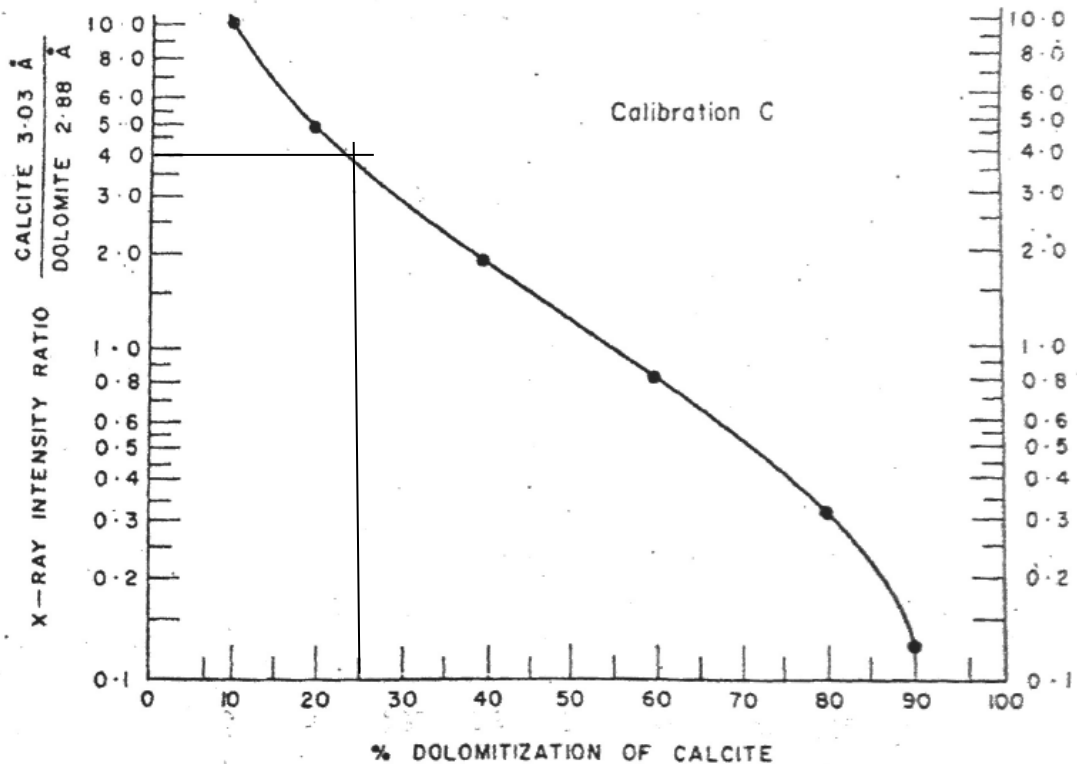


Fig. 34 Calibration curve of % dolomitization versus the intensity ratio of calcite and dolomite peaks. (Obtained from Tennant and Berger, 1957)

Relative % low – Mg Calcite was determined by using calibration curves for

$$\frac{\text{Peak Area of low – Mg Calcite}}{\text{Peak Area of Dolomite}} \quad (\text{Tennant \& Berger, 1957})$$

Relative % Dolomite = 1 – Relative % low – Mg Calcite

$$\text{Ratio} \frac{\text{low – Mg Calcite}}{\text{Dolomite}} = \frac{\text{Relative \% low – Mg Calcite}}{\text{Relative \% Dolomite}}$$

$$\begin{aligned}
 & \text{Low - Mg Calc}\% \\
 & = \frac{TIC \times 100}{\text{Ratio} \frac{Ar}{\text{low - Mg Calc}} + \left(\frac{\text{Ratio} \frac{Ar}{\text{low - Mg Calc}}}{\text{Ratio} \frac{Ar}{\text{high - Mg Calc}}} \right) + 1 + \left(\frac{1}{\text{Ratio} \frac{\text{low - Mg Calc}}{Dol}} \right)} \\
 & \text{Aragonite}\% = \text{Ratio} \frac{\text{Aragonite}}{\text{low - Mg Calcite}} \times \text{Low - Mg Calc}\%
 \end{aligned}$$

$$\text{High - Mg Calc}\% = \frac{\text{Aragonite}\%}{\text{Ratio} \frac{\text{Aragonite}}{\text{high - Mg Calcite}}}$$

$$\text{Dolomite}\% = \frac{\text{Low - Mg Calc}\%}{\text{Ratio} \frac{\text{low - Mg Calcite}}{\text{Dolomite}}}$$

The Carbonate Factory Over The Last 20.000 Yrs In The Nw Saronikos Gulf

SAR4 samples	Depth (cm)	Aragonite/ Low Mg- Calcite	Aragonite/ High Mg- Calcite	Calcite/ Dolomite	Low Mg Calcite%	Aragonite%	High Mg- Calcite%	Dolomite%	TC%
2-3	2.50	1.00	1.94	24.00	19.00	19.00	9.79	0.79	48.59
9-10	9.50	1.44	2.13	24.00	17.10	24.61	11.58	0.71	54.00
18-19	18.50	2.13	2.85	7.70	15.69	33.34	11.71	2.04	62.78
24-25	24.50	3.00	3.76	10.11	12.51	37.54	9.98	1.24	61.27
33-34	33.50	2.85	4.56	15.67	14.27	40.61	8.91	0.91	64.70
43-44	43.50	5.67	11.50	7.33	9.59	54.34	4.73	1.31	69.97
53-54	53.50	10.11	10.11	7.70	5.87	59.39	5.87	0.76	71.91
56-57.5	57.00	11.50	9.00	6.69	5.41	62.26	6.92	0.81	75.40
64-65	64.50	49.00	32.33	4.00	1.58	77.30	2.39	0.39	81.67
68-69	68.50	39.00	32.33	2.45	1.81	70.56	2.18	0.74	75.29
78-80	79.00	39.00	34.71	4.88	1.89	73.58	2.12	0.39	77.98
97-98	97.50	99.00	39.00	5.25	0.79	77.95	2.00	0.15	80.88
109.5-110	109.75	99.00	99.00	3.00	0.72	71.75	0.72	0.24	73.44
119-120	119.50	199.00	99.00	1.27	0.37	72.94	0.74	0.29	74.33
144-145	144.50	249.00	199.00	1.63	0.34	85.15	0.43	0.21	86.13
168-169	168.50	499.00	199.00	1.22	0.17	83.78	0.42	0.14	84.50
224-225.5	225.00	24.00	499.00	4.88	3.22	77.29	0.15	0.66	81.32
232-233	232.50	13.29	11.50	5.25	5.43	72.18	6.28	1.03	84.92
242-243.5	242.75	10.11	15.67	7.33	6.87	69.42	4.43	0.94	81.65
251-252.5	251.75	5.25	10.11	5.67	11.30	59.31	5.87	1.99	78.47
252-253	252.50	6.69	11.50	15.67	9.58	64.13	5.58	0.61	79.90
291-292	291.50	7.33	11.50	6.69	8.31	60.93	5.30	1.24	75.77

Table 17. Empirical Estimation of the CO₃²⁻% participation in each carbonate mineral for SAR4

The Carbonate Factory Over The Last 20.000 Yrs In The Nw Saronikos Gulf

SAR36 samples	Depth (cm)	Aragonite/ Low Mg- Calcite	Aragonite/ High Mg- Calcite	Calcite/ Dolomite	Low Mg Calcite%	Aragonite%	High Mg- Calcite%	Dolomite%	TC%
2-4	3	1.00	1.94	24.00	14.00	14.00	7.21	0.58	35.80
24-26	25	1.44	2.13	24.00	11.94	17.18	8.08	0.50	37.70
30-32	31	2.13	2.85	7.70	11.20	23.79	8.36	1.45	44.80
66-68	67	3.00	3.76	10.11	7.31	21.93	5.83	0.72	35.80
68-70	69	2.85	4.56	15.67	8.95	25.48	5.59	0.57	40.60
120-122	121	5.67	11.50	7.33	4.88	27.65	2.40	0.67	35.60
124-126	125	10.11	10.11	7.70	3.44	34.77	3.44	0.45	42.10
160-161	161	11.50	9.00	6.69	3.22	36.99	4.11	0.48	44.80
161-162	162	49.00	32.33	4.00	0.66	32.37	1.00	0.17	34.20
181-182	182	39.00	32.33	2.45	0.92	35.80	1.11	0.37	38.20
186-187	187	39.00	34.71	4.88	1.43	55.68	1.60	0.29	59.00
199-200	200	99.00	39.00	5.25	0.64	63.80	1.64	0.12	66.20
202-203	203	99.00	99.00	3.00	0.83	81.77	0.83	0.28	83.70
204-205	205	199.00	99.00	1.27	0.34	68.30	0.69	0.27	69.60
207-208	208	249.00	199.00	1.63	0.35	87.69	0.44	0.22	88.70
216-217	217	499.00	199.00	1.22	0.16	80.11	0.40	0.13	80.80
217-218	218	24.00	499.00	4.88	3.65	87.53	0.18	0.75	92.10
224-225	225	13.29	11.50	5.25	5.05	67.06	5.83	0.96	78.90
227-228	228	10.11	15.67	7.33	7.48	75.58	4.82	1.02	88.90
228-229	229	5.25	10.11	5.67	12.09	63.49	6.28	2.13	84.00

Table 18. Empirical Estimation of the CO₃²⁻% participation in each carbonate mineral for SAR36

The Carbonate Factory Over The Last 20.000 Yrs In The Nw Saronikos Gulf

SAR39 samples	Depth (cm)	Aragonite/ Low Mg- Calcite	Aragonite/ High Mg- Calcite	Calcite/ Dolomite	Low Mg Calcite%	Aragonite%	High Mg- Calcite%	Dolomite%	TC%
6-8	7	0,25	0,54	6,14	23,39	5,85	10,86	3,81	43,91
14-16	15	0,28	0,33	19,00	25,75	7,26	21,79	1,36	56,15
26-28	27	0,43	0,53	19,00	22,21	9,52	18,07	1,17	50,96
34-36	35	0,54	0,56	11,50	15,79	8,50	15,11	1,37	40,78
47-49	48	1,63	2,85	24,00	18,29	29,84	10,48	0,76	59,37
53-55	54	1,50	3,00	6,14	19,23	28,85	9,62	3,13	60,83
70-71.5	70,75	4,71	5,25	9,00	11,18	52,71	10,04	1,24	75,18
75-77	76	15,67	11,50	5,67	4,16	65,13	5,66	0,73	75,68
99-101	100	99,00	49,00	1,44	0,77	76,55	1,56	0,54	79,43
107-109	108	99,00	99,00	0,75	0,88	86,64	0,88	1,16	89,55
123-125	124	99,00	49,00	1,38	0,82	81,55	1,66	0,60	84,64
135-137	136	24,00	32,33	4,00	3,37	80,95	2,50	0,84	87,67
157-159	158	99,00	39,00	3,35	0,91	89,68	2,30	0,27	93,15
162.5-163.5	163	99,00	49,00	3,35	0,85	84,02	1,71	0,25	86,83
171-173	172	15,13	11,50	8,09	3,77	57,11	4,97	0,47	66,32
181-182	181,5	13,29	27,57	6,14	5,56	73,91	2,68	0,91	83,06
186-187	186,5	7,33	4,88	32,33	7,94	58,25	11,93	0,25	78,36
192-193	192,5	6,41	9,00	6,14	8,45	54,16	6,02	1,38	70,00
200-201	200,5	7,47	19,00	6,14	7,93	59,29	3,12	1,29	71,64
206-207	206,5	10,36	11,50	49,00	6,16	63,80	5,55	0,13	75,62
209-211	210	8,09	11,50	32,33	7,60	61,46	5,34	0,23	74,63

Table 19. Empirical Estimation of the CO₃²⁻% participation in each carbonate mineral for SAR39

The Carbonate Factory Over The Last 20.000 Yrs In The Nw Saronikos Gulf

SAR39 samples	Depth (cm)	Aragonite/ Low Mg- Calcite	Aragonite/ High Mg- Calcite	Calcite/ Dolomite	Low Mg Calcite%	Aragonite %	High Mg- Calcite%	Dolomite %	TC %
211-213	212	11,20	13,29	6,14	5,81	65,05	4,90	0,95	76,70
216.5-218	217,25	11,05	7,33	6,14	5,81	64,17	8,75	0,95	79,67
223-224	223,5	10,49	11,50	11,50	6,22	65,30	5,68	0,54	77,74
224-226	225	8,09	13,29	8,09	7,99	64,66	4,87	0,99	78,50
233-234.5	233,75	5,67	9,00	24,00	10,84	61,42	6,82	0,45	79,54
236-237	236,5	11,50	27,57	3,55	6,13	70,54	2,56	1,73	80,96
238-240	239	7,33	13,29	5,25	9,20	67,44	5,08	1,75	83,47
243-244	243,5	12,33	11,50	4,56	5,65	69,67	6,06	1,24	82,62
248-250	249	10,76	15,67	2,33	6,41	68,96	4,40	2,75	82,51
253-255	254	11,50	11,50	6,14	6,08	69,89	6,08	0,99	83,03
258.5-260	259	10,11	13,29	9,00	6,82	68,91	5,19	0,76	81,67

Table 19(continued). Empirical Estimation of the CO₃²⁻% participation in each carbonate mineral for SAR39

The Carbonate Factory Over The Last 20.000 Yrs In The Nw Saronikos Gulf

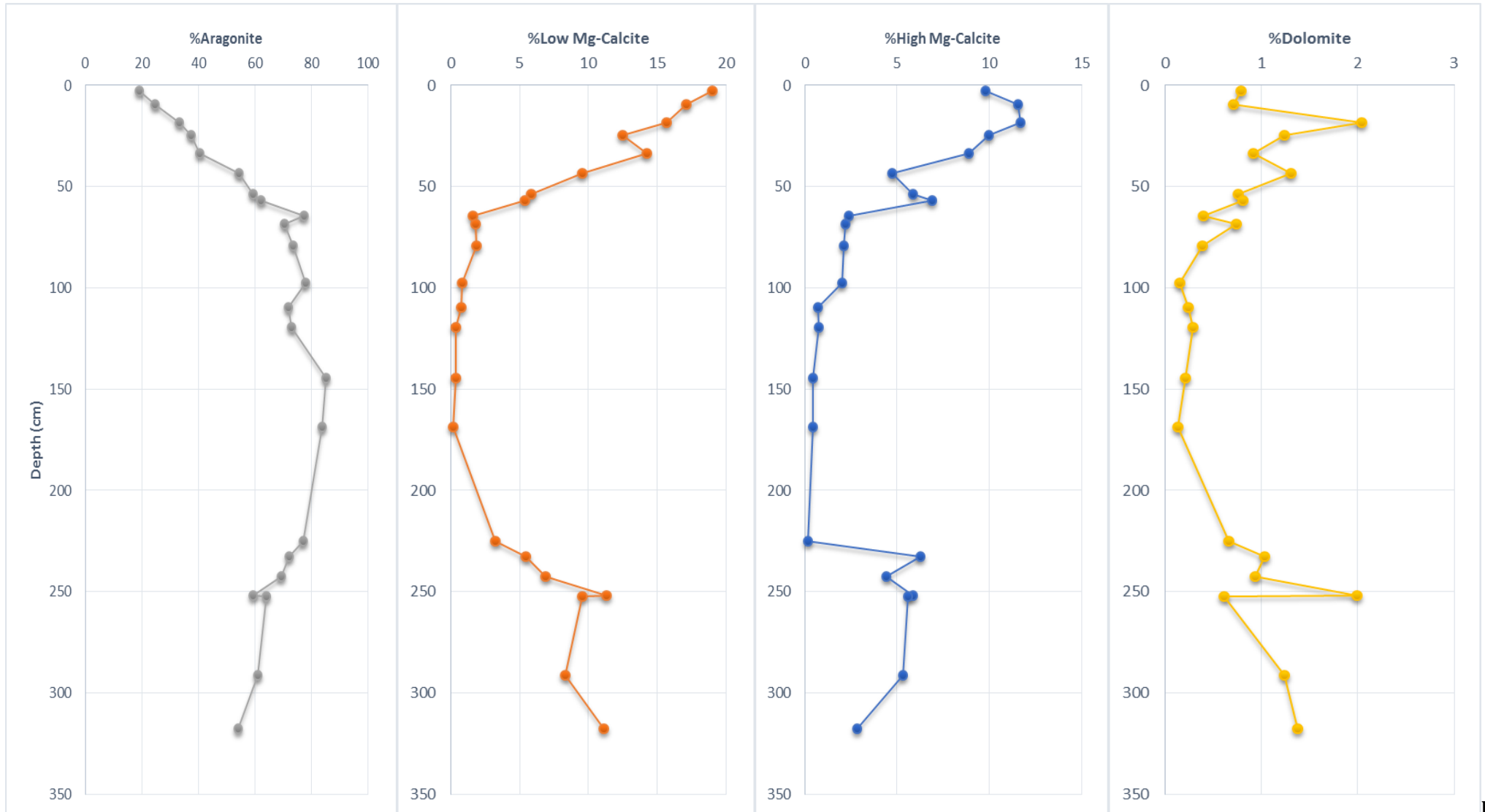


Fig.35 XRD carbonate mineralogy SAR4

Fi

The Carbonate Factory Over The Last 20.000 Yrs In The Nw Saronikos Gulf

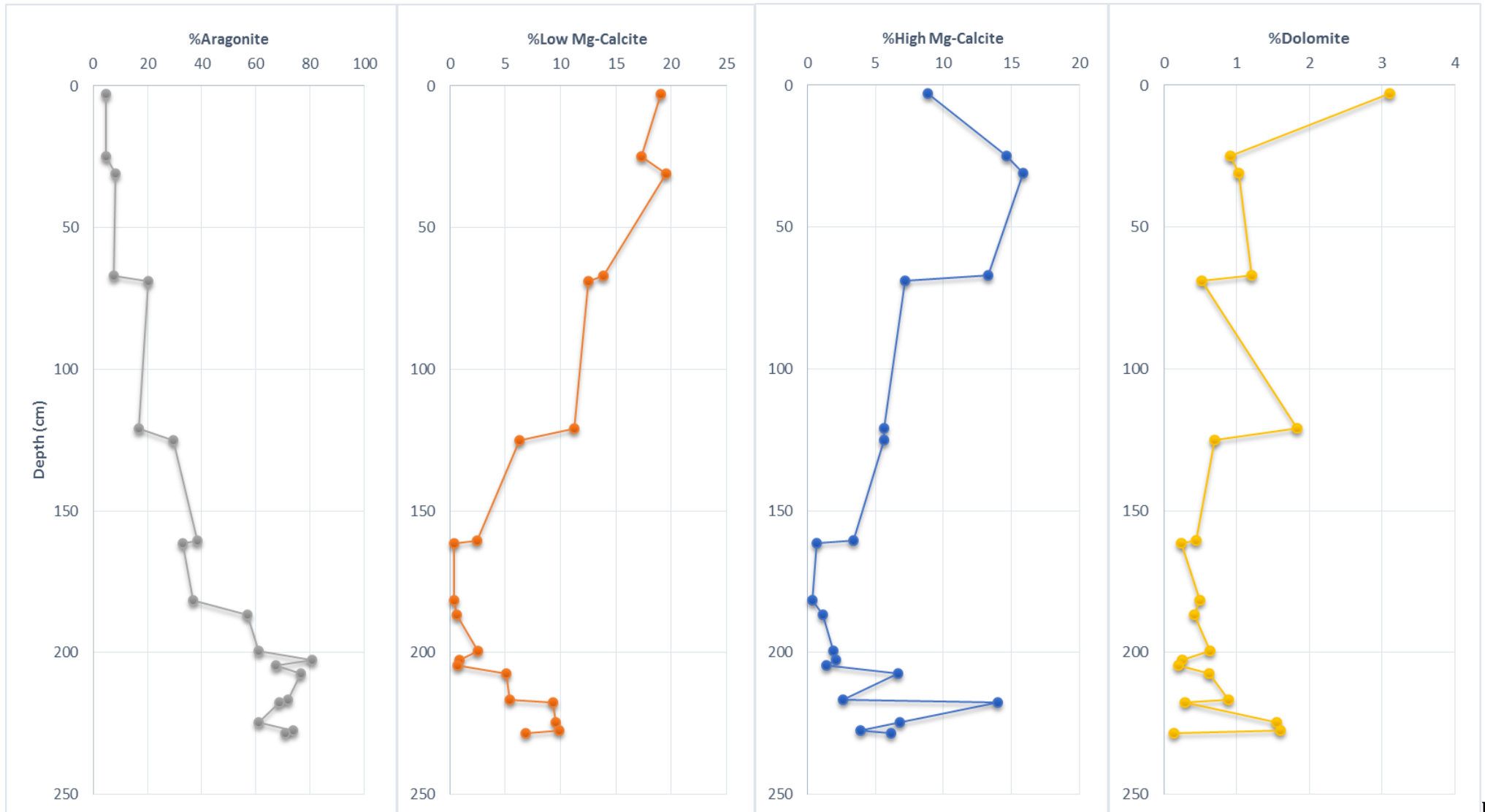


Fig.36 XRD carbonate mineralogy SAR36

FF

The Carbonate Factory Over The Last 20.000 Yrs In The Nw Saronikos Gulf

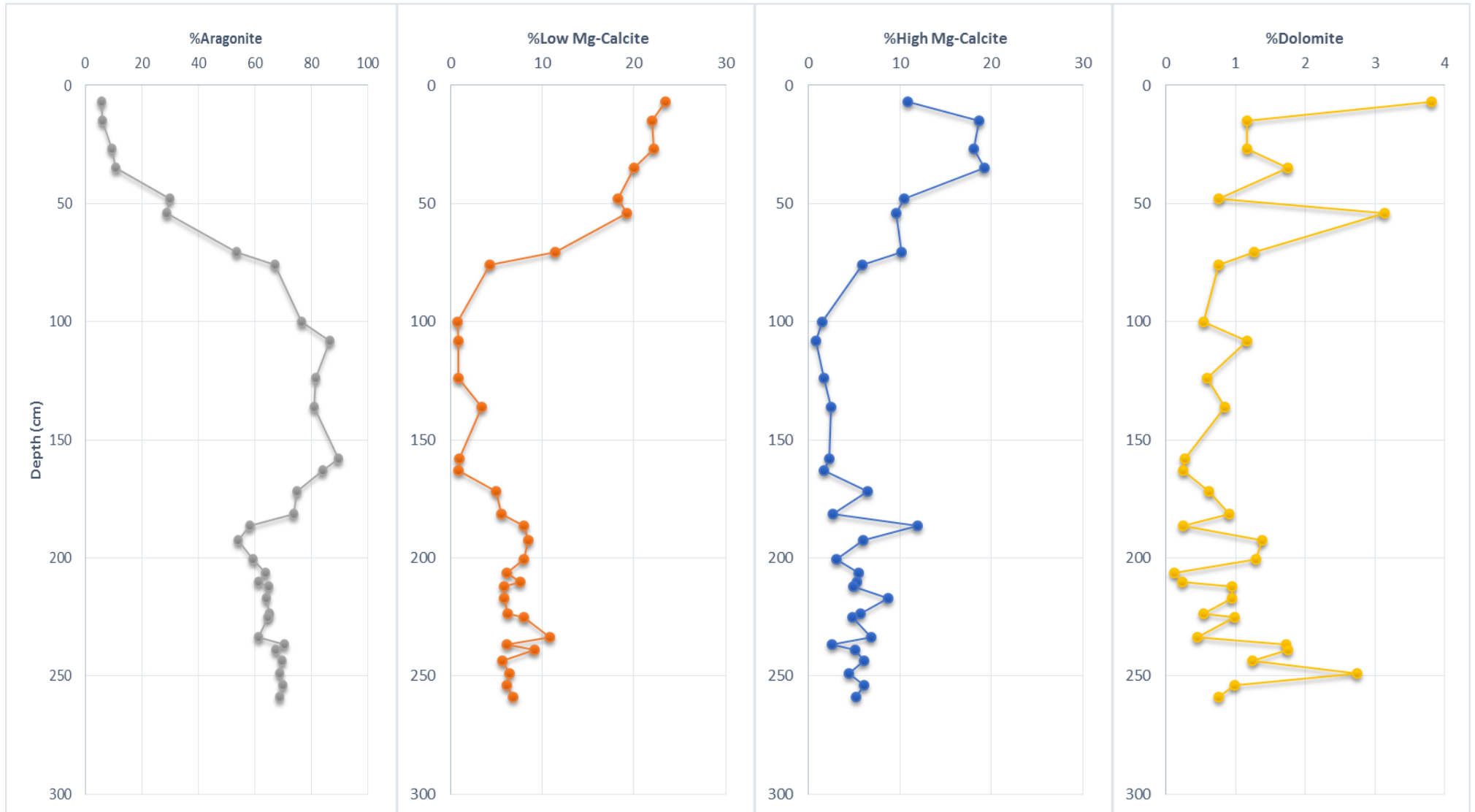


Fig.37 XRD carbonate mineralogy SAR39

The Carbonate Factory Over The Last 20.000 Yrs In The Nw Saronikos Gulf

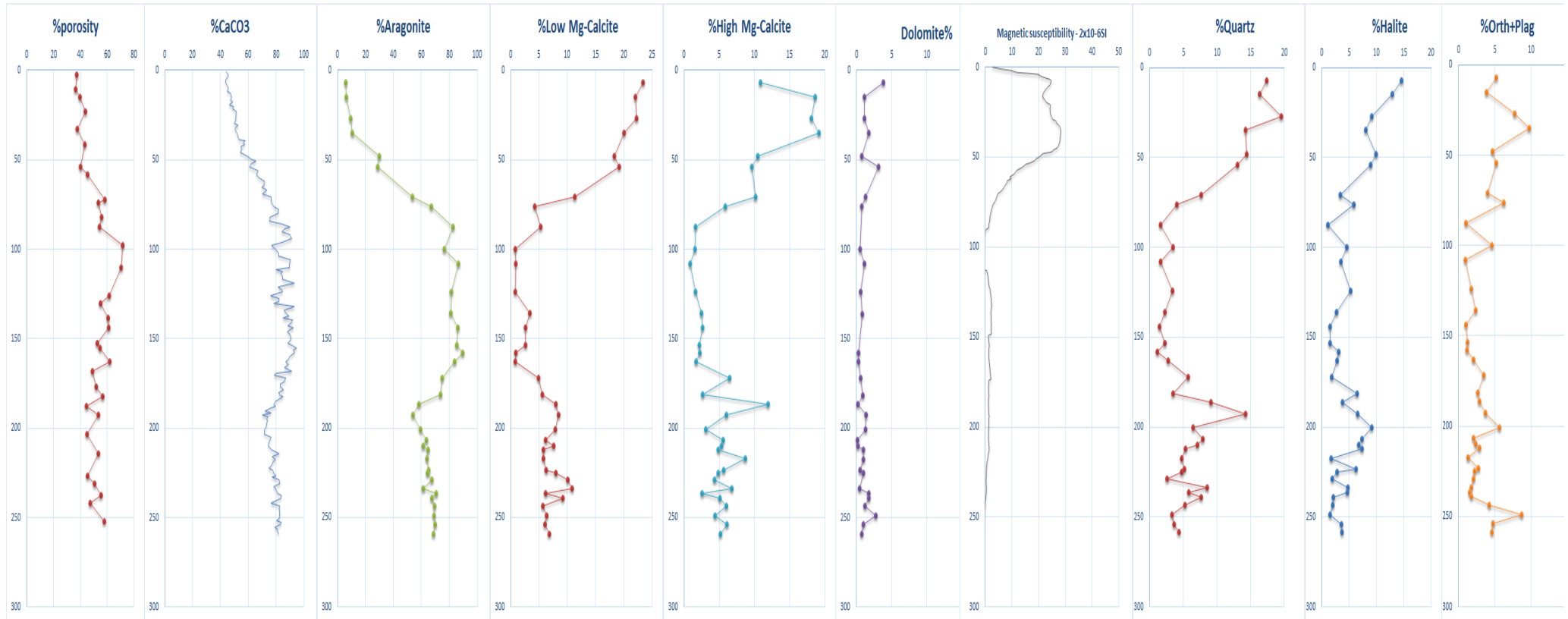


Fig.38 XRD SAR39 Comparison of terrigenous minerals with carbonate minerals

Results

XRD analyses point out one aragonite-dominated sequence from the bottom to 189cm in SAR36 (**Fig.36**), where aragonite ranges between 56-81wt%, one aragonite-dominated sequence from 252 to 64cm in SAR4 (**Fig.35**), where aragonite ranges between 59-85wt% and two distinct aragonite-dominated sequences in SAR39(**Fig.37**): a first one from the bottom to 192cm of the core, where aragonite presents a gradual decrease from 70 to 55wt% and a second one, from 182 to 88cm, where aragonite ranges between 74-90wt%.

In conclusion, XRD analysis of all 3 long cores shows a parallel downward shift of total carbonates and aragonite towards extremely higher values. All the aragonite-dominated sequences correspond to the end of Pleistocene. Regarding the specific time of deposition of these sequences, we discuss it on a later chapter.

Furthermore aragonite seems to be negatively related or unrelated to all the other carbonate minerals. For instance, in all 3 cores it seems that at some point calcite starts to precipitate at the expense of aragonite. This upward transition from an aragonite –dominated sequence to a calcite-dominated sequence in all 3 cores, testifies the exact moment that the sea-level rose enough for the outer sea to connect with Megara basin. Detailed XRD analysis of the terrigenous mineralogy of SAR39 (**Fig.38**) records a similar rapid increase of the terrigenous input over the last 88cm, while aragonite content displays an abrupt decrease, reaching 7wt%, at the top of the core. This abrupt increase of the terrigenous content at the upper part of SAR39 clarifies the reason MS values seem weak at the lower parts of all the cores retrieved from the Saronikos Gulf, proving that Megara basin, before reconnecting with the open sea was a landlocked marine basin disconnected from significant river discharges.

The Carbonate Factory Over The Last 20.000 Yrs In The Nw Saronikos Gulf

Also, this detailed study of SAR39 pointed out that aragonite is unrelated to halite, which means that the proportion of the halite is related to porewater, while no other evaporitic minerals were found e.g. gypsum. One possible explanation for that is described below.

Discussion

As we mentioned before, at the peak of the LGM, around 21-20 ka BP, the sea level has fallen -120 m, resulting to the exposure of large land mass throughout the world. Such a land mass was the N-S oriented plateau in the centre of Saronic Gulf (shaded area) that is responsible for the isolation of both Megara and Epidauros Basin from the rest of the Aegean Sea.

The submarine plateau is distinctively flat and shallow and the connection between Megara and Salamis basin would be at -92 m, while the lowest point for the seawater to enter from the East would be at -80-82m, based on the isobaths and the fact that according to literature no significant tectonic movements took place during that time. This means that since the seawater would be trapped inside Megara Basin at the peak of the LGM, the depth of Megara Basin was around -50m at the site of SAR39, -30m at the site of SAR36 and -90m at the site of SAR4. The fact that the height of the water column wouldn't change significantly within Megara Basin, since its isolation, was pointed out by [Foutrakis, 2016](#) too, who suggested that at 20-18 ka BP the sea level between Salamina and Aegina still stood at -95m.

Based on **Fig. 13** that shows the spatial distributions of aragonite saturation state (Ω_{arag}) at various depth levels, the water column would in fact be supersaturated in aragonite within Megara basin, having these latitudes. The reason for the aragonite sequence in SAR36 being shorter than the rest, even though the depths at this site are shallower is because it is located much closer to the western shores of Saronikos Gulf and

The Carbonate Factory Over The Last 20.000 Yrs In The Nw Saronikos Gulf

therefore records higher terrigenous sedimentation rates during Holocene, being more affected by river discharges.

On the other hand, Usiglio, 1849 (**Fig.18**) pointed out that in order for gypsum to precipitate, only 20% of the initial water volume should survive within the basin. So the water depth within Megara Basin should be -50m>D>-10m at the site of SAR39, -30m>D>-6m at the site of SAR36 and -90m>D>-18m at the site of SAR4 in order to be supersaturated in aragonite without producing any other evaporitic minerals, which means that Megara Basin was probably a relatively shallow saline (definitely not hypersaline) lake, with very small terrigenous supply, during that time.

Other important factors that must be taken into consideration and will be discussed later are:

- In SAR39 between the two aragonite-dominated sequences seems to interfere a transitional facies where calcite seems to slightly increase at the expense of aragonite for a short period.
- The upper aragonite-dominated sequence seems to reach extremely higher values, in relevance to the lower aragonite-dominated sequence, implying the assistance of an external factor e.g. temperature in aragonite precipitation during that time.
- XRD analysis of SAR39 records an Orth+Plag maxima that probably corresponds to Z2(Minoan) tephra layer)
- The upper units of all the studied long cores record a normal marine environment with calcite carbonate sedimentation probably of biogenic origin and rich terrigenous supply. The length of the upper units depends on the rate of the terrigenous input at each site.

4.4 AMS CHRONOLOGY

Lykousis et al. 1993 collected 14 piston cores from Saronikos Gulf from depths between 82 and 380m and they noticed the same aragonite-dominated sequence while they also recognized that the aragonite trend follows the TIC curve. Radiocarbon dating of this sequence within two cores (one from Megara Basin located very close to SAR39 and SAR4 and one from Epidavros Basin) gave 16,560± 260 ka BP and 3 ages: 18.380±130 and 17.870± 110, 18.960± 120 respectively.

Source	Age
SAR39, Megara Basin (this thesis)	16.935 ka ± 50 yrs
Megara Basin Lykousis et al., 1993	16,560± 260 ka
Epidavros Basin Lykousis et al., 1993	18.380±130
Epidavros Basin Lykousis et al., 1993	17.870± 110
Epidavros Basin Lykousis et al., 1993	18.960± 120

Table 20. Radiocarbon ages of aragonite-dominated sequence

AMS radiocarbon dating was also conducted for this thesis at 196-198cm of SAR39. The reason we chose SAR39 for a detailed examination is because this specific long core is the only one that records two distinctive aragonite-dominated sequences and the interval 196-198cm is positioned near the upper boundary of the lower aragonite-dominated sequence.

The estimated radiocarbon age was 16,935 ± 50 ka. This age corresponds to the cold Heinrich Stadial Event 1. According to *Hemming (2004)* HS1 dates at 16.8 ka BP, which explains the slight decrease of aragonite for the benefit of the calcite mineral, as recorded within the transitional facies between the two aragonite-dominated sequences. This minor decline of

The Carbonate Factory Over The Last 20.000 Yrs In The Nw Saronikos Gulf

the aragonite might indicate that HS1 didn't have the same «catastrophic» impact it had in most tropical regions, verifying theories that supported that SST became only slightly cooler than before (1-3°C) in eastern Mediterranean and did not last long.

On the other hand, the deposition of larger quantities of aragonite than before, as recorded within the upper aragonite-dominated sequence (74-90%), implies that this cold event was followed shortly after by a warmer event that quickly accelerated aragonite production.

As it is known, temperature is the most significant controlling factor on the compositions of recent marine carbonate sediments, especially because it affects the Mg:Ca ratio of the seawater, which means that this boost that followed, regarding aragonite production might be related to warmer conditions, confirming none other than the onset of the Bolling-Allerod period.

Furthermore, estimated mean sedimentation rates (with the help of Z2(Minoan) tephra layer recorded in SAR39) during the Bolling-Allerod period, seem to exceed >20cm/1000 years, which means that this carbonate factory might had survived till Early Holocene (88cm in SAR39), much later than the rest semi-gulfs in the Aegean sea.

Finally, we should mention that the impact of YD is not distinctive in the carbonate sediments from Megara Basin, though this is not uncommon.

4.5 SEM

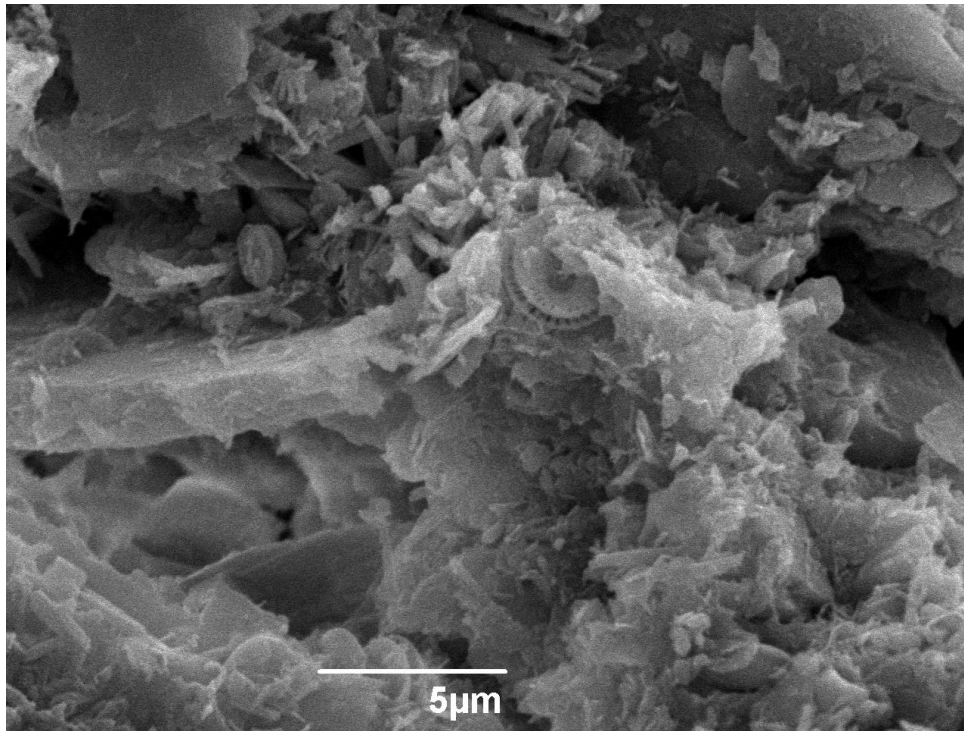


Fig. 39 SEM photomicrographs of *Emiliana Huxley* and *Syracosphaera* in SAR39 58cm

Some photos were taken using a scanning electron microscope (SEM). As we can see the *E.Huxleyi* is present although this species is presumed to be one of the most euryhaline and eurythermal coccolithophore species". Other coccolithophores were also detected however the lack of data does not permit us to make any assumptions. The most dominant mineral in all sections is aragonite and as we can see by its texture it is in the form of needles. The origin of aragonite in modern marine environments is more difficult to be clarified, even though there are numerous studies ([Milliman, 1974](#); [Bathurst, 1975](#); [Scoffin, 1987](#) and [Morse&Mackenzie, 1990](#)) regarding the source of aragonite, especially in the form of carbonate needle muds. According to literature, attempts of interpreting their chemistry and the needles' morphology, defining their biogenic supply, even replicating carbonate production have been made with very contradicting results.

The Carbonate Factory Over The Last 20.000 Yrs In The Nw Saronikos Gulf

For instance, regarding needles' morphology, the precipitation of fine-grained aragonite crystals from seawater is in the same form and size as to those produced by the codiacean algae, while even discrimination based on their chemical characteristics is not always accurate (e.g. *Lowenstam&Epstein, 1957; Milliman, 1974; Bathurst, 1975*).

Also, according to literature in some areas biogenic supply is sufficient (e.g. British Honduras and Florida Bay), while in others is not (e.g. Great Bahama Bank and the Persian Gulf) and an abiotic origin for the aragonite needles is vital in order to justify the precipitation of massive calcareous muds. Quite so, various studies support this hypothesis, as whittings in both areas are proven to be of chemical origin, having precipitated instantaneously from seawater that has become supersaturated with respect to calcium carbonate (*Wells&Illing 1964; Shinn et al., 1989; Robbins&Blackwelder, 1992; Macintyre&Reid, 1992; Milliman et al., 1993*). Nevertheless the presence of aragonite needles at this amount is typical indicator of a carbonate factory similar to the modern carbonate banks and we support that this high precipitation rate recorded within the aragonite sequences must be the result of chemical distribution, rather than biogenic.

On the other hand, calcite contents are probably more related to biogenic origin. Finally we detected well preserved diatoms and authigenic framboidal pyrite.

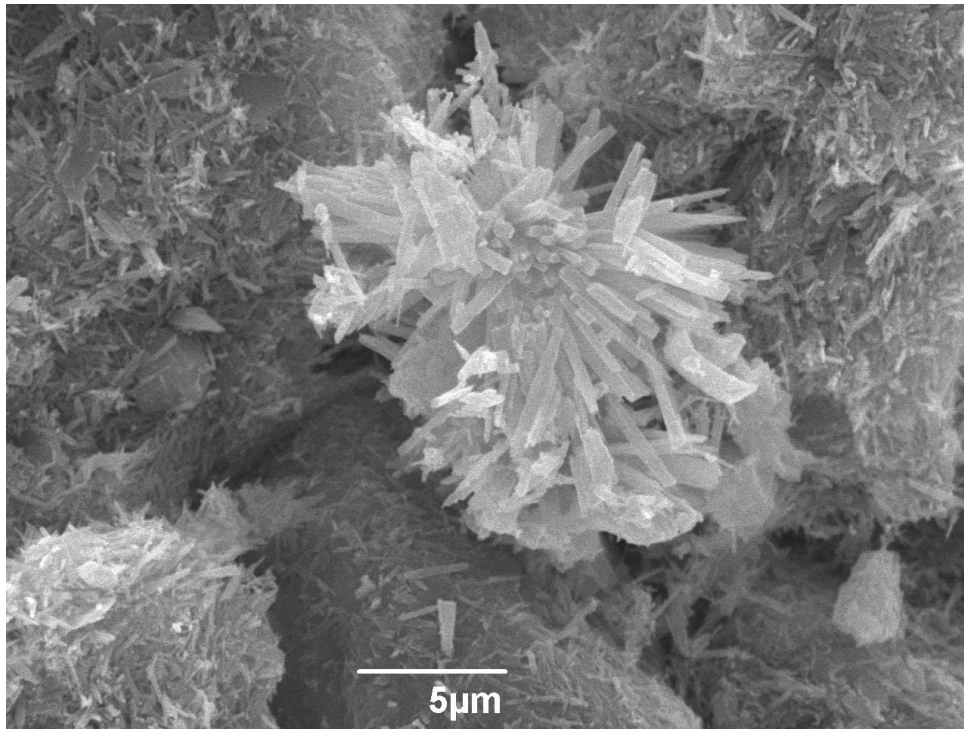


Fig. 40 SEM photomicrographs of Aragonitic needles in SAR39 168cm

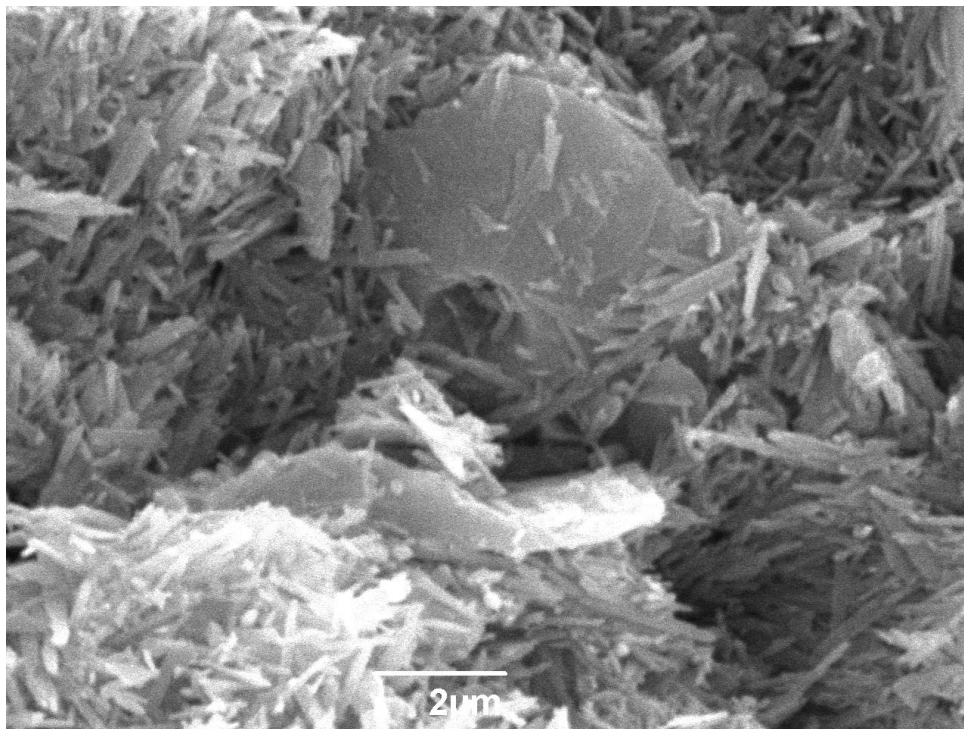


Fig. 41 Calcidiscus surrounded by aragonitic needles in SAR39 168cm

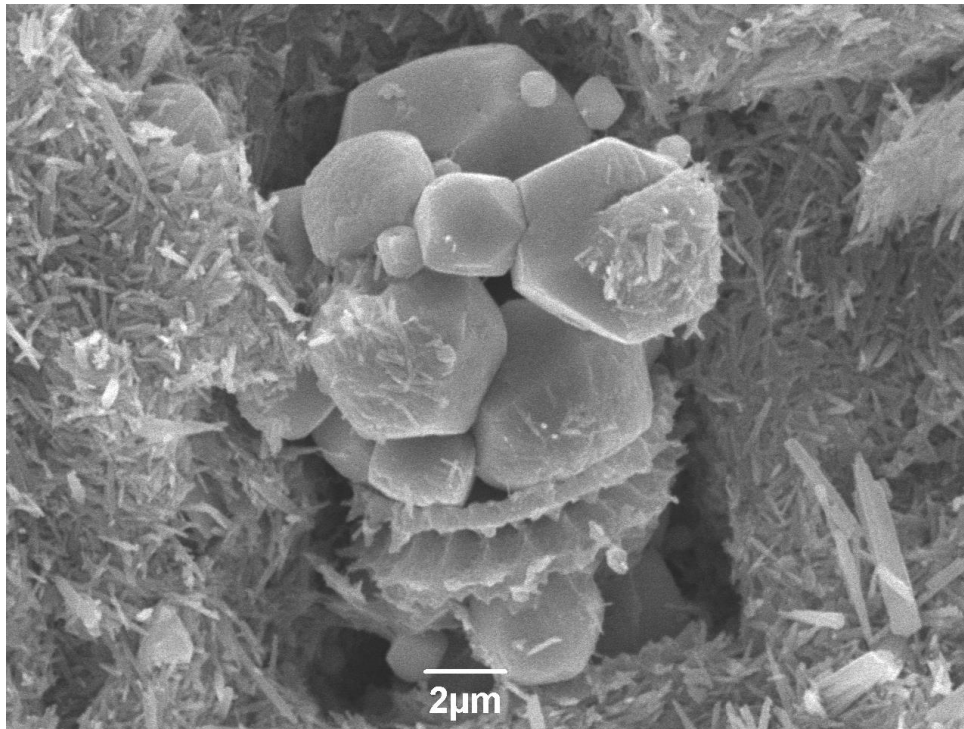


Fig. 42 SEM photomicrographs of Calcite crystals and nanofossil trapped in SAR39 168cm

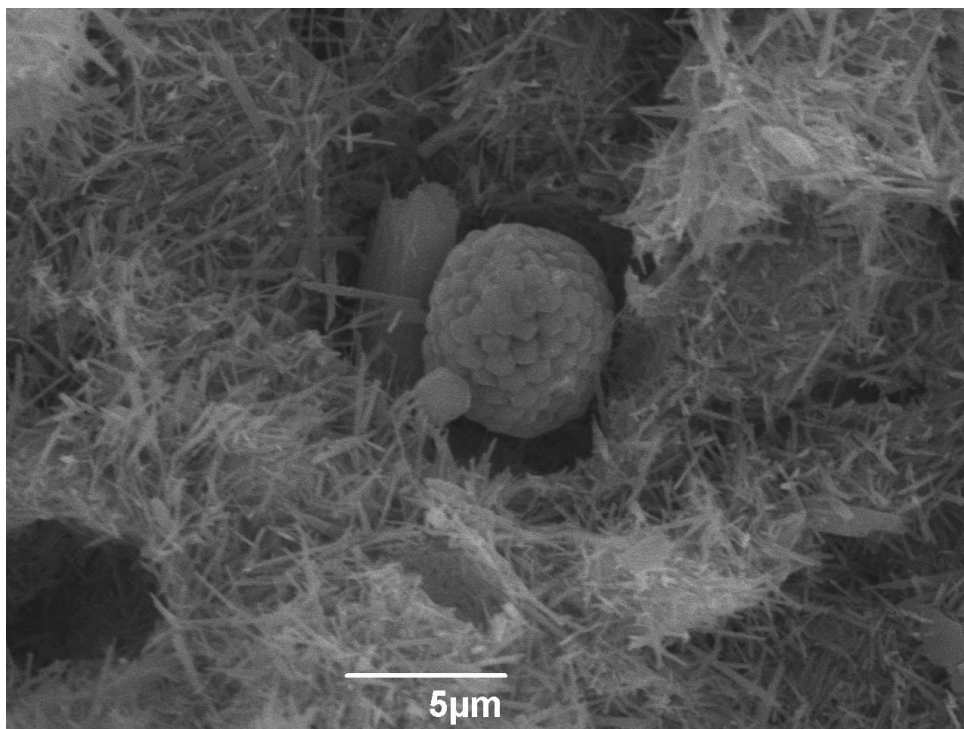


Fig.43 SEM photomicrographs of Authigenic framboidal pyrite in SAR39 168cm

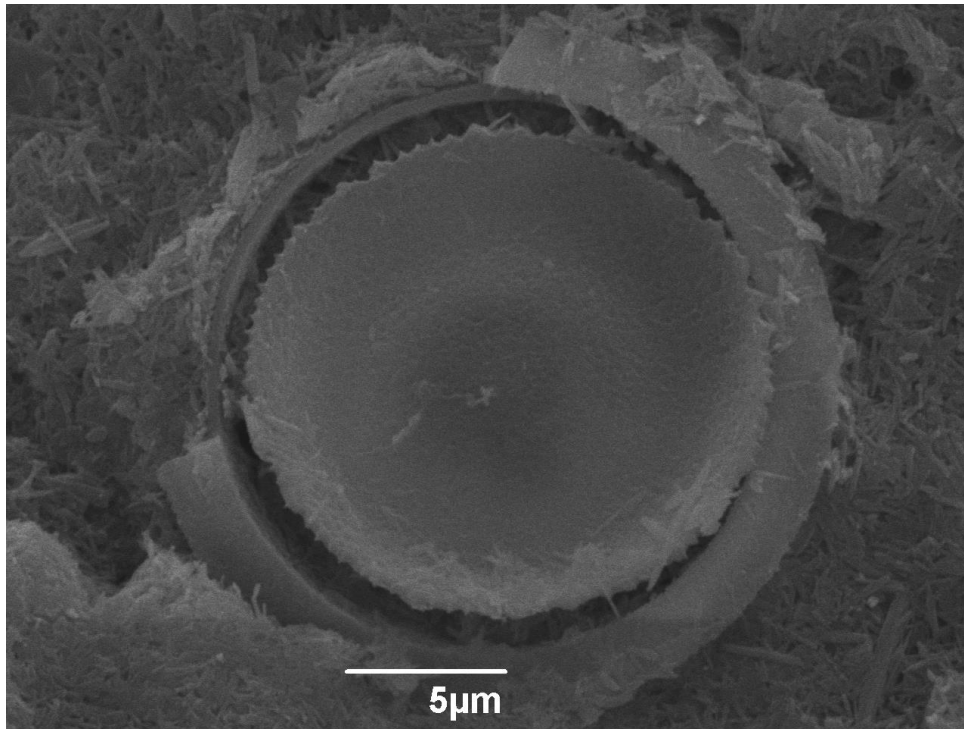


Fig. 44 SEM photomicrographs of Diatom in SAR39 237cm

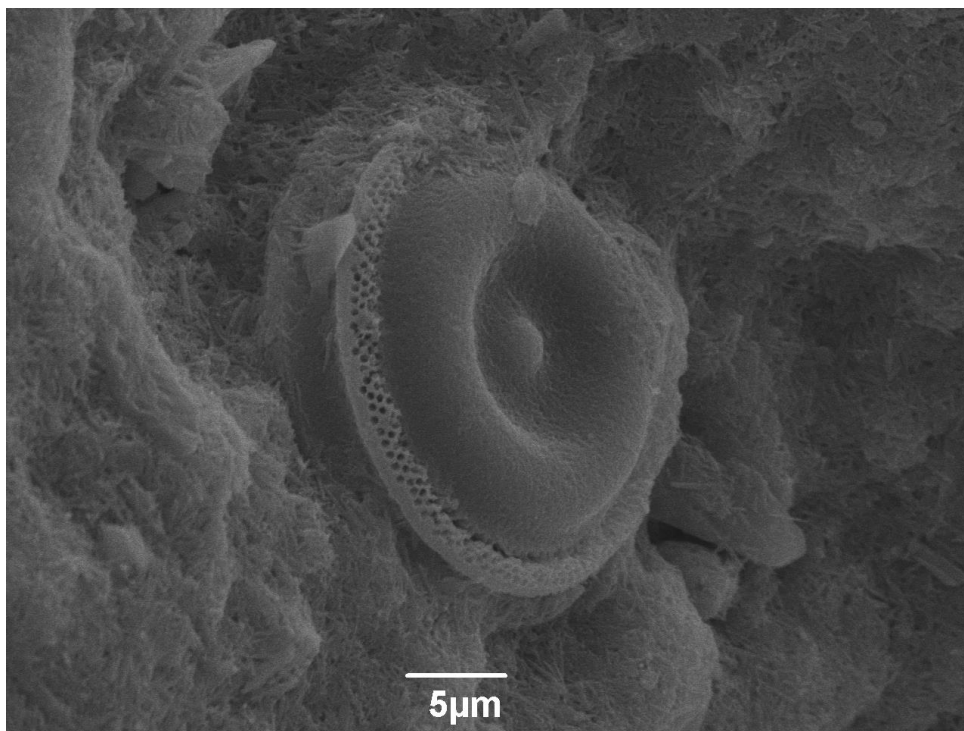


Fig. 45 SEM photomicrographs of Diatom in SAR39 237cm

CHAPTER 5. Conclusions

All the long cores retrieved from the NW Saronikos Gulf support the idea that not long ago, the formation of carbonate proportions was really high (marley lime to pure lime facies) while the supply of terrigenous detritus decreased simultaneously (weak MS, terrigenous mineralogy in SAR39). Based on XRD estimates from the long cores SAR39, SAR4 and SAR36, the dominant carbonate mineral during that period was aragonite. This period of time corresponds to the time interval between LGM and Late Glacial-Holocene transition (based on radiocarbon chronology), which means that during that time Megara basin was a landlocked, shallower saline lake that operated as a carbonate factory, being constantly supersaturated in aragonite, even though there is no evidence of typical evaporitic environment. Furthermore detailed examination of the long core SAR39 shows a dramatic change in aragonite production, reaching extreme proportions (aragonite% $\approx 90\%$), just before its termination, that is possibly related to the warm Bolling-Allerod period, during which the mean sedimentation rate exceeded $>20\text{cm}/1000$ years. The abrupt termination of this carbonate factory corresponds probably to the Meltwater Pulse 1A, one of the strongest and most rapid –glacial sea level benefactors that began soon after the onset of Bolling warming, though there are indications that this carbonate factory might had survived till Early Holocene (88cm in SAR39), when Megara basin was properly reconnected with the open sea. Aragonite-dominated sequences were recorded also in other semi-Gulfs (e.g. Pagasitikos) till 13-14ka, however only in Megara Basin this carbonate factory survived for so long. The thin layers of sand (marine transgression) within the interval of 95-125cm of SAR39, testifies an earlier attempt of the sea to connect with NW Saronikos Gulf likewise, possible related with a temporary inflow from the Salamis basin, through the Salamina-Aegina strait. We propose that the most likely reason for this long delay for the open sea to reconnect with Megara basin is its position, having a second shallow basin in the east interfering between Megara Basin and Aegean Sea that possible got the first inflow of marine waters.

REFERENCES

- [1] **Anastasakis G. and Piper D. J.W., 2005.** Late Neogene evolution of the western South Aegean volcanic arc: Sedimentary imprint of volcanicity around Milos. *Marine Geology*. 215, 135-158
- [2] **Anastasakis G., Piper D.J.W., Dermitzakis M.D. and Karakitsios V. 2006** Upper Cenozoic stratigraphy and palaeogeographic evolution of Myrtoon and adjacent basins, Aegean Sea, Greece. *Marine and Petroleum Geology*, 23, 353-369.
- [3] **Antonarakou A., Kontakiotis G., Mortyn P.G., Drinia H., Sprovien M. , Besiu E., Tripsanas E. (2015)** Biotic and geochemical ($\delta^{18}\text{O}$, $\delta^{13}\text{C}$, Mg/Ca, Ba/Ca) responses of *Globigerinoides ruber* morphotypes to upper water column variations during the last deglaciation, Gulf of Mexico. *Geochimica et Cosmochimica Acta* 170 (2015) 69-93
- [4] **Armijo R, Meijer B, King GCP, Rigo A, Papanastassiou D (1996)** Quaternary evolution of the Corinth Rift and its implications for the Late Cenozoic evolution of the Aegean. *Geophys J Int* 126:11–53
- [5] **Banks, K. W., Riegl, B. M., Shinn, E. A., Piller, W. E., and Dodge, R. E., 2007.** Geomorphology of the Southeast Florida continental reef tract (Miami-Dade, Broward, and Palm Beach Counties, USA). *Coral Reefs*, 26, 617–633.
- [6] **Barber, D. C., et al., 1999.** Forcing of the cold event of 8,200 years ago by catastrophic drainage of Laurentide lakes, *Nature*, 400, 344–348.
- [7] **Bard, E., Hamelin, B., Fairbanks, R.G., Zindler, A., 1990a.** Calibration of the ^{14}C timescale over the past 30,000 years using mass spectrometric U–Th ages from Barbados corals. *Nature* 345, 405–410.
- [8] **Bard, E., Hamelin, B., Fairbanks, R.G., 1990b.** U/Th ages obtained by mass spectrometry in corals from Barbados — sea-level during the past 130,000 years. *Nature* 346,456–458.
- [9] **Bard, E., Hamelin, B., Arnold, M., Montaggioni, L., Cabioch, G., Faure, G., Rougerie, F., 1996.** Sea level record from Tahiti corals and the timing of deglacial meltwater discharge. *Nature* 382, 241–244.

The Carbonate Factory Over The Last 20.000 Yrs In The Nw Saronikos Gulf

- [10] **Bar-Matthews, M., Ayalon, A., Gilmour, M., Matthews, A., and Hawkesworth, C., 2003.** Sea-land oxygen isotopic relationships from planktonic foraminifera and speleothems in the Eastern Mediterranean region and their implication for paleorainfall during interglacial intervals, *Geochimica et Cosmochimica Acta*, 67: 3181–3199.
- [11] **Barkan, E., B. Luz, and B. Lazar (2001),** Dynamics of the carbon dioxide system in the Dead Sea, *Geochim. Cosmochim. Acta*, 65, 355 – 368
- [12] **Bathurst R. G. C. (1975)** Carbonate Sediments and their Diagenesis, 2nd edn., *Developments in Sedimentology No. 12.* Elsevier, Amsterdam, 658p
- [13] **Beget, J. E. (1983)** Radiocarbon-dated evidence of worldwide early Holocene climate change, *Geology* 11: 89-93
- [14] **Berger, J-F., and J. Guilaine. 2009.** The 8200 cal bp Abrupt Environmental Change and the Neolithic Transition: A Mediterranean Perspective, *Quaternary International* 200, pp. 31–49.
- [15] **Berner, R.A., 1975. The role of magnesium in the crystal growth of calcite and aragonite from seawater. *Geo. chim. Cosmochim. Acta*, 39: 489-504.**
- [16] **Bischoff JL, Fyfe WS, 1968** Catalysis, inhibition, and the calcite-aragonite problem: 1. The aragonite-calcite transformation. *American Journal of Science* 266, 65–79.
- [17] **Blanchon, P., and J. Shaw, 1995.** Reef drowning during the last deglaciation: Evidence for catastrophic sea-level rise and ice-sheet collapse, *Geology*, 23, 4–8.
- [18] **Blanchon, P., Jones, B., and Ford, D. C., 2002.** Discovery of a sub-merged relic reef and shoreline off Grand Cayman: further support for an early Holocene jump in sea level. *Sedimentary Geology*, 147, 253–270.
- [19] **Burton EA, Walter LM (1987)** Relative precipitation rates of aragonite and Mg calcite from seawater: Temperature or carbonate ion control? *Geology* 15: 111–114. doi: 10.1130/0091-7613(1987)
- [20] **Burton EA, Walter LM, 1991** The effect of pCO₂ and temperature on magnesium incorporation in calcite in seawater and MgCl₂- CaCl₂ solutions. *Geochimica et Cosmochimica Acta* 55, 777–785

The Carbonate Factory Over The Last 20.000 Yrs In The Nw Saronikos Gulf

- [21] **Cacho I., Grimalt I., Pelejero C. Canals M., Sierro F.J., Flores J.A., Shackleton N., 1999.** Dansgaard-Oeschger and Heinrich event imprints in Alboran Sea paleotemperatures. *Paleoceanography*, Vol. 14, 6, p. 698-705, Dec. 1999
- [22] **Calvert, S.E., Fontugne, M.R., 2001.** On the late Pleistocene–Holocene sapropel record of climatic and oceanographic variability in the eastern Mediterranean. *Paleoceanography* 16, 78–94.
- [23] **Carlson, A.E., Legrande, A.N., Oppo, D.W., Came, R.E., Schmidt, G.A., Anslow, F.S., Licciardi, J.M. and Obbink, E.A., 2008.** Rapid early Holocene deglaciation of the Laurentide ice sheet, *Nature Geoscience*, 1: 620-624.
- [24] **Casford, J. S. L., Rohling, E. J., Abu-Zied, R. H., Jorissen, F. J., Leng, M., and Thomson, J., 2003** A dynamic concept for eastern Mediterranean circulation and oxygenation during sapropel formation, *Palaeogeography, Palaeoclimatology, Palaeoecology*, 190: 103-119.
- [25] **Chappell, J., Polach, H., 1991.** Post-glacial sea-level rise from a coral record at Huon Peninsula, Papua New Guinea. *Nature* 147–149.
- [26] **Clark, P. U., McCabe, A. M., Mix, A. C., and Weaver, A. J., 2004.** Rapid rise of sea level 19,000 years ago and its global implications. *Science*, 304, 1141–1144.
- [27] **Clarke, M.L. & Rendell, H. M. 2009.** The impact of North Atlantic storminess on western European coasts: A review. *Quaternary International* 195, 31–41.
- [28] **Collier REL, Dart CJ (1991)** Neogene to Quaternary rifting, sedimentation and uplift in the Corinth Basin, Greece. *J Geol Soc London* 148:1049–1065
- [29] **Collier, R.E.L., Lykousis, V., Chronis, G., Pavlakis, P., 1992.** Temporal and Lateral Changes in Recent Extensional Subsidence and Uplift Rates: W. Saronic Gulf and Corinth Isthmus, Greece, VI, EGS, *Terra Abstracts*, 3/1: 350
- [30] **Collier, R.E.L., Leeder, M.R., Trout, M., Ferentinos, G., Lyberis, E., Papatheodorou, G., 2000.** High sediment yields and cool, wet winters: test of last glacial paleoclimates in the northern Mediterranean. *Geology* 28/11, 999–1002.

The Carbonate Factory Over The Last 20.000 Yrs In The Nw Saronikos Gulf

- [31] Copin-Montegut, C., 1988. A new formula for the effects of temperature on the partial pressure of CO₂ in seawater. *Marine Chemistry* 25, 29-37.
- [32] Cronin, T.M., Voigt, P.R., Willard, D.A., Thunell, R.C., Halka, J., Berke, M., Pohlman, J., 2007. Rapid sea level rise and ice sheet response to 8200-year climate event. *Geophysical Research Letters* 34, L20603.
- [33] De Choudens-Sanchez V., Gonzalez L.A., 2009. Calcite and Aragonite Precipitation Under Controlled Instantaneous Supersaturation: Elucidating the Role of CaCO₃ Saturation State and Mg/Ca Ratio on Calcium Carbonate Polymorphism *Journal of Sedimentary Research* 79(6):363-376
- [34] Debenay J. P., Andre J. P., and Lesourd M. (1999) Production of lime mud by breakdown of foraminiferal tests. *Mar. Geol.* 157, 159–170.
- [35] De Lange, G.J., Middelburg, J.J., Pruysers, P.A., 1989. Discussion: Middle and Late Quaternary depositional sequences and cycles in the eastern Mediterranean. *Sedimentology* 36, 151–156.
- [36] De Lange, G. J., J. Thomson, A. Reitz, C. P. Slomp, M. Speranza Principato, E. Erba, and C. Corselli, 2008. Synchronous basin-wide formation and redox-controlled preservation of a Mediterranean sapropel, *Nat. Geosci.*, 1, 606–610
- [37] Deleuze, M., and S. L. Brantley (1997), Inhibition of calcite crystal growth by Mg²⁺ at 100 °C and 100 bars: Influence of growth regime, *Geochim Cosmochim Acta*, 61.
- [38] De Rijk, S., A. Hayes, and E. J. Rohling, 1999 Eastern Mediterranean sapropel S1 interruption: An expression of the onset of climatic deterioration around 7 ka BP, *Mar. Geol.*, 153, 337–343
- [39] Deuser, W. G., E. H. Ross, and R. F. Anderson (1981), Seasonality in the supply of sediment to the deep Sargasso Sea and implications for the rapid transfer of matter to the deep ocean, *Deep Sea Res.*, 28, 495 – 505.
- [40] Deuser, W. G., P. G. Brewer, T. D. Jickells, and R. F. Commeau (1983), Biological control of the removal of abiogenic particles from the surface ocean, *Science*, 219, 388 – 391.

The Carbonate Factory Over The Last 20.000 Yrs In The Nw Saronikos Gulf

[41] Dietrich V. J., Mercolli I., Oberhänsli R., 1988. Dazite, High-Alumina-Basalte und Andesite als Produkte amphiboldomierter Differentiation (Aegina und Methana, Ägäischer Inselbogen)*. Schweiz. Mineral. Petrogr. Mitt. 68: 21-39

[42] Dietrich V., Gaitanakis P., Mercolli I., Oberhänsli R. 1993 Geological map of Greece, Aegina Island, scale 1:25.000 Bulletin, Geological Society of Greece, 28 (1993), pp. 555–566

[43] Dittrich, M., P. Kurz, and B. Wehrli (2004), The role of autotrophic picocyanobacteria in calcite precipitation in an oligotrophic lake, Geomicrobiol. J., 21, 45 – 53.

[44] Drakatos G., Karastathis V., Makris J., Papoulia J., Stavrakakis G., 2005. 3D crustal structure in the neotectonic basin of the Gulf of Saronikos (Greece). Tectonophysics, 400: 55-65.

[45] Dromgoole, E.L., And Walter, L.M., 1990, Iron and manganese incorporation into calcite: Effects of growth kinetics, temperature and solution chemistry: Chemical Geology, v. 81, p. 311–336.

[46] Doutsos T, Piper DJW (1990) Listric faulting, sedimentation, and morphological evolution of the Quarternary eastern Corinth rift, Greece: first stages of continental rifting. Geol Soc Am Bull 102:812–829

[47] Eberli G.P., Westphal, H., Riegl, B., 2010. Carbonate Depositional Systems: Assessing Dimensions and Controlling Parameters: The Bahamas, Belize and the Persian/Arabian Gulf. Springer Science & Business Media.

[48] Edwards, R. L., Beck, W. J., Burr, G. S., Donahue, D. J., Chappell, J. M. A., Bloom, A. L., Druffel, E. R. M., & Taylor, F. W., 1993. A large drop in atmospheric $^{14}\text{C}/^{12}\text{C}$ reduced melting in the Younger Dryas, documented with ^{230}Th ages of corals. Science, 260,962-968.

[49] Efstratiou, N., A. Karetsoy, E. Banou, and D. Margomenou. 2004. “The Neolithic Settlement of Knossos: New Light on an Old Picture,” in Knossos: Palace, City, State. Proceedings of the Conference in Herakleion Organised by the British School of Athens and the 23rd Ephoreia of Prehistoric and Classical Antiquities, in November 2000, for the Centenary of Sir Arthur Evans’s

The Carbonate Factory Over The Last 20.000 Yrs In The Nw Saronikos Gulf

Excavations at Knossos (BSA Studies 12), G. Cadogan, E. Hatzaki, and A. Vasilakis, eds., London, pp. 39–51.

[50] Emeis, K. C., Struck, U., Schulz, H. M., Bernasconi, S., Sakamoto, T., and Martinez-Ruiz, F., 2000 Temperature and salinity of Mediterranean Sea surface waters over the last 16,000 years: Constraints on the physical environment of S1 sapropel formation based on stable oxygen isotopes and alkenone unsaturation ratios, *Palaeogeography, Palaeoclimatology, Palaeoecology*, 158: 259-280.

[51] Emeis, K.-C., H. Schulz, U. Struck, M. Rossignol-Strick, H. Erlenkeuser, M.W. Howell, D. Kroon, A. Mackensen, S. Ishizuka, T. Oba, T. Sakamoto and I. Koizumi, 2003 Eastern Mediterranean surface water temperatures and $\delta^{18}\text{O}$ composition during deposition of sapropels in the late Quaternary”, *Paleoceanography*, 18, 1, 1005.

[52] Fairbanks, R.G., 1989. A 17,000-year glacio-eustatic sea level record: Influence of glacial melting rates on the Younger Dryas event and deep-ocean circulation. *Nature* 342,637–642.

[53] Flügel E., 2004 Microfacies of Carbonate Rocks: Analysis, Interpretation and Application Springer-Verlag, Berlin (2004) p. 976

[54] Foutrakis M. P. (2016) Geological Evolution of Saronikos Gulf during Quaternary (PhD thesis in Greek). National Kapodistrian University of Athens p 319. (unpublished)

[55] Friedman, G. M. (1993), Biochemical and ultrastructural evidence for the origin of whittings— A biologically induced calcium carbonate precipitation mechanism, *Comment, Geology*, 21, 287 – 288.

[56] Friedman, G. M. (1994), Great Bahama Bank aragonitic muds, mostly inorganically precipitated, mostly exported—Discussion, *J. Sediment. Res.*, 64, 921 – 922.

[57] Füchtbauer, H., and Hardie, L. A., 1976, Experimentally determined homogeneous distribution coefficients for precipitated magnesian calcites: Application to marine carbonate cements: *Geological Society of America Abstracts with Programs*, v. 8, p. 877.

The Carbonate Factory Over The Last 20.000 Yrs In The Nw Saronikos Gulf

- [58] Fytikas M., Innocenti F., Kolios N., Manetti P., Mazzuoli R., 1986 b. The PlioQuaternary volcanism of Saronikos area (western part of the active Aegean volcanic arc). *Annales Geologiques des Pays Helleniques*, 33: 23-45.
- [59] Gaitanakis, P., and A. D. Dietrich (1995). Geological map of Methana peninsula, scale 1:25 000, Swiss Federal Institute of Technology, Zurich.
- [60] Gavrieli I. and Stein M. (2006). On the origin and fate of the brines in the Dead Sea basin. In *New Frontiers in Dead Sea Paleoenvironmental Research* (eds. Y. Enzel, A. Agnon and M. Stein). GSA Special Paper 401, pp. 183–194.
- [61] Geraga M. , Tsaila-Monopolis St., Ioakim C., Papatheodorou G., Ferentinos G. (2000) Evaluation of palaeoenvironmental changes during the last 18.000 years in the Myrtoon basin, SW Aegean Sea. *Palaeogeography, Palaeontology, Palaeoecology* 156 (2000) 1-17
- [62] Gogou, A., I. Bouloubassi, V. Lykousis, M. Arnaboldi, P. Gaitani and P.A. Meyers, 2007. Organic geochemical evidence of abrupt late Glacial-Holocene climate changes in the North Aegean Sea, *Palaeogeography, Palaeoclimatology, Palaeoecology*, 256, 1-20.
- [63] Goldsworthy M, Jackson J, Haines J (2002) The continuity of active fault systems in Greece. *Geophys J Int* 148:596–618
- [64] Gornitz, V. (Ed.), 2009: *Encyclopedia of Paleoclimatology and Ancient Environments*. Encyclopedia of Earth Sciences Series. Springer.
- [65] Green, M. A., and R. C. Aller (2001), Early diagenesis of calcium carbonate in Long Island Sound sediments: Benthic fluxes of Ca and minor elements during seasonal periods of net dissolution, *J. Mar. Res.*, 59, 769 – 794.
- [66] Gvirtzman, G. and Wieder, M., 2001. Climate of the last 53,000 years in the Eastern Mediterranean based on soil-sequence stratigraphy in the coastal plain of Israel. *Quaternary Science Reviews*, 20: 1827-1849.
- [67] Hanebuth, T., Stattegger, K., Grootes, P.M., 2000. Rapid flooding of the Sunda shelf: a late-glacial sea-level record. *Science* 288, 1033–1035.
- [68] Hanebuth, T., Stattegger, K., Bojanowski, A., 2009. Termination of the Last Glacial Maximum sea-level lowstand: the Sunda Shelf data revisited. *Global and Planetary Change* 66, 76–84.

The Carbonate Factory Over The Last 20.000 Yrs In The Nw Saronikos Gulf

- [69] **Harris, P. T., Heap, A. D., Marshall, J.F., and McCulloch, M., 2008.** A new coral reef province in the Gulf of Carpentaria, Australia: colonization, growth and submergence during the early Holocene. *Marine Geology*, 251, 85–97.
- [70] **Hazan N, Stein M, Agnon A, Marco S, Nadel D, Schwab M, Negendank J, Neev D. 2005** Forthcoming. The late Pleistocene-Holocene history of the Sea of Galilee (Lake Kinneret). *Quaternary Research*
- [71] **Hilgen, F.J., 1991a.** Astronomical calibration of Gauss to Matuyama sapropels in the Mediterranean and implication for the geomagnetic polarity time scale. *Earth Planet. Sci. Lett.* 104, 226–244.
- [72] **James, N.P., Bone, Y. & Kyser, T.K. 2005:** Where has all the aragonite gone? mineralogy of holocene neritic cool-water carbonates, Southern Australia. *Journal of Sedimentary Research* 75, 454–463.
- [73] **Jiang, L.-Q., R. A. Feely, B. R. Carter, D. J. Greeley, D. K. Gledhill, and K. M. Arzayus 2015** Climatological distribution of aragonite saturation state in the global oceans, *Global Biogeochem. Cycles*, 29 (10)
- [74] **Jordan, N., Allison, P. A., Hill, J. & Sutton, M. D. 2015.** Not all aragonitic molluscs are missing: taphonomy and significance of a unique shelly lagerstätte from the Jurassic of SW Britain. *Lethaia*, Volume 48, Issue 4 Pages 540–548
- [75] **John V.C, Coles S.L, Abozed A.L., 1990.** Seasonal cycles of temperature, salinity and water masses of the Western Arabian Gulf. *Oceanologica Acta* 1990 Vol. 13,3.
- [76] **Jolly, D., S.P. Harrison, B. Damnati and R. Bonnefille, 1998.** Simulated climate and biomes of Africa during the Late Quaternary: comparison with pollen and lake status data. *Quaternary Science Reviews*, 17, 629-57.
- [77] **Kallel, N., Paterne, M., Duplessy, J., Vergnaud-Grazzini, C., Pujol, C., Labeyrie, L., Arnold, M., Fontugne, M., Pierre, C., 1997b.** Enhanced rainfall in the Mediterranean region during the last sapropel event. *Oceanologica Acta* 20, 697–712.
- [78] **Karageorgis A., & Kanellopoulos T., Mavromatis V. Anagnostou C. Koutsopoulou E. Schmidt M., Pavlopoulos K., Tripsanas E., Hallberg R. 2013** Authigenic carbonate mineral formation in the Pagassitikos palaeolake during the latest Pleistocene, central Greece. *Geo-Mar Lett* (2013) 33:13–29

The Carbonate Factory Over The Last 20.000 Yrs In The Nw Saronikos Gulf

- [79] **Kienast, M., Hanebuth, T. J. J., Pelejero, C., and Steinke, S., 2003.** Synchronicity of meltwater pulse 1a and the Bolling warming: New evidence from the South China Sea. *Geology*, 31, 67– 70.
- [80] **Klein, B., W. Roether, B. B. Manca, D. Bregant, V. Beitzel, V. Kovacevic, and A. Luchetta (1999),** The large deep water transient in the eastern Mediterranean, *Deep Sea Res. Part I*, 46, 371 – 414.
- [81] **Kolaiti E., Mourtzas N. 2015.** Upper Holocene sea level changes in the West Saronic Gulf, Greece. *Quaternary International* 401, 71-90
- [82] **Kontakiotis G. 2012.** Palaeoceanographic and palaeoclimatic study of Eastern Mediterranean during Late Quaternary, based on planktonic foraminiferal assemblages, PhD Thesis, National & Kapodistrian University of Athens, Greece, pp. 1-247.
- [83] **Kotthoff, U., U. C. Muller, J. Pross, G. Schmiedl, I. T. Lawson, and H. Schulz, 2008.** Late glacial and Holocene vegetation dynamics in the Aegean region: an integrated view based on pollen data from marine and terrestrial archives. *Holocene* 18:1019–1032.
- [84] **Kotthoff U., Koutsodendris A. Pross J., Gerhard S., Bornemann A., Kaul C., Marino G., Peyron O., Schiebel R. (2011)** Impact of lateglacial cold events on the northern Aegean region reconstructed from marine and terrestrial proxy data. *Journal of Quaternary Science* (2011) 26(1) 86-96
- [85] **Kranis HD, Papanikolaou DI (2001)** Evidence for detachment faulting on the NE Parnassos mountain front (Central Greece). *Bull Geol Soc Greece* 34(1):281–287
- [86] **Ku, T.C.W., Walter, L.M., Coleman, M.L., Blake, R.E. & Martini, A.M. 1999:** Coupling between sulfur recycling and syndepositional carbonate dissolution: evidence from oxygen and sulfur isotope composition of pore water sulfate, South Florida Platform, U.S.A. *Geochimica et Cosmochimica Acta* 63, 2529–2546
- [87] **Kuper, R., and S. Kropelin. 2006.** Climate-controlled Holocene occupation in the Sahara: motor of Africa’s evolution. *Science* 313:803–807.
- [88] **Lambeck, K. 1996.** Sea Level change and shore-line evolution in Aegean Greece since Upper Palaeolithic time, *Antiquity*, 70/269, p 588-611.

The Carbonate Factory Over The Last 20.000 Yrs In The Nw Saronikos Gulf

- [89] Lambeck, K., Chappell, J., 2001. Sea-level change through the last glacial cycle, *Science* 292, 679–686.
- [90] Lambeck, K., 2002. Sea-level change from mid-Holocene to recent time: an Australian example with global implications, in: J.X. Mitrovica, B. Vermeersen (Eds.), *Glacial Isostatic Adjustment and the Earth System*, Am. Geophys. Union, Washington, DC, pp. 33–50.
- [91] Leeder M. R., 2011. *Sedimentology and Sedimentary Basins: From Turbulence to Tectonics*, 2nd Edition. © Wiley-Blackwell
- [92] Liu, J.P., Milliman, J., 2004. Reconsidering melt-water pulses 1A and 1B: global impacts of rapid sea-level rise. *Journal of Ocean University of China* 3, 183–190.
- [93] Lourens, L.J.A., Antonarakou, F.J., Hilgen, F.J., Van Hoof, A.A.M., Vergnaud-Grazzini, C., Zachariasse, W.J., 1996. Evaluation of the Plio-Pleistocene astronomical timescale. *Palaeoceanography* 11, 391–431.
- [94] Lowenstam H. A. and Epstein S. (1957) On the origin of sedimentary aragonite needles of the Great Bahama Bank. *J. Geol.* 65, 364–375.
- [95] Lykousis, V., Anagnostou, C., 1994. Sedimentological and paleogeographic evolution of Saronikos Gulf during the Late Quaternary, *Bull. Geol. Soc. Greece* 28 (1), 501–510 (in Greek).
- [96] Lykousis, V., D. Sakellariou, I. Moretti and H. Kaberi (2007). Late Quaternary basin evolution of the Gulf of Corinth: Sequence stratigraphy, sedimentation, fault-slip and subsidence rates, *Tectonophysics*, 440(1-4), 29-51
- [97] Mackenzie, F. T. and Morse, J. W.: Sedimentary carbonates through Phanerozoic time, *Geochim. Cosmochim. Acta*, 56, 3281–3295, 1992.
- [98] Makris, J., Papoulia, J. & Drakatos, G. 2004 Tectonic deformation and microseismicity of the Saronikos Gulf, Greece. *Bull. Seismol. Soc. Am.* 94:3, pp. 920–929
- [99] Mariolakos I (1976) Thoughts and viewpoints on certain problems of the geology and tectonics of the Peloponnesus (Greece). *Annu Geol Pays Hellenique* 27:215–313

The Carbonate Factory Over The Last 20.000 Yrs In The Nw Saronikos Gulf

- [100] **Mariolakos H.; Theocharis D., 2001.** Displacements of Saronikos coastlines over the last 18,000 years and the Kihria palaeolake. Δ.Ε.Γ.Ε. XXXIV/1, σ. 405-413.(greek)
- [101] **Melim, L.A., Westphal, H., Swart, P.K., Eberli, G.P., Munnecke, A., 2002.** Questioning carbonate diagenetic paradigms: evidence from the Neogene of the Bahamas. *Mar. Geol.* 185, 27–53.
- [102] **Meyer, H.J., 1984,** The influence of impurities on the growth rate of calcite: *Journal of Crystal Growth*, v. 66, p. 639–646.
- [103] **Millero F.J. 1996.** *Chemical Oceanography*, Second Edition CRC Press
- [104] **Milliman J. D. (1974)** *Recent Sedimentary Carbonates 1, Marine Carbonates.* Springer, New York.
- [105] **Milliman J. D., Freile D., Steinen R. P., and Wilber R. J. (1993)** Great Bahama Bank argonitic muds: mostly inorganically precipitated, mostly exported. *J. Sediment. Petrol.* 63, 589–595.
- [106] **Morris A., 2000** Magnetic fabric and palaeomagnetic analyses of the Plio-Quaternary calc-alkaline series of Aegina Island, South Aegean Volcanic Arc, Greece *Earth and Planetary Science Letters*, 176 (2000), pp. 91–105
- [107] **Morse J. W. and Mackenzie F. T. (1990)** *Geochemistry of Sedimentary Carbonates.* Elsevier, Amsterdam
- [108] **Morse JW, Wang Q, Tsio MY, 1997.** Influences of temperature and Mg: Ca ratio on CaCO₃ precipitates from seawater. *Geology* 25, 85–87
- [109] **Morse. J. W., Gledhill, D. K. and Millero, F. J.:2003** CaCO₃ precipitation kinetics in waters from the Great Bahama Bank: Implications for the relationship between Bank hydrochemistry and whittings, *Geochim. Cosmochim. Ac.* 67. 2819-2826. 2(X)3
- [110] **Mucci A. 1983.** The solubility of calcite and aragonite in seawater at various salinities, temperatures, and one atmosphere total pressure. *American Journal of Science.* American Journal of Science Vol..283. p.780-799
- [111] **Mucci A. and Morse J. W. (1983)** The incorporation of Mg²⁺ and Sr²⁺ into calcite overgrowths: Influences of growth rate and solution composition. *Geochim. Cosmochim. Acta* 47, 217-233.

- [112] **Mucci, A., B. Sundby, M. Gehlen, T. Arakaki, S. Zhong, and N. Silverberg (2000)**, The fate of carbon in continental shelf sediments of eastern Canada: A case study, *Deep Sea Res. Part II*, 47, 733 – 760.
- [113] **Nakada, M., Lambeck K., 1989**. Late Pleistocene and Holocene sea-level change in the Australian region and mantle rheology. *Geophysical Journal*, 96 pp. 497–517
- [114] **Neev D. And Emery K. O. (1967)** The Dead Sea, depositional processes and environments of evaporites. *Geol. Surv. Israel Bull.* 41, 147p.
- [115] **Papanikolaou D, Lykousis V, Chronis G, Pavlakis P (1988)** A comparative study of neotectonic basins across the Hellenic Arc: The Messiniakos, Argolikos and Southern Evoikos Gulfs. *Basin Res* 1:167–176
- [116] **Papanikolaou D., Mpasis E.K., Kranis C. and Danamos G. 2004** **Paleogeographical evolution of Athens basin from Upper Miocene up to today** *Bulletin of the Geological Society of Greece Vol. Xxxvi*, 2004 *Proceedings of the 10th International Congress, Thessaloniki, April 2004 (greek)*
- [117] **Passier, H. F., J. J. Middelburg, B. J. H. Van Os, and G. J. De Lange (1996)**, Diagenetic pyritisation under eastern Mediterranean sapropels caused by downward sulphide diffusion, *Geochim. Cosmochim. Acta*, 60, 751 – 763.
- [118] **Peltier, W.R., Fairbanks, R.G., 2006**. Global ice volume and Last Glacial Maximum duration from an extended Barbados sea-level record. *Quaternary Science Reviews* 25, 3322–3337.
- [119] **Perissoratis C. and van Andel T.H., 1991** Sea-level changes and tectonics in the Quaternary extensional basin of the South Evoikos Gulf, Greece. *Terra Nova* 3, 294-302.
- [120] **Perissoratis, C., Piper, D.J.W., Lykousis, V., 1993**. Late Quaternary sedimentation in the Gulf of Corinth: the effects of marine-lake fluctuations driven by eustatic sea level changes. *Special Publication Dedicated to Prof. A. Panagos. Nat. Tech. Univ. of Athens*, pp. 693–744.
- [121] **Perissoratis, C., Piper, D.J.W., Lykousis, V., 2000**. Alternating marine and lacustrine sedimentation during late Quaternary in the Gulf of Corinth rift basin, central Greece. *Mar. Geol.* 167, 391–411.

The Carbonate Factory Over The Last 20.000 Yrs In The Nw Saronikos Gulf

- [122] **Pe G.G., 1973** Petrology and geochemistry of volcanic rocks of Aegina, Greece Bulletin Volcanologique, 37 (4) (1973), pp. 491–514
- [123] **Pe-Piper G., Pipier D.J.W., Reynolds P.H. 1983** Paleomagnetic stratigraphy and radiometric dating of the Pliocene volcanic rocks of Aegina, Greece Bulletin Volcanologique, 47 (1983), pp. 1–7
- [124] **Perry, C. T., Taylor K. G. 2006** Inhibition of dissolution within shallow water carbonate sediments: impacts of terrigenous sediment input on syn-depositional carbonate diagenesis. Sedimentology Volume 53, Issue 3, p. 495–513
- [125] **Plummer, L. N., Parkhurst, D. L., Fleming, G. W., and Dunkle, S. A., 1988**, A computer program incorporating Pitzer's equations for calculation of geochemical reactions: U.S. Geological Survey Water-Resources Investigations Report 88-4153, 310 p.
- [126] **Poulimenos G, Doutsos T (1996)** Barriers on seismogenic faults in central Greece. J Geodynamics 22(1/2):119–135
- [127] **Reddy, M M., and Wang, K.K. (1980)** Crystallization of calcium carbonate in the presence of metal ions. Journal of Crystal Growth, 50, 470- 480
- [128] **Reid R. P., Macintyre I. G., and Post J. E. (1992)** Micritized skeletal grains in Northern Belize Lagoon: a major source of Mg-calcite mud. J. Sediment. Petrol. 62, 145–156
- [129] **Ries J. B., Anderson M. A, Hill R. T (2008)** Seawater Mg/Ca controls polymorph mineralogy of microbial CaCO₃: A potential proxy for calcite-aragonite seas in Precambrian time. Geobiology 6, 106–119
- [130] **Robbins, L. L., and Blackwelder P. L., 1992.** Biochemical and ultrastructural evidence for the origin of whittings: A biologically induced calcium carbonate precipitation mechanism, Geology, 20, 464 – 468.
- [131] **Rochford, D. J. (1964)**, Salinity maxima in the upper 1000 metres of the north Indian Ocean, Aust. J. Mar. Freshwater Res., 15, 1–24.
- [132] **Roeser, P., Franz, S.O.,Litt T. (2016)** Aragonite and calcite preservation in sediments from Lake Iznik related to bottom lake oxygenation and water column depth Sedimentology 2016

The Carbonate Factory Over The Last 20.000 Yrs In The Nw Saronikos Gulf

- [133] Rohling, E. J., and Hilgen, F. J., 1991. The eastern Mediterranean climate at times of sapropel formation: a review, *Geologie en Mijnbouw*, 70: 253-264.
- [134] Rohling, E. J., P. A. Mayewski, R. H. Abu-Zied, J. S. L. Casford, and A. Hayes, 2002. Holocene atmosphere-ocean interactions: Records from Greenland and the Aegean Sea, *Clim.Dyn*, 18, 587–593,
- [135] Rohling, E. J., Cane, T. R., Cooke, S., Sprovieri, M., Bouloubassi, I., Emeis, K. C., Schiebel, R., Kroon, D., Jorissen, F. J., Lorre, A., and Kemp, A. E. S., 2002b. African monsoon variability during the previous interglacial maximum, *Earth and Planetary Science Letters*, 202: 61-75.
- [136] Rossignol-Strick, M., 1983. African monsoons, an immediate response to orbital insolation. *Nature* 304, 46–49.
- [137] Rossignol-Strick, M., 1985 Mediterranean Quaternary sapropels, an immediate response of the African monsoon to variations of insolation, *Palaeogeography, Paleoclimatology, Palaeoecology*, 49, 237-63.
- [138] Rossignol-Strick, M., 1995 Sea-land correlation of pollen records in the eastern Mediterranean for the glacial-interglacial transition: biostratigraphy versus radiometric time-scale, *Quaternary Science Reviews*, 14, 893-915, Pergamon, Elsevier, Oxford.
- [139] Rutten, A., G. J. de Lange, A. Hayes, E. J. Rohling, A. F. M. de Jong, and K. van der Borg (1999), Deposition of sapropel S1 sediments in oxic pelagic and anoxic brine environments in the eastern Mediterranean: Differences in diagenesis and preservation, *Mar. Geol.*, **153**, 319–335.
- [140] Sanders_D., 2003 Syndepositional dissolution of calcium carbonate in neritic carbonate environments: Geological recognition, processes, potential significance. *Journal of African Earth Sciences* 36(3):99-134
- [140] Seymour St. K., 1996 The Kakoperato rhyodacite flow, Aegina volcano: a window to the intricacies of a calcalkaline subvolcanic magma chamber *Neues Jahrbuch für Mineralogie - Abhandlungen*, 171 (1) (1996), pp. 61–89
- [142] Sorel D (2000) A Pleistocene and still-active detachment fault and the origin of the Corinth-Patras rift, Greece. *Geology* 28(1):83– 86

The Carbonate Factory Over The Last 20.000 Yrs In The Nw Saronikos Gulf

- [143] **Stanford, J.D., Rohling, E.J., Hunter, S.E., Roberts, A.P., Rasmussen, S.O., Bard, E., McManus, J., Fairbanks, R.G., 2006.** Timing of meltwater pulse 1a and climate responses to meltwater injections. *Paleoceanography* 21 (4)
- [144] **Stanford, J.D., Hemingway, R., Rohling, E.J., Challenor, P.G., Medina-Elizalde, M., Lester, A.J., 2011.** Sea-level probability for the last deglaciation: a statistical analysis of far-field records. *Glob. Planet. Chang.* 79 (3), 193–203.
- [145] **Stanley, S. M. and Hardie, L. A. 1999,** Hypercalcification: Paleontology links plate tectonics and geochemistry to sedimentology. *GSA Today* 9: 1-7.
- [146] **Starinsky A. (1974)** Relation between Ca-chloride brines and sedimentary rocks in Israel. Ph.D. thesis, The Hebrew University, Jerusalem.
- [147] **Stein M, Starinsky A, Goldstein SL, Katz A, Machlus M, Schramm A. 1997.** Strontium isotopic, chemical, and sedimentological evidence for the evolution of Lake Lisan and the Dead Sea. *Geochimica et Cosmochimica Acta* 61:3975–92
- [148] **Stothers, R. B., and M. R. Rampino (1983).** Volcanic eruptions in the Mediterranean before A.D. 630 from written and archeological sources, *J. Geophys. Res.* 88, 6357–6371
- [149] **Sumner DY, Grotzinger JP (1996a)** Herringbone calcite: Petrography and environmental significance. *J Sed Res* 66:419-429
- [150] **Sumner DY, Grotzinger JP (1996b)** Were kinetics of Archean calcium carbonate precipitation related to oxygen concentration? *Geology* 24:119-122
- [151] **Sun, W., Jayaraman, S., Chen, W., Persson, K., and Ceder, G. (2015).** Nucleation of metastable aragonite CaCO₃ in seawater. *Proc. Natl. Acad. Sci. U.S.A.* 112, 3199–3204. doi: 10.1073/pnas.1423898112
- [152] **Thomson, J., Higgs, N.C., Wilson, T.R.S., Croudace, I.W., De Lange, G.J., Van Santvoort, P.J.M., 1995.** Redistribution and geochemical behaviour of redox-sensitive elements around S1, the most recent eastern Mediterranean sapropel. *Geochim. Cosmochim. Acta* 59, 3487–3501
- [153] **Thompson, J., S. Schultze-Lam, S., T. J. Beveridge, T. J. and DesMarais, D. J., 1997.** Whiting events: Biogenic origin due to the photosynthetic activity of cyanobacterial picoplankton, *Limnol. Oceanogr.*, 42, 133 – 141.

The Carbonate Factory Over The Last 20.000 Yrs In The Nw Saronikos Gulf

- [154] Thomson, J., Crudeli, D., de Lange, G. J., Slomp, C. P., Erba, E., Corselli, C., 2004. Florisphaera profunda and the origin and diagenesis of carbonate phases in eastern Mediterranean sapropel units. *Paleoceanography*, Vol. 19
- [155] Thunell, R.C., Williams, D.F., 1989. Glacial–Holocene salinity changes in the Mediterranean Sea: hydrographic and depositional effects. *Nature* 338, 493–496.
- [156] Tooley, M.J., 1989. Floodwaters mark sudden rise. *Nature* 342, 20e21.
- [157] Tornqvist, T. E., S. J. Bick, J. L. Gonzalez, K. van der Borg, and A. F. M. de Jong, 2004. Tracking the sea-level signature of the 8.2 ka cooling event: New constraints from the Mississippi Delta, *Geophys. Res. Lett.*, 31,
- [158] Toscano, M.A., Macintyre, I.G., 2003. Corrected western Atlantic sea-level curve for the last 11,000 years based on calibrated 14C dates from Acropora palmate framework and intertidal mangrove peat. *Coral Reefs* 22, 257–270.
- [159] Trask P.D. Relation of salinity to the calcium carbonate content of marine sediments. U.S. Geological Survey Professional Paper 186-N
- [160] Triantaphyllou, M.V., P. Ziveri, A. Gogou, G. Marino, V. Lykousis, I. Bouloubassi, K.-C. Emeis, K. Kouli, M. Dimiza, A. Rosell-Mele, M. Papanikolaou, G. Katsouras and N. Nunez, 2009 “Late Glacial-Holocene climate variability at the south-eastern margin of the Aegean Sea”, *Marine Geology*, 266, 182-97.
- [161] Triantaphyllou, M.V., A. Antonarakou, K. Kouli, M. Dimiza, G. Kontakiotis, M. Papanikolaou, P. Ziveri, P.G. Mortyn, V. Lianou, V. Lykousis and M.D. Dermitzakis (2009b) Comparing Late Glacial-Holocene plankton ecozones and pollen assemblage zones: basis for a multiproxy ecostratigraphy in the South-Eastern Aegean Sea (E. Mediterranean) *Geomarine Letters*, 29, 4, 249-67.
- [162] Tribble G. W., 1993. Organic Matter Oxidation and Aragonite Diagenesis in a Coral Reef. *Journal of Sedimentary Research* 63(3):523-527
- [163] Tucker, M.E. 1992 Limestones through time. In *Understanding the Earth, a New Synthesis* (eds Brown, G.C., Hawkesworth, C.J. & Wilson, R.C.L.). Cambridge University Press, Cambridge; 347-363.

The Carbonate Factory Over The Last 20.000 Yrs In The Nw Saronikos Gulf

- [164] **Tynan, S. & Opdyke, B.N. 2011:** Effects of lower surface ocean pH upon the stability of shallow water carbonate sediments. *The Science of the Total Environment* 409, 1082–1086.
- [165] **Tzedakis, P. C., Frogley, M. R., Lawson, I. T., Preece, R. C., Cacho, I., and de Abreu, L. (2004),** Ecological thresholds and patterns of millennial-scale climate variability: the response of vegetation in Greece during the last glacial period, *Geology*, 32: 109-112
- [166] **Van Andel, T.H., Shackleton, J.C., 1982.** Late Paleolithic and Neolithic coastlines of Greece and the Aegean. *J. Field Archaeol.* 9, 445±454.
- [167] **Van Heuven, S., D. Pierrot, E. Lewis, And D. W. R. Wallace. 2009.** Matlab program developed for CO₂ system calculations (<http://cdiac.ornl.gov/oceans/co2rprt.html>). Carbon Dioxide Information Analysis Center, Oak Ridge National Laboratory, U.S. Department of Energy, Oak Ridge, Tennessee.
- [168] **Van Hinsbergen DJJ, Snel E, Garstman SA, Marunteanu M, Langereis CG, Wortel MJR, Meulenkamp JE (2004)** Vertical motions in the Aegean volcanic arc: evidence for rapid subsidence preceding in situ volcanism. *Mar Geol* 209:329–345
- [169] **Van Hinsbergen, D. J. J., D. G. van der Meer, W. J. Zachariasse, and J. E. Meulenkamp (2006),** Deformation of western Greece during Neogene clockwise rotation and collision with Apulia, *Int. J. Earth Sci.*, 95, 463–490, doi:10.1007/s00531-005-0047-5.
- [170] **Walter LM, 1986** Relative efficiency of carbonate dissolution and precipitation during diagenesis: a progress report on the role of solution chemistry. In *Roles of Organic Matter in Sediment Diagenesis* (ed. Gautier D). SEPM (Society for Sedimentary Geology) Special Publication no. 38, SEPM, Tulsa, Oklahoma, pp. 1–11.
- [171] **Wansard G., De Deckker P., Julia R. (2016)** Combining the Mg/Ca of the ostracod *Cyprideis torosa* with its ontogenic development for reconstructing a 2 kyr temperature record for Lake Banyoes (NE Spain). *Journal of Microplaeontology* doi:10.1144/jmpaleo2015-009

The Carbonate Factory Over The Last 20.000 Yrs In The Nw Saronikos Gulf

[172] Wenk, H.-R. & Bulakh, A. 2004. Minerals. Their Constitution and Origin. xxii+646 pp. Cambridge, New York, Melbourne

[173] Wehausen, R., and H. J. Brumsack. 2000. Chemical cycles in Pliocene sapropel bearing and sapropel-barren eastern Mediterranean sediments. *Palaeogeography, Palaeoclimatology, Palaeoecology* 158:325–352.

[174] Wheeley, J.R., Cherns, L. & Wright, V.P. 2008: Provenance of microcrystalline carbonate cement in limestone–marl alternations (LMA): aragonite mud or molluscs? *Journal of the Geological Society* 165, 395–403

[175] Wilkinson, B., Algeo, T. (1989) Sedimentary carbonate record of calcium-magnesium cycling, *Am. J. Sci.*, 289, 1158 – 1194, 1989.

[176] Yokoyama, Y., Lambeck, K., Deckker, P.D., Johnston, P., Fifield, L.K., 2000. Timing of Last Glacial Maximum from observed sea level minima. *Nature* 406, 713–716.

[177] Yu, S.-Y., Berglund, B.E., Sandgren, P. and Lambeck, K., 2007: Evidence for a rapid sea level rise 7600 yr ago, *Geology*, 35: 891-894.

ACRONYMS AND ABBREVIATIONS

AMS	▪ Accelerator Mass Spectrometry
HS1	Heinrich Stadial Event 1
IAP	ion activity products
ka BP	kilo annum before present
K_{ar}	apparent stoichiometric solubility product of aragonite
K_c	apparent stoichiometric solubility product of calcite
mbsf	meters below seafloor
MS	Magnetic Susceptibility
MWP 1A₀	Meltwater Pulse 1A ₀
MWP 1A	Meltwater Pulse 1A
MWP 1b	Meltwater Pulse 1b
MWP 1c	Meltwater Pulse 1c
SAR	Ref. to core retrieved from Saronikos
SEM	▪ Scanning Electron Microscopy
SOR	Sulphide Oxidation Reaction
TC	Total Carbon
TIC	Total Inorganic Carbon
pCO₂	Partial pressure of carbon dioxide
XRD	X-ray diffractometer
Ω	Saturation State
ppt	permille or parts per thousand
YD	Younger Dryas

LIST OF FIGURES

- Fig.1 Palaeogeographic reconstruction of the Aegean Sea, during the slow-stand at about 16 ka BP (Lambeck, & Chappell, 2001)
- Fig.2 (a) SST in the Alboran sea based on measurements of the relative composition of unsaturated C₃₇ alkenones, (b) $\delta^{18}\text{O}$ in *G.bulloides* (c) Relative abundance (%) of *N. pachyderma* (s) and (d) $\delta^{18}\text{O}$ record from an ice core. (Graph borrowed from Cacho et al. 1999)
- Fig. 3 Most significant deglacial events to global changes in sea level from 23 ka to the present (Gornitz, 2009)
- Fig.4 Holocene Temperature Variations interpreted by ice cores, sediment cores and pollen analysis by Robert A. Rohde (dark blue: SST from Eastern Tropical Atlantic: Zhao et al., 1995 blue: paleotemperature from Central Antarctica: Petit et al., 1999 light blue: paleotemperature from Greenland: Alley et al., 2000 green: SST from Kilimanjaro in Eastern Central Africa: Thompson et al., 2002 yellow: SST from North Atlantic: Lea et al., 2003, orange: Pollen distributions, interpreted temperature, Europe: Davis et al., 2003, red: SST obtained from ice core from Central Antarctica: EPICA community members, 2004), dark red: SST from Western Tropical Pacific: Stott et al., 2004).
- Fig.5 Sea levels based on clinofolds (Foutrakis, 2016)
- Fig.6 Batymetric map of Saronikos Gulf. (Foutrakis, 2016)shaded area: Coastline when global sea level was -120 m, Red dotted line: possible route of Kifissos river. (map adopted by unpublished Foutrakis&Anastassakis)
- Fig.7 Megara Basin remains isolated. Coastline when global sea level was -90 m, Red dotted line: possible route of Kifissos river. (map modified: adopted by Foutrakis, 2016)
- Fig.8 Shaded area: Coastline when global sea level was -75 m (map modified: adopted by Foutrakis, 2016)
- Fig.9 CO₂ exchange and the chemical reactions of the dissolved CO₂ with the other solutes

The Carbonate Factory Over The Last 20.000 Yrs In The Nw Saronikos Gulf

Fig.10 (left) pH (at 25 deg C) as a function of depth in the Atlantic and Pacific oceans. (right) Depth profile of Ω for calcite and aragonite as a function of ocean basin. Also the depth at which the dotted line crosses the $\Omega=1$ gives the depth below which aragonite and calcite dissolve

Fig.11 Experimentally determined nucleation fields of low-Mg calcite with MgCO_3 content <6 mol% (red), high-Mg calcite + aragonite (blue), and aragonite (green) in $\text{MgCl}_2\text{-CaCl}_2\text{-Na}_2\text{CO}_3\text{-H}_2\text{O}$ solutions at 28 °C, atmospheric pCO_2 and 1 atm total pressure. MgCO_3 content of high-Mg calcite increases systematically with increase in the Mg:Ca ratio in the aqueous solution (data of Füchtbauer&Hardie, 1976, 1980). Black star SW: modern seawater. (Diagram borrowed by Stanley&Hardie, 1999)

Fig.12 Kinetic phase diagram of the relative nucleation rate between calcite and aragonite (color-coded) as a function of solution Mg:Ca ratio and the supersaturation. For Mg: Ca =5.2 (present seawater) only aragonite is preferred to nucleate. Concurrent nucleation of calcite and aragonite occurs for a broad span of supersaturations near Mg:Ca= 2. (Sun et al. 2015)

Fig.13 Spatial distributions of aragonite saturation state (Ω_{arag}) today at depth levels of (a) 50 m, (b) 100 m, (c) 200 m, and (d) 500 m in the global oceans. Colors show gridded values based on Data Interpolating Variational Analysis (DIVA). Black dots show the sampling stations.

Fig.14 The solubility product of calcite (CaCO_3) depending on the water temperature and salinity during precipitation (values according to Mucci, 1983). For instance, at $S=35$ and 1 atmosphere pressure, the K_{sp}^* decreases slightly as the temperature rises

Fig.15 Graph above: The acidity constants for the first dissociation of carbonic acid in freshwater and seawater as a function of the water temperature at salinities of 0, 5, 15, 25, and 35‰. Second Graph: The acidity constants for the second dissociation of carbonic acid in seawater as a function of the water temperature at salinities of 0, 5, 15, 25, and 35‰. The values are according to Millero&Roy (1997). The marine values are equal those reported by Mehrbach et al. (1973) as discussed by

The Carbonate Factory Over The Last 20.000 Yrs In The Nw Saronikos Gulf

Dickson&Millero (1987)

- Fig.16 Values for the first and second dissociation constants of dissolved carbonic acid as a function of the salinity (Millero&Roy, 1997). The values are valid for a water temperature of 20°C. Available dissociation constants of carbonic acid, K_1, K_2 , as a functions of salinity
- Fig.17 Relative precipitation rates of aragonite vs. calcite (R_a/R_c), as a function of temperature in seawater five times supersaturated with respect to calcite (After Burton&Walter, 1987)
- Fig.18 Usiglio Model (1849)(Evaporation Sequence of seawater)
- Fig.19 Photos of the cores retrieved from the Megara Basin
- Fig.20 MS variations of the piston cores from Saronikos Gulf
- Fig.21 Fig. 21 Downcore trends illustrating the inverse relationship of TIC to MS within cores SAR36 and SAR39
- Fig.22 Classification of carbonate-clay mixtures (modified after Barth et al., 1939)
- Fig.23 Plots with the primary facies of the long cores based on their carbonate-clay composition
- Fig.24 SAR36 subunits based on carbonate content-MS relationship
- Fig.25 Photos of SAR36 (a. nodules within marl (facies I), b. transitional facies II, c. heavily bioturbated marley lime)
- Fig.26 SAR36 facies based on carbonate-clay mixture
- Fig. 26b SAR38 subunits based on carbonate content-MS relationship
- Fig.27 photos of SAR38 (a. facies I-facies II b. facies II-facies III)
- Fig.28a SAR39 subunits based on carbonate content-MS relations
- Fig.28b Fig.28b SAR39 facies based on carbonate-clay mixture
- Fig.29 photos of SAR39 a.calcite-dominated sequence b. upper aragonite sequence c.d. thin layers of sand show possible marine transgression e. transitional facies (brownish) between the two aragonite sequences
- Fig.30 Fig.30 SAR4 facies based on carbonate-clay mixture
- Fig.31 SAR34 based on carbonate content-MS relationship (one facies, marl is present, SAR34 represents typical marine environment)

The Carbonate Factory Over The Last 20.000 Yrs In The Nw Saronikos Gulf

- Fig.32 SIEMENS D5000 X-ray diffractometer
Calibration curves for the determination of relative percentages of
- Fig.33 aragonite and calcite i.e. aragonite and high-magnesian calcite
(Obtained from Muller and Muller, 1967).
- Fig.34 Calibration curve of % dolomitization versus the intensity ratio of
calcite and dolomite peaks. (Obtained from Tennant and Berger, 1957
- Fig.35 XRD carbonate mineralogy SAR4
- Fig.36 XRD carbonate mineralogy SAR36
- Fig.37 XRD carbonate mineralogy SAR39
- Fig.38 XRD SAR39 Comparison of terrigenous minerals with carbonate
minerals
- Fig.39 SEM photomicrographs of Emiliana Huxley and Syracosphaera in
SAR39 58cm
- Fig.40 SEM photomicrographs of Aragonitic needles in SAR39 168cm
- Fig.41 Calcidiscus surrounded by aragonitic needles in SAR39 168cm
- Fig.42 SEM photomicrographs of Calcite crystals and nanofossil trapped in
SAR39 168cm
- Fig.43 SEM photomicrographs of Authigenic framboidal pyrite in SAR39
168cm
- Fig.44 SEM photomicrographs of Diatom in SAR39 237cm
- Fig.45 SEM photomicrographs of Diatom in SAR39 237cm

LIST OF TABLES

Table 1	MELTWATER PULSE 1A ₀
Table 2	MELTWATER PULSE 1A
Table 3	MELTWATER PULSE 1B
Table 4	MELTWATER PULSE 1C
Table 5	Saronikos Gulf
Table 6	Production/ Consumption of CO ₂
Table 7	Solubility products (K) and ion activity products(IAP) for carbonate minerals in surface seawater at 25°C. Note that surface seawater is supersaturated with respect to all these carbonate minerals (Leeder, 2011)
Table 8	Salinities of Modern Environments
Table 9	Typical carbonate factories
Table 10	Info of the long cores retrieved from NW Saronikos Gulf
Table 11	Classification of minerals based on their MS
Table 12	SAR36 Info
Table 13	SAR38 Info
Table 14	SAR39 Info
Table 15	SAR4 Info
Table 16	SAR34 Info
Table 17	Empirical Estimation of the CO ₃ ²⁻ % participation in each mineral for SAR4
Table 18	Empirical Estimation of the CO ₃ ²⁻ % participation in each mineral for SAR36
Table 19	Empirical Estimation of the CO ₃ ²⁻ % participation in each mineral for SAR39
Table 20	Radiocarbon ages of aragonite-dominated sequence